THE NONLINEAR EVOLUTION OF SECONDARY INSTABILITIES IN BOUNDARY LAYERS

by

Jeffrey D. Crouch

Dissertation submitted to the Faculty of the
Virginia Polytechnic Institute and State University
in partial fulfillment of the requirements for the degree of

Doctor of Philosophy

in

Engineering Mechanics

APPROVED:

Th. Herbert, chairman

D.T. Mook

S.L. Hendricks

S.A. Ragab

M. Renardy

April, 1988

Blacksburg, Virginia

THE NONLINEAR EVOLUTION OF SECONDARY INSTABILITIES IN BOUNDARY LAYERS

by

Jeffrey D. Crouch

Committee Chairman: Thorwald Herbert
Engineering Science and Mechanics

(ABSTRACT)

Following the concepts of stability analysis, a study is made of the pre-breakdown stage of transition to turbulence in boundary layers. The first step consists of a 'decoupling' of the primary and secondary instabilities. A perturbation method is used to solve for the primary wave, in the absence of any secondary disturbances. Once the wave is calculated, it is decomposed into a basic flow portion and an interaction portion. The basic flow portion acts as a parametric excitation for the secondary wave. The interaction portion then captures the resonance effects of the secondary back onto the primary. A perturbation method is also used for the secondary and interaction components. The results obtained are in three principal forms: Landau constants, amplitude growth curves, and velocity functions. While in good agreement with experiments and simulations, these results offer new explanations to the observed processes. In addition, a physically-based transition criteria is established.

Acknowledgements

The author would like to express his gratitude to for the many suggestions during the course of this work. From conception to completion interactions with him have been enormously rewarding in terms of encouragement and the fostering of new ideas. Thanks also to the committee members

, for their contributions toward this effort.

In addition, the author would like to thank and . Their comments and criticisms have played an important role in the development of this work. The many discussions with them have been an invaluable asset. Thanks to for help in the administrative aspects, which made things run much more smoothly. Finally, thanks to for help with the typing and for continued encouragement and support.

Table of contents

1. Introduction

1.1 Motivation

The process of transition from laminar to turbulent flow is of fundamental significance to the analysis of fluid flows. Many of the variables used in design applications depend dramatically on the state of the flow. Boundary layers, in particular, demonstrate considerable quantitative and qualitative differences between the laminar and turbulent states.

Transition is a process by which an unstable ordered state undergoes qualitative changes toward a disordered and chaotic state. Energy, extracted from the mean flow, is pumped into disturbance waves which then interact and cause changes in one another and in the mean flow itself. Although certain qualitative changes necessarily occur, the process details are not unique.

Attempts to study transition have revolved around the induction and subsequent growth of disturbances within the boundary layer. In low noise environments, experiments have shown distinct stages in the development of these disturbances. The first stage begins with the onset of a two-dimensional TS instability. The dominate mode (most unstable or highest initial amplitude) then grows within a virtually two-dimensional framework, having no spanwise variations. At some point, however, these TS waves 'give over' to a three-dimensional wave field. Once initiated, spanwise variations rapidly grow and in most cases lead to the ultimate breakdown of the laminar flow.

The early work of Schubauer and Skramstad (1948) demonstrates the actual presence of the TS wave within the laminar boundary layer. For sufficiently small amplitudes, these waves harmlessly grow and decay. However, if larger amplitudes are reached, peak-valley splitting occurs, resulting in periodic spanwise variations (Klebanoff, Tidstrom. and Sargent 1962). This disturbance field is characterized by a streamwise wavelength equal to that of the TS wave and a spanwise wavelength of the same order. Unlike the TS wave, these three-dimensional disturbances grow rapidly, leading to breakdown within a few TS wavelengths.

Other experments establish another form of three dimensionality, where the streamwise wavelength is twice that of the TS wave (Knapp and Roache 1968; Kachanov and Levchenko 1982). This behavior is observed for intermediate amplitudes of the TS wave. In addition to demonstrating a similar occurrence of three dimensionality for lower disturbance amplitudes, these experiments show the process to be non-unique. These detailed studies have stimulated much activity focused on finding the mechanisms associated with the onset and evolution of the three dimensionality.

1.2 Previous Work

Attempts at analysis of this transitional flow field begin with the two-dimensional linear stability theory applied to a parallel basic flow. This theory provides a good description of the onset and evolution of the TS wave, based on either a temporal or spatial growth rate. The inclusion of nonparallel effects

shows stronger growth rates over a slightly wider range of Reynolds numbers, giving better agreement with experiments (Gaster 1974; Saric and Nayfeh 1977).

Most of the analytic work dealing with the nonlinear self interaction of the TS wave has been done for plane Poiseuille flow. This strictly parallel flow allows for a cleaner mathematical description of the basic physics. Perturbation methods developed for growing waves yield a Landau equation that describes the two-dimensional wave amplitude. These methods use either the amplification rate (Stuart 1960) or the wave amplitude (Watson 1960) as the expansion parameter. These schemes, however, have an arbitrariness in the evaluation of the Landau constants due to the particular definition of the amplitude. Herbert devised a new scheme with a modified definition of the amplitude which yields a unique solution (Herbert 1983). Many studies on Poiseuille flow and similar work on the boundary layer (Herbert 1975) show the nonlinear self-interaction effects to be small and qualitatively insignificant, at the observed two-dimensional amplitudes.

Proceeding beyond the two-dimensional region, dramatic changes occur with the onset of three-dimensional variations. The origin and evolution of these variations have given rise to many different theoretical approaches. The majority of these approaches fall under one of two headings, namely mutual resonant interaction models or parametric interaction models (Nayfeh 1987; Herbert 1988a). This distinction characterizes how the three-dimensional wave interacts with the two-dimensional wave.

The mutual resonant interaction models consist of one or more two-

dimensional waves and a pair of three-dimensional waves which interact through resonance (Nayfeh 1985). The wave amplitudes are considered to be of the same order so that a mutual interaction occurs without any bias given to the two-dimensional wave. At first order, these waves are simple solutions to the two- or three-dimensional Orr-Sommerfeld equation or Squire's equation. At second order, the two-dimensional/three-dimensional resonance occurs, consisting of interactions between the different Squire and Orr-Sommerfeld modes. The most successful of these models is the Craik resonant triad (Craik 1971). Even though this model requires, a priori, a particular spanwise wave number for the resonance to occur, it gives good results for low amplitude two-dimensional waves. In addition it establishes, analytically, the subharmonic path to transition. The mutual interaction models seem justified for small two-dimensional amplitudes but fail to reflect the bias present when larger two-dimensional amplitudes occur.

The parametric interaction model is based on the preeminence of the two-dimensional wave at the onset of three-dimensionality. This model consists of a two-dimensional primary wave of amplitude A and a three-dimensional secondary wave of amplitude B (Herbert 1984a). Although both amplitudes are small with respect to the mean flow, the secondary wave amplitude, B, is also considered small with respect to A. This assumption results in a linear Floquet system governing the secondary wave. This system admits a wide variety of solutions which vary in prominence depending on the value of A. For large values of A, primary resonance occurs, producing the fundamental mode associated

with peak valley splitting. At smaller A, the principle parametric resonance dominates, yielding the subharmonic modes. In the limit $A \rightarrow 0$, the spanwise wave number for maximum growth is consistent with Craik's mechanism. The resulting disturbance profiles and amplitude growth curves are in good agreement with the experiments of Klebanoff et al. (1962) and Kachanov and Levchenko (1982) (Herbert 1984a; 1985).

This parametric approach, in conjunction with experimental work, provides a good working model for the early stages of transition (Herbert 1988b). The first stage consists of a primary instability; the onset and evolution of the TS wave. In the second stage, as this TS wave reaches sufficiently large A, the onset of a secondary instability occurs. Once the secondary amplitude, B, becomes comparable with A, the waves interact, producing modifications to the primary wave and the mean flow. This interaction gives rise to the third stage which is characterized by the breakdown of the laminar flow. The modifications of B on A, however, are not accessible in the linear treatment of the parametric interaction.

Following this parametric approach, Croswell (1985) analyzed the energy exchanges between mean flow, two-dimensional waves, and three-dimensional waves for plane Poiseuille flow. This work establishes a possible feedback loop by which the three-dimensional wave could be self-sustained. The initial energy transfer occurs with the mean flow giving rise to a two-dimensional wave. This wave in turn acts as a catalyst for the stronger transfer from the mean flow into the three-dimensional wave. A portion of the energy received by the three-

dimensional wave is dissipated, but the majority either goes into an increase in amplitude or is transferred to the two-dimensional wave. As shown in Figure 1.1, this chain of energy transfers suggests a feedback loop. If, in addition, the modified two-dimensional wave continues to stimulate the three-dimensional wave, self-sustained growth would be established.

In addition to the analytical and asymptotic approaches, direct numerical simulations have been done for both the plane Poiseuille flow and the Blasius boundary layer. Although these methods remove some of the approximations present in analytical approaches, they do require some a priori information. In particular, the inflow and outflow boundary conditions for the region of computation under consideration. Most of the transition simulations are based on a temporal evolution of disturbances in a spatially periodic domain (Orszag and Patera 1983; Zang and Hussaini 1985; Spalart and Yang 1987). An alternative approach is to consider a spatial evolution, which can also allow for nonparallel effects (Fasel and Konzelmann 1987).

The results of the simulations show good agreement with the experiments and permit easier access to details of the flow. Thus, they offer an additional perspective with their own biases, building a fuller view of the actual transition process. This broader view supports the analytical and asymptotic efforts, which are able to more fully decompose the flow field, to uncover the physical mechanisms.

1.3 Scope of Present Work

This endeavor is focused on the mechanisms associated with the nonlinear stages of the transition process. The details of these mechanisms lie hidden in the intricate interactions of finite amplitude waves. Under certain conditions these waves may interact to produce a disturbance field which in turn will stimulate their own growth. The establishment of such positive feedback offers a good criteria for the onset of breakdown. Therefore. in addition to focusing on the mechanisms, an attempt is made to determine the threshold conditions for the ultimate transition to turbulence.

To this end, a model is formulated for the geometrically simple case of Blasius flow, under the parallel flow assumption. Recognizing the initial prominence of the TS wave, this model contains both the parametric and mutual interaction models as special cases. Like the linear-parametric model, the initial stages of the secondary instability account for the already established primary wave. However, when the secondary wave becomes larger, it is allowed to affect the primary wave, similar to a mutual interaction model. This analytic/asymptotic approach allows for a piecewise examination of the wave interactions, leading to new insights into the physical mechanisms.

This paper is intended to present the key components of the interaction model along with some results and their implications. To begin, the details of the problem formulation are discussed. An attempt is made to establish this model as a general perturbation approach to biased systems, in which one mode is permitted to become substantially larger then other modes, before the modes

interact nonlinearly. In addition, problem specific details are given in the light of previous work. Following the formulation is a description of the method of solution. Results are then presented, for both comparison with other work and demonstration of new findings. Finally, an appraisal of the model is given along with a description of the conditions necessary for self-sustained growth.

2. Problem formulation

The key to the analysis of wave interactions in the boundary layer is in the recognition of the initial prominence of the TS wave. This prominence suggests that the TS wave be calculated as a primary wave, in the absence of any three-dimensional disturbances. Once the primary wave is calculated, it is split into a strong basic flow portion and a weak interaction portion. The basic flow portion, in conjunction with the Blasius flow, gives rise to a secondary wave which is three dimensional. This secondary wave then interacts with the interaction portion of the primary wave, producing corrections to both the primary and secondary waves. The only restriction on the arbitrary splitting of the primary is that the interaction portion be 'small' compared to the basic flow portion. The appendix offers an example of this approach applied to a simple two-degree-of-freedom nonlinear dynamics problem.

Motivating this approach is the need to account for higher-order resonance interactions between the primary and secondary modes. The strong agreement between theory, experiment and simulation establish the parametric origins of the secondary. Once the secondary becomes 'significantly' large, however, some degree of mutual interaction must be permitted. Any attempt to apply a purely mutual interaction will result in the loss of the secondary mode, leaving only multiple primary modes. As an alternative, the two-dimensional disturbance field can be decomposed into parametric forcing and mutually interacting com-

ponents.

This decomposition could be accomplished by adding an additional secondary mode which is two-dimensional. This mode would be parametrically generated and would provide a two-dimensional/three-dimensional resonance interaction. The resonance provided, however, would not be between the primary and secondary waves but between two secondary waves, one of which is two dimensional. An additional shortcoming is that the two-dimensional secondary mode is without physical justification. The primary mode alone contains the complete two-dimensional field in the absence of any three-dimensional disturbances.

An alternative approach, used here, is to decompose the primary wave. Although more complicated analytically, this approach permits a two-dimensional/three-dimensional interaction without the addition of a two-dimensional secondary. Since the decomposition is somewhat arbitrary, the resonance effects can be distributed over the entire primary wave (as described in section 3.2.2).

2.1 Governing equations

The analysis begins with the equations governing the motion of an incompressible fluid. Namely, the continuity equation (conservation of mass)

$$\nabla \cdot \mathbf{v} = 0 \tag{2.1}$$

and the Navier-Stokes equations (conservation of momentum)

$$\frac{\partial \mathbf{v}}{\partial t} + (\mathbf{v}\cdot\nabla)\,\mathbf{v} = -\nabla p + \frac{1}{Re}\nabla^2 \mathbf{v} \ . \tag{2.2}$$

Here the Cartesian coordinates (x',y,z) are used, decomposing the velocity, $\mathbf{v}$, into the respective components (u,v,w). The streamwise direction is taken to be x', the spanwise direction z, and the surface normal direction y. The boundary conditions governing the flow are

$$u = v = w = 0 \qquad at \quad y = 0 \ , \tag{2.3}$$

$$u \to 1 \ , \ w \to 0 \qquad as \quad y \to \infty \ . \tag{2.4}$$

The curl of the momentum equation in conjunction with continuity removes the explicit dependence on pressure, p, and produces the vorticity transport equation

$$\frac{1}{Re}\nabla^2\boldsymbol{\omega} - \frac{\partial \boldsymbol{\omega}}{\partial t} - (\mathbf{v}\cdot\nabla)\boldsymbol{\omega} + (\boldsymbol{\omega}\cdot\nabla)\mathbf{v} = 0 \ . \tag{2.5}$$

These are three scalar equations for the vorticity components, which in turn yield the Cartesian velocity components through

$$\nabla \times \mathbf{v} = \boldsymbol{\omega} = (\xi, \eta, \varsigma) \ . \tag{2.6}$$

At the expense of generating higher order equations, derivatives and combinations of derivatives yield useful forms of the equations. In particular, taking $\partial/\partial z$ of the η -vorticity equation leads to Squire's equation.

$$L^s(\mathbf{v}) - \frac{\partial}{\partial t}M^s(\mathbf{v}) + N^s(\mathbf{v},\mathbf{v}) = 0 \tag{2.7}$$

where

$$L^s(\mathbf{v}) = (\frac{1}{R}\nabla^2)\ \frac{\partial \eta}{\partial z} \tag{2.7a}$$

$$M^s(\mathbf{v}) = \frac{\partial \eta}{\partial z} \tag{2.7b}$$

$$N^s(\mathbf{v},\mathbf{v}) = -\frac{\partial}{\partial z}(\mathbf{v}\cdot\nabla)\eta + \frac{\partial}{\partial z}(\omega\cdot\nabla)\mathbf{v} \quad . \tag{2.7c}$$

Likewise, taking $\partial/\partial x$ of the ς -vorticity equation and subtracting $\partial/\partial z$ of the ξ -vorticity equation leads to the Orr-Sommerfeld equation,

$$L^o(\mathbf{v}) - \frac{\partial}{\partial t}M^o(\mathbf{v}) - N^o(\mathbf{v},\mathbf{v}) = 0 \tag{2.8}$$

where,

$$L^o(\mathbf{v}) = (\frac{1}{R}\nabla^2)\nabla^2\mathbf{v} \tag{2.8a}$$

$$M^o(\mathbf{v}) = \nabla^2\mathbf{v} \tag{2.8b}$$

$$N^o(\mathbf{v},\mathbf{v}) = -\frac{\partial}{\partial x}(\mathbf{v}\cdot\nabla)\varsigma + \frac{\partial}{\partial x}(\omega\cdot\nabla)w - \frac{\partial}{\partial z}(\mathbf{v}\cdot\nabla)\xi - \frac{\partial}{\partial z}(\omega\cdot\nabla)u \quad . \tag{2.8c}$$

To examine the evolution of disturbances within the boundary layer, the velocity is decomposed into a one-dimensional mean flow, a two-dimensional primary wave, and a general three-dimensional disturbance,

$$\mathbf{v}(x',y,z,t) = \mathbf{v}_0(y) + \mathbf{v}_1(x',y,t) + \mathbf{v}_2(x',y,z,t) \quad . \tag{2.9}$$

The velocity $\mathbf{v}_0$ is the mean flow, consisting of the Blasius profile subject to the parallel flow assumption. The velocity $\mathbf{v}_1$ represents a TS wave calculated as an instability of the Blasius flow. The velocity $\mathbf{v}_3$ consists of the three-dimensional secondary wave as well as higher order terms both two- and three-dimensional produced by resonant wave interaction. Substituting (2.9) into (2.7), (2.8), (2.3), and (2.4) and subtracting the equations for the mean-basic flow yields,

$$L_0^s(\mathbf{v}_1) - \frac{\partial}{\partial t}M^s(\mathbf{v}_1) + N^s(\mathbf{v}_1,\mathbf{v}_1) + L_0^s(\mathbf{v}_3)$$

$$-\frac{\partial}{\partial t}M^s(\mathbf{v}_3) + N^s(\mathbf{v}_1,\mathbf{v}_3) + N^s(\mathbf{v}_3,\mathbf{v}_3) = 0 \tag{2.10}$$

$$L_0{}^o(\mathbf{v}_1) - \frac{\partial}{\partial t}M^o(\mathbf{v}_1) + N^o(\mathbf{v}_1,\mathbf{v}_1) + L_0{}^o(\mathbf{v}_3)$$

$$-\frac{\partial}{\partial t}M^o(\mathbf{v}_3) + N^o(\mathbf{v}_1,\mathbf{v}_3) + N^o(\mathbf{v}_3,\mathbf{v}_3) = 0 \tag{2.11}$$

$$\mathbf{v}_1 = \mathbf{v}_3 = 0 \qquad at \quad y = 0 \tag{2.12}$$

$$\mathbf{v}_1 \to 0 \ , \quad \mathbf{v}_3 \to 0 \qquad as \quad y \to \infty \ . \tag{2.13}$$

For the stability analysis, $\mathbf{v}_0$ is considered known: therefore, new linear operators are introduced, defined as $L_0{}^s(\mathbf{v}) = L^s(\mathbf{v}) + N^s(\mathbf{v}_0,\mathbf{v})$ for the Squire's equation, and similarly for the Orr-Sommerfeld equation.

2.2 Primary wave

The first step in analyzing equations (2.10) and (2.11) is to consider the two-dimensional mode $\mathbf{v}_1$ as a primary wave, independently satisfying

$$L_0{}^s(\mathbf{v}_1) - \frac{\partial}{\partial t}M^s(\mathbf{v}_1) + N^s(\mathbf{v}_1,\mathbf{v}_1) = 0 \ . \tag{2.14}$$

$$L_0{}^o(\mathbf{v}_1) - \frac{\partial}{\partial t}M^o(\mathbf{v}_1) + N^o(\mathbf{v}_1,\mathbf{v}_1) = 0 \ . \tag{2.15}$$

These nonlinear equations contain all the self interaction which goes into the formation of a finite amplitude two-dimensional wave in the presence of a Blasius mean flow. To solve these equations, a perturbation method expanding about the linear solution at fixed R and α is used. Following Herbert (1983), the temporal growth concept leads to a Landau equation for the representative amplitude. This equation will be incomplete, however, if interaction with the

secondary wave is also to be considered.

2.2.1 Fourier expansion

Because the coefficients in (2.14) and (2.15) are independent of x', i.e. $\mathbf{v}_0 = u_0(y)$, the velocity $\mathbf{v}_1$ can be expanded in a Fourier series in x'. Extrapolating from the form of the linear solution while including higher order harmonics, a mean flow distortion, and a modification to the wave itself yields

$$\mathbf{v}_1(x',y,t) = \sum_{k=-\infty}^{\infty} \tilde{\mathbf{v}}_{1_k}(y,t)e^{ik\theta} \qquad \theta = \alpha x' - \gamma(t) \tag{2.16}$$

where $\tilde{\mathbf{v}}_{1_{-k}}$ is equal to the complex conjugate of $\tilde{\mathbf{v}}_{1_k}$. The key factor in making a selection of this form is the need to account for the modification of both the frequency and growth rate due to finite amplitude. The function $\gamma(t)$ contains the temporal oscillation, while $\tilde{\mathbf{v}}_{1_k}(y,t)$ contains the growth. Substituting (2.16) into (2.14) and (2.15) produces a set of coupled nonlinear partial differential equations in y and t.

2.2.2 Amplitude expansion

Using perturbation methods, the set of partial differential equations, generated from (2.14) and (2.15), is further reduced to a set of ordinary differential equations. Recognizing the harmonics of the fundamental function, $\tilde{\mathbf{v}}_{1_1}(y,t)$, to be of higher order suggests defining

$$\tilde{\mathbf{v}}_{1_k}(y,t) = A^{|k|}\mathbf{v}_{1_k}(y,t) \ . \tag{2.17}$$

This brings about a decoupling of the nonlinear equations, since $\tilde{\mathbf{v}}_{1_k}$ contains no

terms smaller than $O(A^k)$. As a result of the time derivative in (2.14) and (2.15), (2.16) and (2.17) produce coefficients which contain the frequency (or wave speed) and the growth rate. These can be coupled as a single complex coefficient,

$$\lambda = a - i\omega = a - i\alpha c_r \tag{2.18}$$

where a is the growth rate and c_r is the wave speed, defined by,

$$a = \frac{dA}{A\,dt} \quad , \quad c_r = \frac{\omega}{\alpha} = \frac{d\gamma}{\alpha\,dt} \quad . \tag{2.19}$$

Following the method of strained parameters, both the function, $\mathbf{v}_{1_k}(y,t)$, and the coefficient, λ, are expanded in terms of the amplitude A. Only even powers of A are included, however, since the odd power terms have been found to drop out (Herbert 1983). The resulting forms of these expansions are,

$$\mathbf{v}_{1_k}(y,t) = \sum_{p=0}^{\infty} \mathbf{v}_{1_{kp}}(y) A^{2p} \quad , \tag{2.20}$$

$$\lambda = \sum_{p=0}^{\infty} \lambda_p A^{2p} \quad , \quad \lambda_p = a_p - i\alpha c_{r_p} \quad . \tag{2.21}$$

Making this final substitution and collecting terms results in two coupled ordinary differential equations for each harmonic at every given order of A. The ultimate order of a function depends on which harmonic as well as which term in the expansion it is. An expansion of this form accounts for all resonances of A with itself up to a given order. In consideration of the secondary mode and its interaction with the primary mode, similar expressions are used.

As a result of this procedure, the expanded form of the primary wave (to third order) is,

$$\mathbf{v}_1(x',y,t) = 1/2(A^2\mathbf{v}_{1_{01}}(y)) + (A\mathbf{v}_{1_{10}}(y) + A^3\mathbf{v}_{1_{11}}(y))e^{i\theta} + (A^2\mathbf{v}_{1_{20}}(y))e^{i2\theta} + (A^3\mathbf{v}_{1_{30}}(y))e^{i3\theta} + c.c. \quad . \tag{2.22}$$

In addition to the fundamental wave, $\mathbf{v}_1$ now contains a mean flow correction and a second harmonic. Likewise, the growth rate and wave speed can be expanded as

$$\frac{dA}{Adt} = a_0 + A^2 a_1 \quad , \tag{2.23}$$

$$c_r = c_{r_0} + A^2 c_{r_1} \quad . \tag{2.24}$$

Given an initial amplitude, equation (2.23) describes its growth in time, while (2.24) provides the corresponding change in wave speed. A third order solution of this problem gives the velocity functions $\mathbf{v}_{1_{10}}, \mathbf{v}_{1_{01}}, \mathbf{v}_{1_{20}}, \mathbf{v}_{1_{11}}$ and the constants $a_0, a_1, c_{r_0}, c_{r_1}$, independent of the value of A. The actual velocity functions, the growth rate, and the wave speed, however, depend on the value of A.

If the value of A were to take into account the interaction with the secondary wave, then the modified velocity functions and wave speed will also via (2.22) and (2.24), respectively. Simply modifying A, however, will not capture the effects of the interaction on the velocity functions. To this end, additional functions of higher order must be included in $\mathbf{v}_3$.

2.2.3 Two-dimensional basic flow

With the primary wave calculated to within an initial amplitude, $\mathbf{v}_1$ could be substituted into equations (2.10) and (2.11) as a basic flow of fixed amplitude. This is the standard procedure for the parametric analysis of secondary instabilities. By selecting an amplitude and substituting the primary mode into the secondary mode equations, a purely parametric interaction is obtained. Thus, no modification of the primary wave due to the secondary wave is taken into account.

To allow for modifications to the primary wave due to interactions with the secondary wave, the primary wave amplitude is decomposed into a predefined portion, A^*, and a variable portion, $\hat{A}$, namely $A = A^* + \hat{A}$ where $\hat{A} < A^*$. The actual choices of A^* and $\hat{A}$ are arbitrary, requiring only that they together satisfy equation (2.23) in the absence of any secondary wave. In this way, the primary wave can be split into a basic flow, containing only A^*, and a perturbation, containing also the variable $\hat{A}$. The basic flow interacts parametrically (one-way interaction) with the secondary wave. while the perturbation interacts through resonance (two-way interaction). Since A^* will be predefined, only $\hat{A}$ needs to be determined so as to fix A and fully define the primary wave.

Substituting for A in (2.22) and collecting coefficients of powers of $\hat{A}$ yields the expression,

$$\mathbf{v}_1 = \mathbf{v}_1^* + \hat{\mathbf{v}}_1 \tag{2.25}$$

where,

$$\mathbf{v}_1^* = 1/2(A^{*2}\mathbf{v}_{1_{01}}) + A^*(\mathbf{v}_{1_{10}} + A^{*2}\mathbf{v}_{1_{11}})e^{i\theta} + (A^{*2}\mathbf{v}_{1_{20}})e^{i2\theta} + (A^{*3}\mathbf{v}_{1_{30}})e^{i3\theta} + c.c. \ ,$$

$$\hat{\mathbf{v}}_1 = \hat{A}\,\mathbf{v}_A + \hat{A}^2\,\mathbf{v}_{A^2} + \hat{A}^3\,\mathbf{v}_{A^3} + O(A^{*4}) \ ,$$

and,

$$\mathbf{v}_A = (A^*\mathbf{v}_{1_{01}}) + (\mathbf{v}_{1_{10}} + 3A^{*2}\mathbf{v}_{1_{11}})e^{i\theta} + (2A^*\mathbf{v}_{1_{20}})e^{i2\theta} + (3A^{*2}\mathbf{v}_{1_{30}})e^{i3\theta} + c.c. \ ,$$

$$\mathbf{v}_{A^2} = 1/2(\mathbf{v}_{1_{01}}) + (3A^*\mathbf{v}_{1_{11}})e^{i\theta} + (\mathbf{v}_{1_{20}})e^{i2\theta} + (3A^*\mathbf{v}_{1_{30}})e^{i3\theta} + c.c. \ ,$$

$$\mathbf{v}_{A^3} = (\mathbf{v}_{1_{11}})e^{i\theta} + (\mathbf{v}_{1_{30}})e^{i3\theta} + c.c. \ .$$

The first term, $\mathbf{v}_1^*$, is independent of $\hat{A}$ and constitutes a fully known basic flow. The other term contains an expansion in terms of the perturbation amplitude $\hat{A}$. Similarly, substitution for A into (2.24) gives the expanded form of the wave speed

$$c_r = c_r^* - c_r^{\wedge} \tag{2.26}$$

where,

$$c_r^* = (c_{r_0} + A^{*2}c_{r_1}) \ ,$$

$$c_r^{\wedge} = \hat{A}(2A^*c_{r_1}) + \hat{A}^2(c_{r_1}) + O(A^{*4}) \ .$$

Finally, substituting for A and collecting coefficients of $\hat{A}$, (2.23) becomes

$$\frac{dA^*}{dt} + \frac{d\hat{A}}{dt} = (A^*a_0 - A^{*3}a_1) - \hat{A}(a_0 - 3A^{*2}a_1)$$

$$+ \hat{A}^2(3A^*a_1) + \hat{A}^3(a_1) + O(A^{*5}) \ . \tag{2.27}$$

In order to get an evolution equation for $\hat{A}$, the amplitude A^* is defined such that

$$\frac{dA^*}{dt} = A^*a_0 + A^{*3}a_1 \ . \tag{2.28}$$

This yields the equation for the growth of $\hat{A}$ due purely to self interaction of the primary wave,

$$\frac{d\hat{A}}{dt} = \hat{A}(a_0 + 3A^{*2}a_1) + \hat{A}^2(3A^*a_1) + \hat{A}^3(a_1) + O(A^{*5}) \ ,$$

or,

$$\frac{d\hat{A}}{dt} = \hat{A}a_A + \hat{A}^2a_{A^2} + \hat{A}^3a_{A^3} + O(A^{*5}) \ . \tag{2.29}$$

Thus far, no consideration has been given to the effects of a secondary wave back onto the primary wave.

2.3 Secondary wave and interaction modes

The consideration of the primary wave in the absence of interaction with the secondary yields a $\mathbf{v}_1$ which satisfies (2.14) and (2.15). To account for the primary/secondary interaction, two additional effects must be considered. The first effect is a modification of the primary amplitude, $\hat{A}$, due to higher order resonances with the secondary wave. When this occurs, (2.29) acquires additional terms which result in residuals $R^s(\hat{\mathbf{v}}_1)$ and $R^o(\hat{\mathbf{v}}_1)$, in (2.14) and (2.15), respectively. The exact form of these residuals is yet to be determined. The second effect of the primary/secondary interaction is a modification of the disturbance velocity functions. To account for this, two-dimensional functions will be included in $\mathbf{v}_3$.

Subtracting the primary equations (2.14) and (2.15) from (2.10) and (2.11), respectively, yields the governing equations for the secondary and interaction

modes

$$L_0^{\,e}(\mathbf{v}_3) - R^e(\hat{\mathbf{v}}_1) - \frac{\partial}{\partial t}M^e(\mathbf{v}_3) + N^e(\mathbf{v}_1,\mathbf{v}_3) + N^e(\mathbf{v}_3,\mathbf{v}_3) = 0 \ , \tag{2.30}$$

$$L_0^{\,o}(\mathbf{v}_3) - R^o(\hat{\mathbf{v}}_1) - \frac{\partial}{\partial t}M^o(\mathbf{v}_3) + N^o(\mathbf{v}_1,\mathbf{v}_3) + N^o(\mathbf{v}_3,\mathbf{v}_3) = 0 \ . \tag{2.31}$$

Substituting $\mathbf{v}_1 = \mathbf{v}_1^{\,*} + \hat{\mathbf{v}}_1$ gives,

$$L_0^{\,e}(\mathbf{v}_3) + L_1^{\,e}(\mathbf{v}_3) - R^e(\hat{\mathbf{v}}_1) - \frac{\partial}{\partial t}M^e(\mathbf{v}_3)$$

$$+ N^e(\hat{\mathbf{v}}_1,\mathbf{v}_3) + N^e(\mathbf{v}_3,\mathbf{v}_3) = 0 \ , \tag{2.32}$$

$$L_0^{\,o}(\mathbf{v}_3) - L_1^{\,o}(\mathbf{v}_3) - R^o(\hat{\mathbf{v}}_1) - \frac{\partial}{\partial t}M^o(\mathbf{v}_3)$$

$$+ N^o(\hat{\mathbf{v}}_1,\mathbf{v}_3) + N^o(\mathbf{v}_3,\mathbf{v}_3) = 0 \ . \tag{2.33}$$

Since $\mathbf{v}_1^{\,*}$ is now considered known, new linear operators, $L_1^{\,e}(\mathbf{v}_3) = N^e(\mathbf{v}_1^{\,*},\mathbf{v}_3)$ and $L_1^{\,o}(\mathbf{v}_3) = N^o(\mathbf{v}_1^{\,*},\mathbf{v}_3)$, have been introduced. These equations contain both a linear-parametric forcing of $\mathbf{v}_3$ and a nonlinear interaction with $\hat{\mathbf{v}}_1$ and itself.

Recall that the self interaction of the two dimensional wave only produces higher order one- and two-dimensional waves without resonating with the three-dimensional wave. The self interaction of the three-dimensional wave, however, produces both two- and three-dimensional higher order terms. Therefore, $N(\hat{\mathbf{v}}_1,\mathbf{v}_3)$ and $N(\mathbf{v}_3,\mathbf{v}_3)$ together provide the primary/secondary interaction.

To enable better analytical treatment of the secondary wave, a key assumption is made about the amplitude A^*. Namely, $dA^*/dt=0$, which is equivalent to saying A^* is locally an equilibrium amplitude. Although in general this is not

the case, the variation of A' relative to the secondary amplitude is quite small. Equation (2.28) is used to determine how A^* will evolve in time (or equivalently in space) after which the secondary and interaction terms are considered. This assumption is similar to doing an expansion about a finite amplitude, A^*. In such a case, the secondary amplitude, B, and the primary interaction amplitude, $\hat{A}$, are considered small in relation.

After this assumption, the variable coefficients associated with $L_1^{\,s}$ and $L_1^{\,o}$ can be simplified since the basic flow component , $\mathbf{v}_1^*$, of the primary wave is periodic in x' and t. To achieve this simplification, the problem is transformed into a Galilean frame moving with the two-dimensional wave. Introducing a new variable $x = x' - \gamma(t)/\alpha$, $\mathbf{v}_1^*$ becomes,

$$\mathbf{v}_1^*(x',y,t) = \mathbf{v}_1^*(x,y) = \mathbf{v}_1^*(x+\lambda_x,y) \tag{2.34}$$

where $\lambda_x = 2\pi/\alpha$ is the wavelength. The time dependence of $\mathbf{v}_1^*$ is totally removed, since A^* is considered fixed after it is calculated using (2.28). Expressing the periodic portion of the basic flow in terms of the stream function, $\psi_1^*(x,y)$, yields the typical form for the linear secondary operators $L_1^{\,s}$ and $L_1^{\,o}$ (Herbert 1984b).

2.3.1 Fourier expansion

Since the coefficients in (2.30) and (2.31) are independent of z, the velocity $\mathbf{v}_3$ can be expanded in a Fourier series in z

$$\mathbf{v}_3(x,y,z,t) = \sum_{m=-\infty}^{\infty} \tilde{\mathbf{v}}_{3_m}(x,y,t)\, e^{im\beta z} \quad . \tag{2.35}$$

If a time modulation $e^{-im\delta(t)}$ (similar to the primary mode) were included, it would have no effect. The function $\delta(t)$ shows up in the equations as the imaginary part of the Landau constant $d\delta/dt$, but since only β^2 appears in the equations, the system is real. Having real velocities then requires the Landau constants to be real.

Substituting (2.35) into (2.32) and (2.33) removes the z dependence. The nonlinear terms in $N^s(\mathbf{v}_3,\mathbf{v}_3)$ and $N^o(\mathbf{v}_3,\mathbf{v}_3)$ require a multiplication of the Fourier series. To account for this, the nonlinear operators can be rewritten as $N^s(\mathbf{v}_{\tilde{3}_\mu},\mathbf{v}_{\tilde{3}_\nu})$ and $N^o(\mathbf{v}_{\tilde{3}_\mu},\mathbf{v}_{\tilde{3}_\nu})$, respectively. The indices μ and ν take the role of m in (2.35). Only terms produced by the combination $\mu+\nu = m$ will contribute to the m^{th} harmonic equation. Substituting (2.35) into the continuity equation and dividing by the index, m, gives an expression for w_{3_m}

$$i\beta w_{3_m} = -\frac{1}{m}\left(\frac{\partial u_{3_m}}{\partial x}+\frac{\partial v_{3_m}}{\partial y}\right) . \tag{2.36}$$

Using this expression and the corresponding μ and ν expressions, w is removed from equations (2.32) and (2.33). For the case of $m = 0$, the term $1/m$ is simply set to zero. The velocity $\mathbf{v}_3$ includes both the first order secondary wave and the higher order resonance terms. For the resonance terms which are two dimensional, m will be equal to zero.

2.3.2 Amplitude expansion

Conceptually, the application of the perturbation method to the secondary and interaction modes is the same as for the primary wave. The presence of two

interacting amplitudes, however, requires a more generalized approach for the construction of the velocity functions and the amplitude growth equations. For simplicity, these can be constructed up to an arbitrary order by examining which interactions will produce a resonance with the primary or secondary wave. This approach is similar to that of Li (1986) used to examine the evolution of the first and second harmonics for the Taylor problem.

Starting with the linear secondary wave $B\mathbf{v}_B(x,y)e^{i\beta z}$ and the first order primary-interaction term $\hat{A}\mathbf{v}_A(x,y)$, higher order terms are generated. For each interaction, a new function is created. Which $\tilde{\mathbf{v}}_{3_m}$ function it will be a part of is determined by the associated value of m. Of particular interest are the terms associated with $m = 1$. These terms will be in resonance with the secondary wave. Constructing $\tilde{\mathbf{v}}_{3_1}$ to third order and noting $\hat{A}=\hat{A}(t)$ and $B=B(t)$ gives,

$$\tilde{\mathbf{v}}_{3_1}(x,y,t) = B\,\mathbf{v}_B(x,y) + \hat{A}B\,\mathbf{v}_{AB}(x,y) + \hat{A}^2B\,\mathbf{v}_{A^2B}(x,y) + B^3\,\mathbf{v}_{B^3}(x,y) \quad . \tag{2.37}$$

Associated with $m = 0$ are the interaction terms in resonance with the primary wave. To third order, $\tilde{\mathbf{v}}_{3_0}$ becomes,

$$\tilde{\mathbf{v}}_{3_0}(x,y,t) = B^2\,\mathbf{v}_{B^2}(x,y) + \hat{A}B^2\,\mathbf{v}_{AB^2}(x,y) \quad . \tag{2.38}$$

In addition to the new functions, the higher order resonance terms also generate Landau constants. The Landau constants monitor the effect of the interaction on the amplitudes associated with the particular resonance. Modifications occur through the amplitude growth equations. Recognizing where the $m = 1$ resonances occur, the secondary amplitude growth equation becomes

$$\frac{dB}{dt} = B\,b_B + \hat{A}B\,b_{AB} + \hat{A}^2B\,b_{A^2B} + B^3\,b_{B^3} \quad . \tag{2.39}$$

A similar consideration of the $m = 0$ resonances provides the the growth equation for $\hat{A}$

$$\frac{d\hat{A}}{dt} = \hat{A}\, a_A + \hat{A}^2\, a_{A^2} + \hat{A}^3\, a_{A^3} + B^2\, a_{B^2} + \hat{A}B^2\, a_{AB^2} \ . \tag{2.40}$$

The first three terms are from the primary self interaction (2.29). The last two terms are additions which account for the primary/secondary interaction. These additional terms produce the residuals in (2.32) and (2.33).

The result of the Fourier analysis and the amplitude expansion is a decoupling of (2.32) and (2.33) into a collection of linear equations. To determine these new equations (2.35), (2.37), and (2.38) are substituted into (2.32) and (2.33). Carrying out differentiation with respect to time produces $d\hat{A}/dt$ and dB/dt coefficients multiplying the M operators. These derivative terms are then replaced with the Landau constants and amplitudes given in (2.39) and (2.40). Collecting coefficients of $Be^{i\beta z}$ yields the linear secondary equations,

$$L_0^{s}(\mathbf{v}_B) + L_1^{s}(\mathbf{v}_B) - b_B\, M^{s}(\mathbf{v}_B) = 0 \ . \tag{2.41}$$

$$L_0^{o}(\mathbf{v}_B) - L_1^{o}(\mathbf{v}_B) - b_B\, M^{o}(\mathbf{v}_B) = 0 \ . \tag{2.42}$$

The solution of this eigenvalue problem yields the linear growth rate b_B and the corresponding x,y velocity function $\mathbf{v}_B$.

At second order, there are equations for both two- and three-dimensional terms. Collecting coefficients of $\hat{A}Be^{i\beta z}$ gives the equations for the secondary wave modification.

$$L_0^{s}(\mathbf{v}_{AB}) + L_1^{s}(\mathbf{v}_{AB}) - (a_A + b_B)\, M^{s}(\mathbf{v}_{AB})$$

$$- b_{AB}\, M^s(\mathbf{v}_B) = (2A^* c_{r_1} \frac{\partial}{\partial x})\, M^s(\mathbf{v}_B) + N^s(\mathbf{v}_A, \mathbf{v}_B) \ , \tag{2.43}$$

$$L_0{}^o(\mathbf{v}_{AB}) + L_1{}^o(\mathbf{v}_{AB}) - (a_A + b_B)\, M^o(\mathbf{v}_{AB})$$

$$- b_{AB}\, M^o(\mathbf{v}_B) = (2A^* c_{r_1} \frac{\partial}{\partial x})\, M^o(\mathbf{v}_B) + N^o(\mathbf{v}_A, \mathbf{v}_B) \ . \tag{2.44}$$

The terms containing c_{r_1} are due to the higher order modifications of the wave speed. They contain only lower order information. Collecting coefficients of $B^2 e^{i0z}$ for the primary wave modification yields,

$$L_0{}^s(\mathbf{v}_{B^2}) + L_1{}^s(\mathbf{v}_{B^2}) - 2a_A\, M^s(\mathbf{v}_{B^2}) - a_{B^2}\, M^s(\mathbf{v}_A) = N^s(\mathbf{v}_B, \mathbf{v}_B) \ , \tag{2.45}$$

$$L_0{}^o(\mathbf{v}_{B^2}) + L_1{}^o(\mathbf{v}_{B^2}) - 2a_A\, M^o(\mathbf{v}_{B^2}) - a_{B^2}\, M^o(\mathbf{v}_A) = N^o(\mathbf{v}_B, \mathbf{v}_B) \ . \tag{2.46}$$

In a similar fashion, higher order equations are generated.

The equations governing the second order constants and functions are nonhomogeneous, yet there structure is similar to the first order homogeneous equations. Therefore, certain parameter values can result in these equations being singular. The most obvious case for this, is in the calculation of $\mathbf{v}_{AB}$. As is discussed in section 2.5, the shape of this function is very similar to that of $\mathbf{v}_B$. If $\mathbf{v}_{AB}$ takes the form of a constant multiplying $\mathbf{v}_B$, then (2.43) and (2.44) will be singular. In particular, this will result in $\mathbf{v}_{AB} = -(b_{AB}/a_A)\mathbf{v}_B$. In such a case $\mathbf{v}_{AB}$ offers nothing new, and can be discarded. Other cases of singular behavior can result from resonances not included in this model. When A^* is 'small' oblique TS waves become relevant and should be considered. By neglecting such modes artificially large responses can occur over narrow bands of the parameters. In general, this type of singular behavior occurs at amplitudes, A^*, below the range

of interest.

2.3.3 Floquet analysis

The final result of the perturbation analysis is a pair of equations for each of the x,y functions in (2.37) and (2.38). Since the coefficients in these equations depend on x and y, Fourier analysis cannot be used to produce functions independent of x or y. With the 'localized' assumption of a fixed A^*, however, the coefficients are purely periodic. with respect to x. These x-periodic coefficients allow the use of Floquet theory to deal with the x dependence.

Earlier work of Herbert (1984a: 1984b; 1985) for linear parallel shear flows provides a guideline to the present application of this theory. The general form of the x,y functions will be $e^{\rho z} f(x,y)$ where f is x-periodic with wavelength λ_x. For the case of temporal stability, the characteristic exponent, ρ, will be zero. Thus the x,y functions can be written as a collection of y functions multiplying x-periodic functions similar to the application of Fourier analysis. The major distinction is that each y function of this collection must be solved for simultaneously. This is due to the coupling provided by the x-periodic coefficients.

In this regard, each of the x,y functions of (2.37) and (2.38) is expanded as

$$f(x,y) = \sum_{n=-\infty}^{\infty} f_n(y) e^{in\hat{\alpha}x} \quad , \qquad \hat{\alpha} = \frac{\alpha}{2} = \frac{\pi}{\lambda_x} \quad , \tag{2.47}$$

where f_{-n} is equal to the complex conjugate of f_n. When this form of expansion is substituted into the governing equations, a decoupling occurs between the modes with n even and n odd. The modes with n even have wavelength λ_x and

are called fundamental modes. These fundamental modes originate from primary resonance with the x-periodic coefficients. The modes with n odd have wavelength $2\lambda_x$ and are designated subharmonic modes. These modes result from principle parametric resonance (Nayfeh and Mook 1979).

2.4 Definition of amplitudes

Calculating the secondary and interaction modes contained in $\mathbf{v}_3$ has been simplified to solving sets of coupled ordinary differential equations. Associated with this decomposition of the velocity field, however, is an ambiguity in the definition of the amplitudes. In particular, the physical amplitudes can reside in both the velocity functions and the defined amplitudes. To establish meaningful evolution equations for $\hat{A}$ and B, a uniqueness condition is applied which ensures that the Landau constants contain the growth information (Herbert 1983).

The solution of the first order problem, (2.41) and (2.42), results in an eigenvalue, b_B, and an eigenfunction, $\mathbf{v}_B$. The phase on this function is fixed by imposing a local norm condition at a fixed point, y_0, in the profile. This point corresponds to the maximum in the primary-wave function, at some initial Reynolds number. The principal reason for using a local norm rather than an integrated norm is the simplicity that results at higher order.

In the second (or higher) order problem, the equations are nonhomogeneous, yet they possess a homogeneous solution. For a nontrivial solution to exist, the nonhomogeneous portion must satisfy a solvability condition which can be

used to calculate the Landau constants. Requiring the real part of the velocity function to be zero at y_0 produces a unique solution for the functions and constants. This ensures that $\hat{A}$ and B contain the major portion of the higher order amplitude modifications. The resulting functions are not normalized, however, so $\hat{A}$ and B are not the physical amplitudes.

To determine the physical two- and three-dimensional amplitudes, the total u composite functions must be considered. Once the total velocity functions are known, the maximum can be calculated to yield the physical amplitudes. The total two-dimensional velocity function will be the sum of (2.22) and (2.38). Following the experimental approach the portion of the disturbance with frequency ω, can be singled out. This requires, for (2.22), setting $k = \pm 1$, as defined in (2.16) and for (2.38), setting $n = \pm 2$, as defined in (2.47). Thus, the total two-dimensional function becomes

$$u_{2D}(x,y,t) = u_1(x',y,t)\big|_{k=\pm 1} + \tilde{u}_{3_0}(x,y,t)\big|_{n=\pm 2} \quad . \tag{2.48}$$

The total three-dimensional function is contained solely in (2.37) where $m = 1$. This function is characterized by one of two frequencies, depending on which mode of secondary instability is being considered. The subharmonic mode at frequency $\omega/2$ is obtained by setting $n = \pm 1$, as defined in (2.47),

$$u_S(x,y,t) = \tilde{u}_{3_1}(x,y,t)\big|_{n=\pm 1} \quad . \tag{2.49}$$

The fundamental mode at frequency ω is obtained by setting $n = \pm 2$, as defined in (2.47),

$$u_F(x,y,t) = \tilde{u}_{3_1}(x,y,t)\big|_{n=\pm 2} \quad . \tag{2.50}$$

Both of these functions are multiplied by $e^{i\beta z}$ which produces a net spanwise

variation in the physical velocities.

Since the fundamental function has the same frequency as the two-dimensional function, they are indistinguishable in experiments. In such a case, it is useful to define a new function which is three dimensional and contains the total velocity field at frequency ω

$$u_\omega (x,y,z,t) = u_{2D} (x,y.t) + u_F (x,y.t)e^{i\beta z} \quad . \tag{2.51}$$

This function is of particular interest at two spanwise locations, $z = 0$ and $z = \lambda_z/2$. At $z = 0$, u_{2D} and u_F combine in phase to produce the characteristic peak velocity function

$$u_P (x,y,t) = u_\omega (x,y.0,t) = u_{2D} (x.y.t) - u_F (x.y.t) \quad . \tag{2.52}$$

At $z = \lambda_z/2$, u_{2D} and u_F combine out of phase to produce the valley velocity function

$$u_V (x,y,t) = u_\omega (x,y,\frac{\lambda_z}{2},t) = u_{2D} (x,y,t) - u_F (x,y,t) \quad . \tag{2.53}$$

Having these total velocity functions, the physical amplitudes can be determined. As an example, the norm for the subharmonic function is $||u_S|| = \sqrt{(u_S,u_S)}$. Here the inner product is defined by

$$(u_S,u_S) = (\tilde{u}_{3_1}|_{n=-1})(\tilde{u}_{3_1}|_{n=-1})^\dagger + (\tilde{u}_{3_1}|_{n=+1})(\tilde{u}_{3_1}|_{n=+1})^\dagger \tag{2.54}$$

where † signifies complex conjugate. This norm provides a magnitude for the velocity function. The physical amplitude is then defined to be the maximum of the norm, $||u_S||_{max}$. Similar norms and amplitudes are calculated for each composite function.

2.5 Landau constants

By following a perturbation method of this type, the details of the wave interactions are cast in terms of Landau constants and disturbance velocity functions. Taken together, these provide a unique description for the evolution of the total two- and three-dimensional disturbance fields. Perhaps the most important advantage in using this approach, however, is the ability to examine the interactions of particular 'pieces' of the flow field. The Landau constants provide both the magnitude and direction (constructive or destructive) of these interactions. Although each constant is associated with a physical process, some can be better understood in analytical terms.

Carrying out the perturbation expansion to third order produces five Landau constants governing the evolution of the interaction portion of the primary wave, $\hat{A}$. These constants, given in (2.40), are a_A, a_{A^2}, a_{A^3}, a_{B^2}, and a_{AB^2}. The first three of these are related to the effects of self interaction whereas the latter two are related to interaction with the secondary mode. The first order constant, $a_A = a_0 + 3A^{*2} a_1$, is principally the linear growth rate. A small correction is added which accounts for the finite amplitude A^*, even though $\hat{A}$ could be considered infinitesimal. The constants $a_{A^2} = 3A^* a_1$ and $a_{A^3} = a_1$ are due solely to the third order self interaction of the primary wave. These constants contain the interaction with both the mean flow distortion and the second harmonic.

The second order constant, a_{B^2}, monitors the effect of the secondary mode onto the primary wave. Associated with the constant a_{B^2} is a velocity function, $\mathbf{v}_{B^2}$. The constant dictates the $O(B^2)$ effects on the amplitude $\hat{A}$, while the

function represents the effect on the total two-dimensional velocity field. This interaction is of key importance since it captures the distinct qualitative changes in the two-dimensional velocity field due to the three-dimensional disturbance. Unlike the secondary wave, which contains the primary/secondary interaction at first order, the primary wave first 'feels' the secondary at second order. Thus, any energy feedback will be first observed at this order. For plane Poiseuille flow, energy analysis has established the presence of a significant feedback from the three-dimensional field into the two-dimensional field (Croswell 1985 ; Herbert 1986). This would suggest that either $a_{B^2}>0$ or $B^2\,\mathbf{v}_{B^2}$ is of the order of the primary. If $a_{B^2}<0$, then higher order interactions must be considered to establish any sustained growth.

At third order, the constant a_{AB^2} contains the effect of the combined velocity field of $\mathbf{v}_A$ and $\mathbf{v}_{B^2}$. This particular interaction, however, offers nothing qualitatively new to the primary evolution. If the second order constant, a_{B^2}, were small, a_{AB^2} would become more relevant.

For the third order expansion, four Landau constants govern the evolution of the secondary amplitude, B. These constants given in (2.39) are b_B, b_{AB}, b_{A^2B} and b_{B^3}. The constant b_B is the linear growth rate of the secondary wave due to the parametric excitation by a TS wave with amplitude A^*. This constant appears as an eigenvalue in (2.41) and (2.42), varying as a function of the parameters (α,β,R,A^*) and the basic flow velocity functions. In the solution of (2.41) and (2.42), b_B is found to be real, which establishes the synchronization of the secondary with the primary wave. A general study of the dependence of the

growth rate, b_B, on the various parameters is given in Herbert (1984a; 1985) and Santos (1987). Of particular interest are the strong growth rates which occur for a broad band of spanwise wave numbers, β.

In the calculation of the first order constant b_B, the primary wave amplitude is considered to be A^*. Actually, however, the amplitude is $A = A^* + \hat{A}$. The second order constant b_{AB} takes the interaction portion of the primary wave, $\hat{A}$, into account. This constant offers nothing qualitatively new but is rather a quantitative modification of the linear growth rate. This is best understood by considering a new growth rate, σ_B, of the physical amplitude $\overline{B}$. The physical amplitude is defined by $\overline{B} = ||u_S||_{\max}$ for the subharmonic mode and by $\overline{B} = ||u_F||_{\max}$ for the fundamental. The growth rate can then be written as

$$\sigma_B = \frac{d\overline{B}}{\overline{B}dt} \quad , \tag{2.55}$$

where $\overline{B} = \overline{B}(\hat{A}(t), B(t), t)$. Expanding the derivative in (2.55) yields

$$\sigma_B = \frac{1}{\overline{B}} \left[\frac{d\overline{B}}{d\hat{A}} \frac{d\hat{A}}{dt} + \frac{d\overline{B}}{dB} \frac{dB}{dt} \right] \quad . \tag{2.56}$$

Substituting for the various components and evaluating the limit as $\hat{A}, B \to 0$ gives

$$\sigma_B = b_B + \hat{A} \left[b_{AB} + \frac{a_A}{2} \left(\left(\frac{u_{AB}}{u_B} \right)_{n=\hat{n}} - \left(\frac{u_{AB}}{u_B} \right)_{n=-\hat{n}} \right) \right] + \cdots \tag{2.57}$$

where $\hat{n} = 1$ for the subharmonic mode or $\hat{n} = 2$ for the fundamental and the functions are evaluated at the point of maximum u_B. Note, when $\hat{A} = 0$, then σ_B reduces to b_B. Taking the derivative of (2.57) with respect to A gives the slope of the growth rate as a function of A, evaluated at A^*. The slope is principally b_{AB}, with a correction due to the corresponding function u_{AB}. Therefore, as the primary amplitude deviates by $\hat{A}$ from A^*, the secondary growth rate is corrected by $\hat{A}$ multiplying the term in square brackets in (2.57). Comparing this slope with that calculated using a finite difference about A^* provides a check for the numerical algorithm.

The third order constant b_{B^3} accounts for the self interaction of the secondary wave. In particular, it describes how the two-dimensional velocity field, produced by the secondary wave, will affect the original three-dimensional wave. If b_{B^3} is negative then the secondary wave will be totally dependent on the primary for its existence. However, if b_{B^3} is positive then the secondary has the potential for self-sustained growth after it reaches some critical amplitude. This constant in conjunction with a_{B^2} most dramatically controls the ultimate fate of the secondary wave. The constant a_{B^2} controls indirectly through the primary whereas b_{B^3} affects directly the secondary.

The final constant to be considered is the third order constant b_{A^2B}. This constant is generated by the interaction of the secondary wave with the higher order portion of the primary wave. Similar to the second order constant b_{AB}, this constant contributes quantitatively but produces nothing qualitatively new.

3. Method of solution

3.1 Solution techniques

3.1.1 Numerical analysis

Following this problem formulation the original problem is successively decomposed into simpler problems. Each step in the decomposition carries assumptions and imposes restrictions based on the fluid physics. The first step is the decoupling of the primary and secondary instabilities. Both of these problems are then addressed using Fourier and perturbation analyses. This results in a collection of pairs of linear differential equations for each case. For the secondary wave, Floquet analysis is also necessary to produce ordinary differential equations governing the flow. Finally, the only difference between the primary and secondary instabilities is that the secondary requires the solution of a collection of coupled pairs of ordinary differential equations. rather than just one pair.

To actually solve the sets of ordinary differential equations the method of spectral collocation is used. To begin, the unbounded domain $y = 0.\infty$ is mapped into the bounded domain $\eta = 1,0$ using the algebraic mapping

$$\eta = \frac{\overline{y}}{y + \overline{y}} \quad . \tag{3.1}$$

The parameter $\overline{y}$ is used to control the distribution of collocation points within the boundary layer.

Next the velocity functions are expanded in terms of coefficients multiplying comparison functions. Here the odd Chebyshev polynomials are used for comparison functions. These polynomials 'automatically' satisfy the boundary conditions at infinity. For any given pair of equations this expansion can be written as

$$u(y) = \sum_{k=1}^{K} c_k T_{2k-1}(y) \quad , \tag{3.2}$$

$$v(y) = \sum_{k=1}^{K} d_k T_{2k-1}(y) \quad . \tag{3.3}$$

Since the Chebyshev polynomials are expressed in terms of η, the chain rule is used to calculate derivatives with respect to y. Owing to the finite sum on k error is introduced by (3.2) and (3.3). In the method of spectral collocation this error is forced to zero at certain collocation points, y_j, across the domain. Rewriting (3.2) and (3.3) at the collocation points yields

$$u(y_j) = \sum_{k=1}^{J+1} c_k T_{2k-1}(y_j) \quad , \tag{3.4}$$

$$v(y_j) = \sum_{k=1}^{J+2} d_k T_{2k-1}(y_j) \quad . \tag{3.5}$$

The additional coefficients (c_{J+1}, d_{J+1}, and d_{J+2}) are the result of explicitly satisfying the boundary conditions at $y = 0$.

Introducing (3.4) and (3.5) into the ordinary differential equations produces and algebraic system for the coefficients. For the primary wave this is a $(2J+3)\times(2J+3)$ complex system. The secondary wave however, requires using (3.4) and (3.5) for each u_n and v_n in the expansion (2.47). Thus a larger system of dimension $(N+1)(2J+3)\times(N+1)(2J+3)$ is produced. These algebraic systems are then solved numerically using Wielandt iteration.

3.1.2 Symbolic manipulation

In order to verify the equations derived during the problem formulation, MACSYMA, a computer algebra program, is used. Special attention is given to the nonlinear secondary instability equations. Beginning with (2.1) and (2.2) the scalar vorticity transport equations are calculated. These equations are then used to derive (2.32) and (2.33). Making the substitutions of (2.35) and (2.36) z and w are removed producing the Orr-Sommerfeld and Squire equations for u_{3_m} and v_{3_m}. From these equations two different checks are made. For the first check the velocities are immediately expanded in x following the form of (2.47). This gives a general expression for the nonlinear terms for an $(n\alpha,\nu\beta),(m\alpha,\mu\beta)$ interaction. This general expression is used in the numerical calculations.

The second check follows the derivation of the equations up to the construction of the algebraic system. Expanding the velocities u_{3_m} and v_{3_m} using (2.37) and (2.38) introduces the amplitudes $\hat{A}(t)$ and $B(t)$ into the equations. Time derivatives are then taken producing $d\hat{A}/dt$ and dB/dt terms. The Landau constants are then introduced by substituting (2.39) and (2.40).

Following this procedure two equations are created containing $\hat{A}$, B, and all the u and v velocities of (2.37) and (2.38). Collecting coefficients of $Be^{i\beta z}$ then yields (2.41) and (2.42). Likewise, collecting coefficients of $\hat{A}Be^{i\beta z}$ yields (2.43) and (2.44). Finally, collecting coefficients of B^2e^{i0z} yields (2.45) and (2.46).

For each pair of equations obtained by collecting coefficients, the Floquet analysis is carried out. The basic flow portion of the primary wave is first expanded as a Fourier series. Then substitution is made for the secondary velocities using the form of (2.47). Each velocity function is then approximated using (3.4) or (3.5). Collecting the terms multiplying the spectral coefficients c_k and d_k of the unknown secondary velocity, an algebraic system is constructed. This system is then transformed into Fortran code and solved. This provides a comparison for the general numerical algorithm.

3.2 Solution scheme

The perturbation scheme in conjunction with the numerical analysis yields the Landau constants and the corresponding functions at any given Reynolds number. The goal of the solution scheme is to convert this discrete information into a continuous evolution (temporal or spatial) of the disturbance field. Prescribing initial amplitudes and integrating the amplitude growth equations provides the building block for such a conversion. Having the various amplitudes and functions, the total disturbance field can be analyzed.

3.2.1 Two phase approach

The simplest scheme for calculating the amplitude growths as a function of R is based on a two-phase approach. This begins with the initial amplitudes for A^*, $\hat{A}$, and B, at some initial R. The first phase consists of calculating primary Landau constants and functions at a succession of R locations. Then, starting with the initial A^*, the basic flow portion of the amplitude is calculated at each R. In the second phase, the secondary and interaction constants and functions are calculated. Using the initial $\hat{A}$ and B, these amplitudes are then calculated at each R.

To solve for the primary wave, (2.14) and (2.15) are analyzed using the perturbation scheme disscribed in section 2.2. This scheme results in a family of velocity functions and the two Landau constants, a_0 and a_1, at each R. The Gaster transformation (Gaster 1962) allows the amplitude growth equation, (2.28), to be recast in terms of the independent variable R. The governing equation for the basic flow portion of the primary wave, A^*, becomes

$$\frac{dA^*}{dR} = \frac{2}{c_g} \left(A^* a_0 + A^{*3} a_1 \right) \quad , \tag{3.6}$$

where c_g is the group velocity, defined as

$$c_g = c_r + \alpha \frac{dc_r}{d\alpha} \quad . \tag{3.7}$$

This equation is integrated to project the amplitude, A^*, from one Reynolds number to the next, where the Landau constants are again evaluated.

With A^* and the primary wave functions at each R, the basic flow and perturbation functions, $\mathbf{v}_1^*$ and $\hat{\mathbf{v}}_1$, are calculated. Once A^* and $\mathbf{v}_1^*$ are known, the secondary wave functions and linear growth rate can be determined. The higher order interaction functions and constants are then calculated using this first order primary and secondary information. Having all the Landau constants, integration is carried out for $\hat{A}$ and B using

$$\frac{d\hat{A}}{dR} = \frac{2}{c_r}\left(\hat{A}\, a_A + \hat{A}^2\, a_{A^2} + \hat{A}^3\, a_{A^3} + B^2\, a_{B^2} - \hat{A}B^2\, a_{AB^2} \right) \tag{3.8}$$

and

$$\frac{dB}{dR} = \frac{2}{c_r}\left(B\, b_B + \hat{A}B\, b_{AB} + \hat{A}^2 B\, b_{A^2B} + B^3\, b_{B^3} \right) \tag{3.9}$$

respectively. These equations follow the form given by Bertolotti (1985) for the linear treatment of the secondary wave. He found this form of equation to be a lowest order approximation to the evolution equation derived from a spatial stability analysis.

After calculating the amplitudes A^*, $\hat{A}$, and B, as well as the various velocity functions, the composite functions can be calculated at each R. Evaluating the maxima of the norms then yields the physical amplitudes.

Following this simple approach the basic flow portion of the primary wave is totally unaffected by the presence of the secondary wave. If the effects of the secondary wave on the primary are small, any changes to the basic flow portion, A^*, can be neglected. However, if these effects are not small, neglecting them is a major shortcoming. To avoid this problem, a pseudo-marching scheme is used

which allows for the total primary wave to be effected by the secondary.

3.2.2 Pseudo marching scheme

The pseudo marching scheme is aimed at distributing the various resonance effects onto both A and B. In the early stages of the amplitude evolutions, the primary/secondary interaction is completely dominated by the parametric resonance. As the secondary amplitude grows, however, mutual resonance becomes increasingly more significant. To accommodate the changeover from the region of linear-parametric resonance to the region where mutual resonance is significant, the primary amplitude, A, is repeatedly split into A^* and $\hat{A}$ and recombined.

To begin, the primary amplitude, A, and the secondary amplitude, B, are specified at some initial R. In addition, the parameter $\Delta = \hat{A}/A$ is specified, from which $\hat{A} = \Delta A$ and $A^* = A - \hat{A}$ are calculated. Solving (2.14) and (2.15) following the perturbation scheme yields the constants and functions for the primary wave. With A^* as defined, the basic flow and interaction functions $\mathbf{v}_1^*$ and $\hat{\mathbf{v}}_1$ are calculated. The secondary and interaction functions and constants are then determined.

Having the complete set of Landau constants, the amplitude growth equations (3.6), (3.8), and (3.9) are integrated to determine A^*, $\hat{A}$, and B at the next R location. At this new location, the total primary amplitude is reevaluated, $A = A^* + \hat{A}$. Then the amplitude is again decomposed using $\hat{A} = \Delta A$ and $A^* = A - \hat{A}$, and the calculation procedure is repeated.

Following this scheme provides an avenue for modification of the basic flow amplitude, A^*. By modifying A^*, the secondary and interaction terms are also modified. The continual redistribution of A, between A^* and $\hat{A}$, takes advantage of the arbitrariness in this split. As long as $\hat{A}$ is small relative to A^*, the evolution of B will be independent of Δ. Since $\hat{A}$ must be small, the maximum distance between R locations is such that $\hat{A}$ does not change 'too radically' relative to A^*. In the regions of strong interaction the R spacing is cut in half if $\hat{A}$ goes below 10^{-5}, and the integration is repeated. Controlling the R spacing is an indirect way to control the rate of exchange between $\hat{A}$ and A^*, and thus between mutual and parametric resonance. All of the amplitude evolution information given in the results is based on the pseudo marching scheme.

4. Results

4.1 Effect of truncations

To facilitate a numerical solution of the final equations, each of the summations introduced is truncated to some finite value. The simplification due to truncation, however, is counteracted by the introduction of errors. Optimal cut off values are chosen to be the minimum values for which a 'reasonable' solution is obtained.

The first truncation considered is that of the Floquet system associated with the streamwise variation. Table 4.1 gives the values of the Landau constants a_A, b_B, and a_{B^2} for the subharmonic problem, with different cut offs. For the linear constant, b_B, a cutoff of $N= 1$ gives good results. The second order constant a_{B^2}, however, changes radically between $N= 1$ and $N= 3$. A further comparison shows $N= 3$ to be sufficient. The other second order constant b_{AB} behaves similar to b_B.

The second truncation considered is in the number of collocation points used. As shown in table 4.2 the first order constants rapidly converge when increasing the number of collocation points, J. The second order constants, however, show a peculiar dependence on J. This results from imposing the uniqueness conditions, $u_{AB}(y_0)= 0$ and $u_{B^2}(y_0)= 0$, at a particular collocation point. As J changes the relative y positions of the collocation points change. Thus the exact position, y_0, where the uniqueness condition is imposed depends

on J and causes slight variations in the second order constants. Since the position y_0 is arbitrary, the real effect of the variation is a redistribution of the growth between the constants and the functions. As long as J is kept fixed for a given run, these variations pose no problem. In light of the preliminary nature of this analysis, a value of $J = 20$ is sufficient.

The third truncation, which is more closely related to the physics. is the order of the primary wave. This is a control over the amount of primary wave self interaction that is considered. By carrying the expansion to third order modifications to the disturbance velocity function and growth rate are determined. As established earlier these modifications are small for the amplitudes of interest (Herbert 1975; Orszag and Patera 1983). The third order Landau constant a_1 is calculated to be $O(1)$. Since these modifications are small in comparison to the radical effects of the primary/secondary interaction, they are neglected.

Contained in the second order self interaction are the mean flow distortion and the second harmonic. Table 3 shows the effect of these second order corrections on the secondary and interaction constants b_B, b_{AB}, and a_{B^2}. Since the effect on these constants is only about one percent, the primary self interaction is neglected in further calculations. A further impetus for neglecting these effects is the inability to calculate the mean flow distortion at a Reynolds number past R_{II}. The governing equation for the mean flow distortion is simply that of a forced harmonic oscillator. In the absence of forcing (i.e. the primary wave) the mean flow distortion should be zero. For the case $a_0<0$, however, the equation

admits a homogeneous solution which is nonphysical. For a further discussion of this problem see Herbert (1983) or Davey and Nguyen (1971).

The remaining truncations to be considered are for the spanwise Fourier series and for the perturbation order of the interaction. As described in section 2.3.2 these truncations are not independent. In particular, for a given order there is an appropriate number of spanwise harmonics to consider. The majority of the calculations are carried out to second order. At third order, some qualitatively different processes are captured. For the specific investigation of these processes the calculations are extended to third order.

4.2 Landau constants

The first and most fundamental results to be considered are the values of the Landau constants. A detailed description of the meaning of each constant is given in section 2.5. Numerical results are now presented which provide the framework for understanding the particulars of the amplitude evolutions. The major focus of this investigation is on the first- and second-order interactions. These interactions capture the most significant features in the growth of the disturbances.

Although the first order results show the subharmonic and fundamental modes to be very similar, at second order there are significant differences between these modes. Because of these differences the results are given in two parts: first for the subharmonic mode, and then for the fundamental.

4.2.1 Subharmonic mode

Following the pseudo-marching scheme the effects of the interaction are extended over the whole primary amplitude A. Since A^* changes during the course of interaction the constants also 'feel' the effect. To understand the evolution of the amplitudes the variation of the constants with respect to R must be considered. Figure 4.1 shows this variation for the subharmonic mode at $F = 124$ and $b = 0.33$, where F is the dimensionless frequency defined by $F = 10^6\, 2\pi f\nu / U_\infty^2$ and b is a fixed dimensionless wave number $b = 10^3\, \beta / R$. The initial amplitudes for figure 4.1 are such that there is a strong primary/secondary interaction beginning at R=640. At this Reynolds number A and B are approximately the same magnitude.

Beginning at R=510 the first order constant a_A is positive, but diminishing in size. At R_{II}=606 the sign changes and the magnitude then increases, unaffected by the interaction. The second order constant a_{B^2} starts out large and negative. Prior to the strong interaction at R=640 its magnitude is increasing. Once the interaction begins its magnitude diminishes rapidly until there is a sign change whence it begins to grow. This sign change produces novel results, which are discussed in section 4.3.

The first order constant b_B begins with a positive magnitude and remains positive throughout the interaction. Initially its magnitude is increasing but the interaction results in a drop in the magnitude, after which it again increases. The second order constant b_{AB} is also positive over the entire range of R. When the magnitude of b_B decreases the magnitude of b_{AB} increases. The changes in

both of these constants are related to changes in A^*.

Another display of the Landau constants as a function of R is given in figure 4.2. This is also for the subharmonic mode, but at F=137 and b=0.40. In this case the primary/secondary interaction is weak, owing to the low amplitudes at which the interaction occurs. The decay and change in sign of both b_B and a_{B^2} are due to the variation of A^*. Unlike figure 4.1, however, this A^* variation is dominated by the first order growth rate a_A.

For cases in which a strong interaction occurs the most dramatically affected constant is a_{B^2}. Once the interaction begins, radical changes occur over a relatively short R distance. This behavior, as well as the weak interaction behavior, can be best understood in terms of the dependence on A^*.

The variation of the Landau constants with A^* is presented in figures 4.3, 4.4, and 4.5. In figure 4.3 the conditions are F= 124 and b= .33 and the fixed Reynolds number location is R= 580. This is before R_{II} so that a_A is positive. The value of a_A does not depend on A^* since only a first-order primary self-interaction is being considered. The second order constant a_{B^2} is positive for small A^* and negative for large A^*. The sign change occurs at $A^*\approx$.275%. Except for a narrow region around this A^* the magnitude of a_{B^2} is quite large. This suggests that the B^2 effects will be strong as long as A^* is away from $A^*\approx$.275%. The implications associated with this constant are discussed in section 4.3. The first order constant b_B is positive and large with respect to a_A. For small amplitudes, $A^*<$.25, the value of b_B rapidly drops toward zero. Thus for smaller values of A^* the subharmonic is not energized by the presence of the

finite amplitude TS wave. Once the amplitude A^* exceeds some threshold, however, the subharmonic shows strong growth. The constant b_{AB} is large and positive for all A^*. Since this constant monitors the change in b_B with respect to A^* its behavior is somewhat predictable. As b_B drops rapidly below $A^*= .25$ the value of b_{AB} increases.

Using the same conditions, figure 4.4 gives the Landau constant variations at $R= 610$. The general behavior of the constants is unchanged. However, since $R= 610$ is just past $R_{II}= 606$, the linear constant a_A is now small and negative. In fact the magnitude of a_A is below 10^{-4}, so it does not appear in the figure. The constant b_B is larger and the threshold for $b_B>0$ occurs at a smaller value of A^*. Also affected by R, is the A^* location at which a_{B^2} changes sign. This here occurs at $A^*\approx.305$.

Finally figure 4.5 shows the variation of the Landau constants with respect to A^* for the conditions $a= .21$ and $b= .14$ and $R= 900$. The variable a is a fixed nondimensional streamwise wave number $a= 10^3\,\alpha/R$. Again the behavior of each constant is much the same as in figures 4.3 and 4.4. with some additional detail for small A^*. These Landau constant variations are seen as typical for the subharmonic mode to transition.

4.2.2 Fundamental mode

Following the line of discussion for the subharmonic, the variation of the Landau constants with respect to R is first considered. Figure 4.6 shows these variations for the conditions $F= 64.4$ and $b= .44$. At a Reynolds number $R\approx770$,

the primary and secondary amplitudes are of the same magnitude, producing strong interaction.

Since this range of R is well before R_{II}, the constant a_A is positive and increasing in magnitude. The constant a_{B^2} begins large and negative at R= 675. Initially its magnitude is decreasing, but it then begins to increase at $R\approx$700. This increase is continued to the point of strong interaction. where the magnitude begins to decrease once again. Unlike the subharmonic mode, no sign change occurs for a_{B^2}. In contrast to a_{B^2}, the constants b_B and b_{AB} behave just as for the subharmonic case. However, the explanation for their behavior is quite different.

Figure 4.7 shows the variation of the constants for the conditions F= 124 and b= .33. Unlike the case of figure 4.6, the primary/secondary interaction occurs past R_{II}. The constant a_A begins positive, but changes sign at R_{II}= 606. The constant a_{B^2} begins large and negative and increases in magnitude up to the point of strong interaction, $R\approx$650. Its magnitude then decreases followed by a rapid increase. Like the case of figure 4.6, the sign of a_{B^2} remains negative. The dramatic changes of a_{B^2} in figures 4.6 and 4.7 can be explained in terms of the variation of A^*.

Initially the constant b_B is positive and increasing in magnitude. Once a strong primary/secondary interaction occurs, the magnitude drops rapidly toward zero. The second order constant b_{AB}, while remaining positive, undergoes a decrease followed by an increase in magnitude. After the occurrence of the strong interaction there is a jump in the magnitude accompanied by a sign

change. This singular behavior occurs at a small A^* value, and is discussed in section 2.3.2.

To understand the details of figures 4.6 and 4.7 the dependence of the constants on A^* must be investigated. Figure 4.8 shows the Landau constant variation as a function of A^*, for the conditions F= 64.4 and b= .44. The constant a_A is positive with a fixed magnitude. The second order constant a_{B^2} is large and negative for small amplitudes, $A^*<1\%$. As A^* increases the magnitude of a_{B^2} rapidly decreases, and then gradually increases. Note however, that the sign of a_{B^2} remains negative for all A^*. Again the behavior of b_B and b_{AB} is just as for the subharmonic case.

Figure 4.9 is another plot of the Landau constant variations, but for the conditions F= 124, b= .33, R= 610. The constant a_A is not shown since its magnitude is below 10^{-4}. The constants a_{B^2} and b_B vary similarly to the case for figure 4.8. At a value of $A^*\approx.7$ the constant b_{AB} drops in magnitude signifying a reduction in the rate of decline of b_B with decreasing A^*. This b_{AB} behavior is unique to the fundamental mode.

4.3 TS equilibrium amplitude

By allowing the resonant interaction to influence the total TS wave through the continued amalgamation and resplitting of A^* and $\hat{A}$, dramatic variations in the wave amplitude are captured. Of particular interest is the damping effect of the secondary amplitude B on A, through the B^2 resonance. This is characterized by a large negative Landau constant a_{B^2}. When this

damping is counterbalanced, an 'equilibrium' state is obtained. Setting the primary-amplitude growth equations to zero yields

$$A_e \approx -\frac{a_{B^2}}{a_A} B^2 \ , \tag{4.1}$$

for a second order interaction. Since $dB/dt \neq 0$, this is not a true equilibrium state. but rather is slowly varying.

4.3.1 Subharmonic mode

During the amplitude evolution for the subharmonic mode, a strong interaction occurs when A and B are approximately of the same magnitude. This results in a radical decay in A, tending to zero within 30–40 Reynolds numbers. The reason for this decay is the large negative Landau constant a_{B^2}. Before the amplitude A goes to zero, however, the sign of a_{B^2} changes. This can be seen in figures 4.3, 4.4, and 4.5. As a result of this sign change the decay is stopped and the amplitude takes on the value A_e.

Figure 4.10 shows the evolution of A^* and B resulting in an equilibrium amplitude A_e. Using different initial amplitudes for B, the location of the strong primary/secondary interaction is shifted. As a result, the rate of decay of A^* is changed. In each case the final equilibrium amplitude is approximately the same. The insensitivity of A_e to the magnitude of B^2 is due to rate of change of a_{B^2} near $a_{B^2} = 0$. There is a narrow 'band' of A^* around $a_{B^2} = 0$ overwhich a_{B^2} goes from a large positive to a large negative value (see for example figure 4.4). The A^* component of the equilibrium amplitude falls within this

narrow band. Once the primary amplitude takes on an equilibrium value its destiny is controlled by the secondary amplitude.

4.3.2 Fundamental mode

Like the subharmonic mode, the strong primary/secondary interaction occurs when the magnitudes of A and B are roughly the same. However, the response of the primary wave is significantly different. Initially the primary amplitude decays rapidly. Since the a_{B^2} Landau constant remains negative as A^* goes to zero, the decay can only be arrested by a large positive a_A. Figure 4.11 shows the evolution of A^* and B for conditions in which a_A is large and positive. In this case the primary amplitude decays to A_e, and then varies slowly.

Figure 4.12 is a case in which a_A is negative (past R_{II}). Under such conditions the primary wave is driven to zero. This results in a leveling off of B due to the lack of A^* forcing. These results suggest that the fundamental type breakdown must be initiated before R_{II}. In addition, lower frequencies with larger growth rates a_A are more susceptible to fundamental (K-type) breakdown. For the case of figure 4.12, as $A^* \rightarrow 0$ the $\mathbf{v}_{B^2}$ function becomes exceptionally large indicating the need to consider additional modes.

4.4 Amplitude growth curves

Having examined the evolution of A and B, attention is now focused on the total disturbance field and the physical amplitudes. By following a wave interaction approach to transition, disturbance characteristics are cast in terms

of amplitudes and functions. These features are directly measurable in experiments and thus provide a window for comparison. Due to the differences in the Landau constants, the subharmonic and fundamental modes are examined separately.

4.4.1 Subharmonic mode

The key to understanding the progression of the physical amplitudes lies in the interrelationship of the various amplitude components. Figure 4.13 shows how these components evolve with Reynolds number for the conditions F= 124, b= .33. As described in section 4.3.1 the secondary amplitude B forces the primary amplitude $A = A^{*} + \hat{A}$ to an equilibrium value. through the B^2 resonance. Simultaneous with the decay of A the secondary growth rate b_B is reduced. This results in a change in the slope of B versus R. Once A settles to the slowly varying equilibrium value, the slope of B versus R becomes almost constant. The composite amplitude $||u_{2D}||_{max}$ is initially equivalent to $A = A^{*} + \hat{A}$. After B crosses A the component $B^2 u_{B^2}$ becomes increasingly dominant. The net effect of the primary/secondary interaction on $||u_{2D}||_{max}$ is thus: an initial reduction due to the decay of A and then a rapid 'liftoff' from the linear solution, due to the presence of the B^2 function. The development of $||u_S||_{max}$ follows closely that of B. The reason for such an observable distinction is that B does not represent the maximum in the u_B profile, but rather the magnitude of u_B at y_0.

A comparison is given in figure 4.14 of the linear and nonlinear amplitude evolutions for the conditions of F= 124 and b= .33. The principle effect of the nonlinearity is to cause $||u_{2D}||_{max}$ to 'dip' and then 'liftoff', and to cause a

reduction in the growth of $||u_S||_{max}$. Figures 4.15 and 4.16 give similar comparisons for the conditions F= 137, b= .40 and F= 82.7, b= .129, respectively. In total, these figures show the general effects of nonlinearity for the subharmonic mode.

In the development of this method the primary amplitude A was arbitrarily split into A^* and $\hat{A}$. The size of the split is defined by the parameter $\Delta = \hat{A}/A$. This split allows for the capture of the nonlinear primary/secondary interaction through the pseudo marching scheme. If the split is truly arbitrary, the results should be virtually independent of Δ and should converge to a fixed solution as $\Delta \rightarrow 0$. Figure 4.17 shows the development of $||u_{2D}||_{max}$ and $||u_S||_{max}$ for different values of Δ. The changes are small and decrease in size as Δ becomes smaller.

Now that the general interaction characteristics have been assessed, comparisons are made to experimental results. The first case considered is for the conditions F= 124 and b= .33. Figure 4.18 shows the theoretical curves with the experimental points of Kachanov and Levchenko (1984). The initial amplitudes were chosen to provide the best linear agreement in the neighborhood of the interaction. This is done as an attempt to isolate the interaction region for a more clear comparison. The agreement is somewhat improved from that of the linear theory given by Herbert (1984a). In particular, the dip in $||u_{2D}||_{max}$ yields a closer fit.

The second case considered is for the conditions F= 137 and b= .40. The experimental data are also from Kachanov and Levchenko (1984). Unfortunately no spanwise wave number is given for their F= 137 results. For an estimate, the values for F= 109 and F= 124 are used to extrapolate a possible value

at $F = 137$. The principal effect of using a different wave number is the change in the linear secondary growth rate b_B. In order to isolate the interaction region for comparisons the experimental points are shifted in R. This is to minimize variations due to unpredictable effects such as; nonparallelism, pressure gradients, and the virtual leading edge. The size of the shift is chosen to be $R = -10$, based on a match up of theory and experiment for an isolated TS wave (see figure 4.19). These results are for small initial amplitudes.

Increasing the initial TS amplitude results in the development of a secondary wave, figure 4.20. The amplitude of the secondary never becomes large enough to allow a strong primary/secondary interaction. Therefore, both waves harmlessly decay as shown by both theory and experiment. A yet larger initial TS amplitude produces significant secondary growth as seen in figure 4.21. For these conditions a strong interaction does occur as conferred by both theory and experiment. Agreement seems good, but the theory predicts a stronger 'liftoff' of the two-dimensional wave. The last comparison for this case is given in figure 4.22. A high initial TS amplitude produces strong secondary growth and strong interaction. For the two-dimensional amplitude the agreement is good but the experiment shows a larger 'dip' before the 'liftoff'. The weaker agreement for the subharmonic may be the result of a mismatch in the spanwise wave number which would produce a different linear growth rate.

The third comparison is for the case $F = 82.7$ and $b = .129$. Figure 4.23 shows the theoretical curves with the data points of Corke and Mangano (1987). Again the initial amplitudes were chosen to provide good linear agreement in

the region of interaction. During these calculations a singularity occurred due to the similarity in shape of $\mathbf{v}_B$ and $\mathbf{v}_{AB}$, as described in section 2.3.2. Therefore, the AB constant and function are not part of this solution. The agreement for the two-dimensional wave is fair. The experimental data do not show a 'dip' or a very large 'liftoff'. The agreement for the subharmonic is very good all the way to breakdown. The nonlinear shift in the rate of growth of $||u_S||_{\max}$ is consistent with the data.

The final case for comparison is $F = 93$ and $b = .174$, given in figure 4.24. The experimental data are from Corke and Mangano (1987). Agreement for the two-dimensional wave is poor. Although the data are taken past R_{II} the experiment does not show a decay in $||u_{2D}||_{\max}$. Rather, the data show some gradual increase throughout the region. The subharmonic agreement is fair, up to breakdown.

In addition to the experimental comparisons, the results are evaluated for the conditions of the numerical simulations of Spalart and Yang (1987). Their simulations involved a two-dimensional wave and the simultaneous growth of the subharmonic and fundamental modes. The qualitative agreement is good, but the theory predicts the two-dimensional 'liftoff' at an earlier point in the evolutions. This seems to be a result of considering only single modes. The presence of a fuller spectrum allows for a broader transfer of energy, which tends to weaken the growth of individual modes.

4.4.2 Fundamental mode

Unlike the subharmonic mode, the occurrence of a strong interaction does not foretell breakdown for the fundamental. Only when the first order growth rate a_A is substantially large will a breakdown be triggered. Figure 4.25 shows the evolution of the different amplitude components for the conditions F= 64.4, b= .44. The amplitude A is driven to A_e by the strong interaction beginning at $R\approx765$. The reduction in A results in a decrease in the secondary growth rate b_B.

The two-dimensional physical amplitude $||u_{2D}||_{max}$ experiences a 'liftoff' from A due to the $B^2u_{B^2}$ component. The corresponding function u_{B^2} is quite large which explains why $||u_{2D}||_{max}$ is larger than $A-B^2$. The three-dimensional amplitude $||u_F||_{max}$ falls on top of B. This results from B being a measure of u_B at y_0 and the maximum of $||u_S||$ also occurring at y_0. Given in figure 4.26 is a comparison of the second order results with the linear theory. The most dramatic variation is nonlinear liftoff of $||u_{2D}||_{max}$. Under such conditions $||u_{2D}||_{max}$ remains larger than $||u_F||_{max}$.

Perhaps an easier way to assess the results for the fundamental mode is in terms of the peak and valley variations. Figure 4.27 gives the results of figure 4.26 recast in terms of peak and valley. The effect of the nonlinear interaction is to produce stronger initial growth in the peak and a more radical increase in the valley.

Finally a comparison is given in figure 4.28 to the experimental results of Cornelius (1985). Agreement for the peak curve is good up to $R\approx776$. This is

where high frequency spikes were first observed for the conditions $F = 64.4$, $b = .21$. Although agreement is good early on, the valley variation seems to be qualitatively different past $R \approx 770$. This might well be a result of spikes, which cause variations in the disturbance levels for the outer portion of the profiles. Another source of variation could be the 'artificially' high level of three dimensionality in the experiment due to the 'spacers' under the forcing ribbon.

4.5 Velocity functions

In conjunction with the amplitude curves, the velocity functions provide a detailed sketch of the disturbance field produced by wave interactions. Variations across the boundary layer are captured in the form of functions multiplied by appropriate amplitudes. These are calculated at each R location with their respective constants. Characteristics of these functions provide an explanation for the evolution of the composite functions, which would be observable in experiments.

4.5.1 Subharmonic mode

In the early stages of the strong interaction the major changes in the composite velocity functions are due to amplitude changes. Since the amplitudes play the role of 'weighting parameters', a rapid change in amplitude produces a restructuring of the velocity field. As the strong interaction progresses, however, the independent functions are affected via A^*.

Figure 4.29 shows the independent functions u_A, u_{B^2}, u_B, and u_{AB} at $R = 580$

for the conditions F= 124, b= .33. The first function u_A is simply the TS wave profile. The second function u_{B^2} is produced by the B^2 resonance of the three-dimensional field with the two-dimensional field. This function has three local maximums; one below the critical layer, one just above the critical layer, and another well outside the critical layer near the outer TS maximum. The third function u_B is the linear subharmonic function. Finally, u_{AB} is the function produced by the $\hat{A}$ variation in the primary wave. This function is fuller than u_B and has a higher maximum. Figures 4.30 - 4.33 present these functions at different R locations through the interaction region. The first order functions u_A and u_B remain virtually unchanged. Meanwhile u_{B^2} undergoes changes toward a fuller profile with a single peak. The function u_{AB} progresses toward the shape of u_B.

Using the independent velocity functions and the amplitude growth curves the total composite functions are constructed. Given in figures 4.34, 4.35, and 4.36 are a sequence of functions u_{2D} for the total two-dimensional velocity field. Initially at R= 630. the function looks like the TS wave profile. As the strong interaction takes place (see figure 4.16) the function is transformed into the characteristic 'bell shape' (Kachanov, Kozlov, and Levchenko 1977). The net effect is a movement of the large amplitude modulations from $y\approx0.6$ to $y\approx1.5$. Over this same region of interaction, R= 630–680, the subharmonic function u_S goes virtually unchanged, as is substantiated by figure 4.37.

A comparison is given in figures 4.38 and 4.39, to the experiment of Kachanov and Levchenko (1984). The two-dimensional profile of figure 4.38

shows good agreement, with some deviations near $y = 0$. The subharmonic profile of figure 4.39 matches very well. However, these two profiles are at $R = 608$ which is before the region of strong interaction.

4.5.2 Fundamental mode

As described in section 4.3.2, the fundamental mode may follow one of two scenarios, interaction leading to breakdown or interaction leading to decay. In either case the functions are basically the same. Attention here is restricted to the conditions $F = 64.4$ and $b = .44$, for which breakdown occurs.

The functions u_A, u_{B^2}, u_B, and u_{AB}, given in figure 4.40 for $R = 725$, look very similar to the subharmonic functions for $R = 580$ (figure 4.29). The development of the functions with R, however, is significantly different as seen in figures 4.40, 4.41, and 4.42. The function u_{B^2} maintains the three local maximums, but the global maximum moves from the middle to the innermost of these. The function u_{AB} changes only slightly for these conditions. The variation of the first order functions u_A and u_B is small, as for the subharmonic.

The composite functions, constructed from amplitudes and the independent functions, are of the form u_P and u_V. Figures 4.43 and 4.44 contain a sequence of peak functions at different R locations. Initially the function shape is similar to the TS wave. Moving downstream the maximum shifts outward and the profile becomes more compact. Given in figures 4.45 and 4.46 is a sequence of corresponding valley functions. The first function given is a mildly distorted TS profile. This gives over to a function containing three local maximums. The

function then becomes 'fuller' again from which a new maximum arises.

Finally, a comparison is given between the composite functions u_p and u_V and the experimental data of Cornelius (1985). The calculated functions correspond to the conditions of figure 4.28. The first three comparisons are for the peak functions at R= 716, 735, and 755. These are given in figures 4.47, 4.48, and 4.49, respectively. The agreement is good for R= 716 and R= 735. At R= 755 the experiment shows larger values on the outer portion of the profile. This may be related to the occurrence of spikes. For the same R locations the valley functions are given in figures 4.50, 4.51, and 4.52. These show very good agreement between the theory and experiment. In total. these comparisons offer strong support for the theoretical treatment of this problem.

5. Conclusions

5.1 Appraisal of the approach

The principal aim of this work is to provide some understanding and explanation of the primary/secondary interaction in boundary layers. The strong agreement between theory, experiment, and simulation have established the parametric origins of the secondary. Under some conditions the assumptions of the parametric approach seem well justified (Herbert 1984a). However, when the amplitude of the secondary becomes large a mutual interaction must be permitted. In such a case a purely mutual interaction would lose the secondary altogether, resulting in the interaction of multiple primary waves. The alternative approach, given here, maintains the parametric secondary wave while permitting modifications to the primary wave.

The pseudo marching scheme, in conjunction with the perturbation method, provides a continuous transition from the purely parametric to the purely mutual interaction. Based on the agreement with experiments and simulations this method seems to capture the significant physics of the problem. Experimental comparisons show good agreement up to breakdown, where the amplitudes are in excess of 6% for the subharmonic (Corke and Mangano 1987) and 10% for the fundamental (Cornelius 1985). The assumptions made appear to be justified and not overly strong.

Perhaps the greatest value in this approach comes from the ability to

decompose the flow field. This decomposition has provided new insights unobtainable in experiments and simulations. These insights provide, for the first time, a physically-based transition criteria.

5.2 Conditions for breakdown

The results of this study provide new scenarios for the early stages of transition. These contain a simple set of parameters which can be monitored to detect the onset of breakdown.

The early transition process begins with the onset of the two-dimensional wave. This wave then evolves within a virtually two-dimensional framework. Given the frequency and an initial amplitude the wave development is fixed. For significantly large initial amplitudes the two-dimensional wave gives rise to a three-dimensional secondary wave. This is characterized by the first occurrence of a positive growth rate b_B at some initial conditions $(R_{1,} A_1)$. From this point the two- and three-dimensional waves undergo simultaneous evolution. Very simply stated, the first stages of transition are:

(a.) Onset of two-dimensional wave growth (at R_1).

(b.) Linear and nonlinear evolution of the two-dimensional wave.

(c.) Onset of three-dimensional wave growth (at R_1, A_1)

(d.) Simultaneous growth of the two- and three-dimensional waves.

Thus far no distinction has been made between the subharmonic and fundamental modes.

Beyond step (d.) the different modes must be considered separately. This

results from the different behaviors of the Landau constants once a strong primary/secondary interaction occurs. For the subharmonic mode this interaction is always favorable to sustained growth and, therefore, leads to breakdown. Alternatively, the strong interaction is destructive for the fundamental mode, requiring a significant linear-primary growth rate to initiate breakdown.

The first discussion is for the subharmonic mode. After a period during which the primary and secondary grow together, the process is characterized by one of three cases. Two of these lead to breakdown while in the other the waves die out. The first case for the subharmonic mode may be summarized as follows:

(1e.) The magnitude of B becomes the same order as A before R_{II}.

(1f.) Growth of the primary amplitude becomes dominated by B, through the B^2 resonance.

(1g.) The secondary amplitude B continues to grow while the two-dimensional field becomes increasingly B^2 dominated.

(1h.) This new disturbance field gives rise to high frequency fluctuations and breakdown.

If the primary begins to decay before it is affected by the secondary, case two or case three will occur. In case two, only step (e.) is altered and breakdown is still the final outcome.

(2e.) The primary reaches R_{II} and begins to decay. Before A falls below A_2 the secondary amplitude B reaches the magnitude of A. The amplitude A_2 represents the value at which b_B goes negative and B begins to decay.

Steps (f.), (g.), and (h.) are as in case one. For the third case conditions are not sufficient for breakdown. This is given by the sequence:

(3e.) The primary reaches R_{II} and begins to decay.

(3f.) The amplitude A falls below A_2 before B reaches the magnitude of A, resulting in the decay of B.

(3g.) Both waves die out without leading to breakdown.

The fundamental mode is also characterized by three distinct sequences beyond step (d.). Only one of these contains the strong mechanisms which seem to precede breakdown. The first case for the fundamental mode is given by:

(1e.) The magnitude of B becomes the same order as A before R_{II}.

(1f.) A strong linear growth rate a_A balances the destructive effects of B.

(1g.) The secondary amplitude B continues to grow while the two-dimensional field becomes increasingly B^2 dominated.

(1h.) This new disturbance field gives rise to high frequency fluctuations and breakdown.

This is the only case for the fundamental mode which leads to breakdown. A necessary condition for the fundamental-type breakdown is that the initial amplitudes be large enough to initiate breakdown before R_{II}. This is not sufficient, however, as seen by the second case.

(2e.) The magnitude of B becomes the same order as A before R_{II}.

(2f.) A weak linear growth rate a_A allows B to suppress A.

(2g.) Growth of the secondary is terminated.

(2h.) Both waves die out without leading to breakdown.

Another alternative for the fundamental mode is given by:

(3e.) The magnitude of B becomes the same order as A after R_{II}.

(3f.) The secondary B accelerates the decay of the primary A.

(3g.) Growth of the secondary is terminated.

(3h.) Both waves die out without leading to breakdown.

Simply stated, a general guideline for the initiation of breakdown can be understood in terms of the relative amplitudes of the primary and secondary waves. When these amplitudes are approximately the same size a strong resonance interaction occurs between the two waves. Conditions which produce continued wave growth under this interaction give rise to breakdown. Once self sustained growth is established the primary amplitude remains virtually constant. This primary amplitude provides the forcing for the continued growth of the secondary wave. The observed energy increase in the two-dimensional field is due to an increasing B^2 component.

Table 4.1 Effect of the Floquet truncation on the Landau constants for the subharmonic mode with $F = 124$, $b = .33$, $J = 40$, $A^* = .00548$ and $R = 450$.

Effect of Floquet Truncation			
N	a_A	b_B	a_{B^3}
1	.00122444	.00159870	−.02952737
3	.00122444	.00160910	−.01997401
5	.00122444	.00160911	−.01988331

Table 4.2 Effect of the number of collocation points on the Landau constants for the subharmonic mode with F= 124, b= .33, N= 3, A^*= .00548 and R= 450.

Effect of Number of Collocation Points			
J	a_A	b_B	a_{B^2}
20	.00121755	.00161445	−.0220841
40	.00122444	.00160910	−.01997401
60	.00122444	.00160799	−.02060788
80	.00122444	.00160755	−.02092833

Table 4.3 Effect of the order of the primary wave on the Landau constants for the subharmonic mode with $F = 124$, $b = .33$, $N = 3$, $J = 40$. The secondary and interaction constants are calculated at different Reynolds number locations, based on a first and second order primary wave.

Effect of Primary Wave Self Interaction					
R	Order of Primary	a_A	b_B	b_{AB}	a_{B^2}
450.76	1st	.00122444	.00161430	.31482046	−.01968543
	2nd	.00122444	.00160910	.31565655	−.01997409
500.76	1st	.00149266	.00417646	.27878575	−.03826735
	2nd	.00149266	.00414546	.28411203	−.03841012
550.76	1st	.00115998	.00695070	.35201577	−.07436246
	2nd	.00115998	.00689253	.35690273	−.07358806
600.76	1st	.00015128	.00923526	.41758746	−.11429141
	2nd	.00015128	.00919522	.43103286	−.11319302

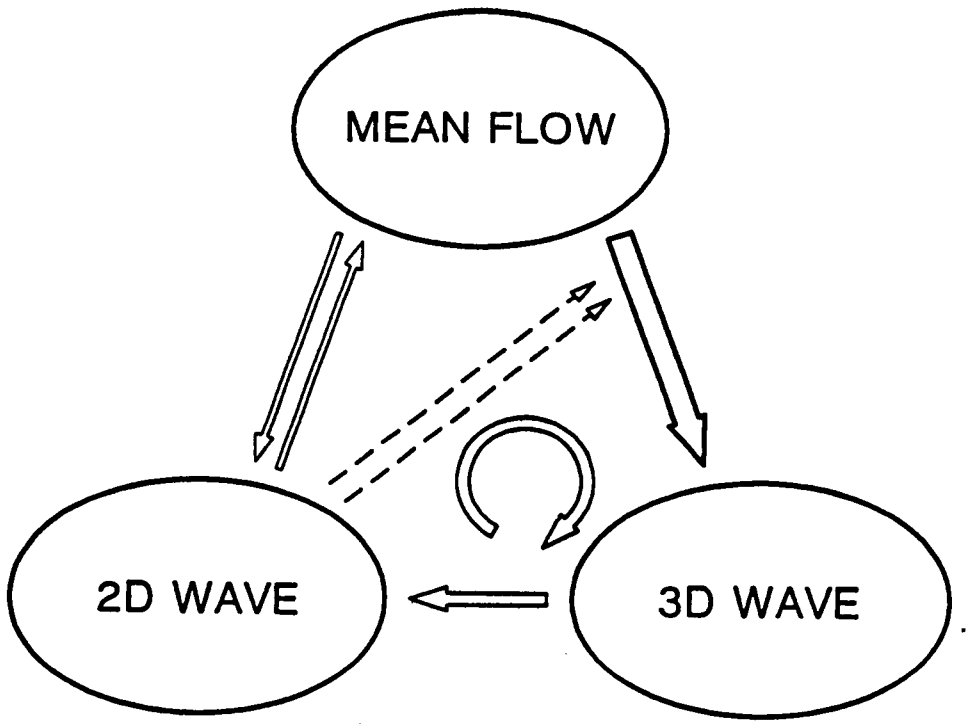

Figure 1.1 Schematic of energy transfer between the mean flow and the two- and three-dimensional waves. The dashed line signifies a catalytic effect. Taken from Herbert (1988a).

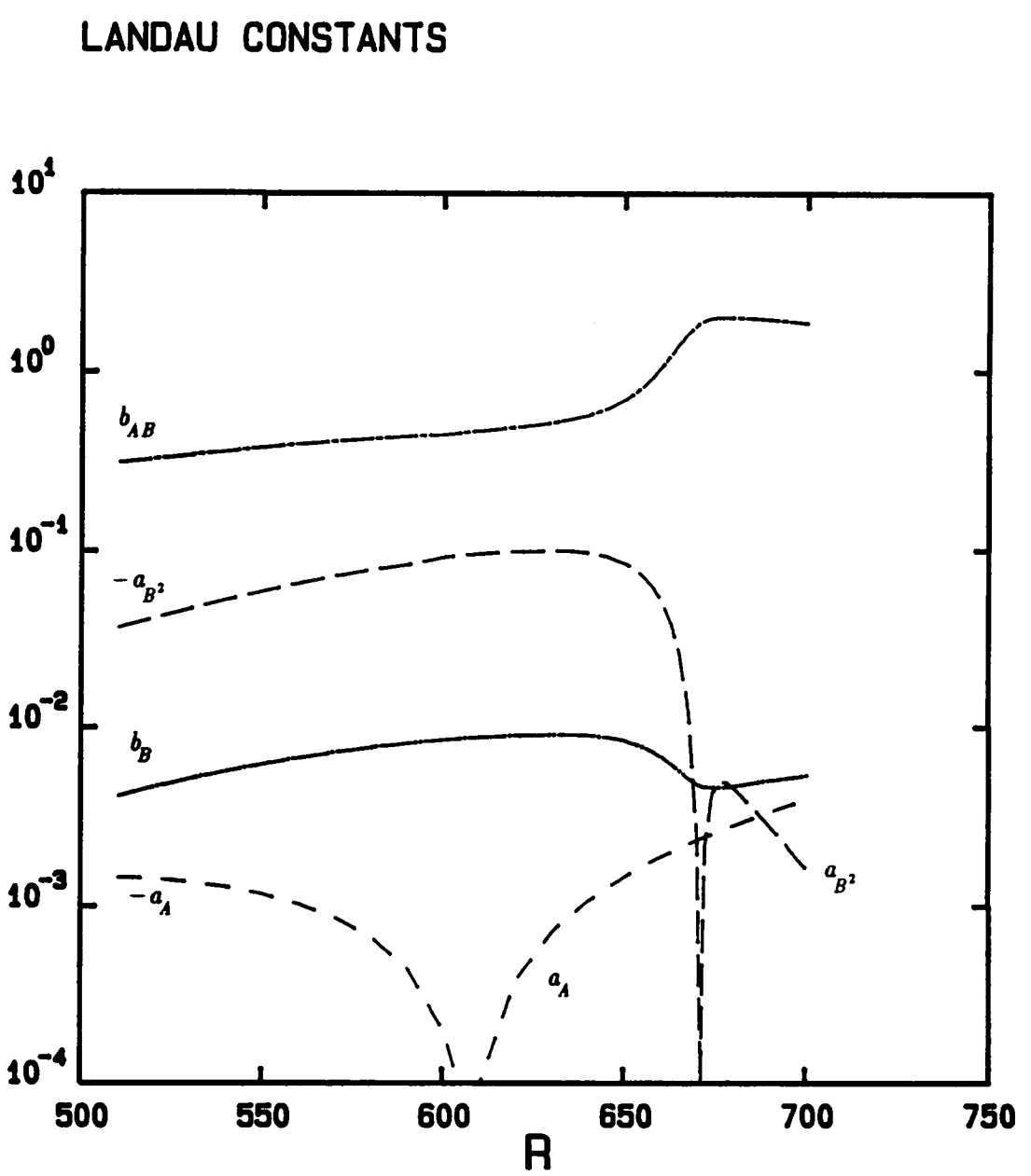

Figure 4.1 Variation of the Landau constants with Reynolds number. Results for the subharmonic mode at $F = 124$ and $b = .33$ with variable amplitudes. Initial values are $A = .00782$, $\Delta = .1$, and $B = .000053$ at $R = 510$.

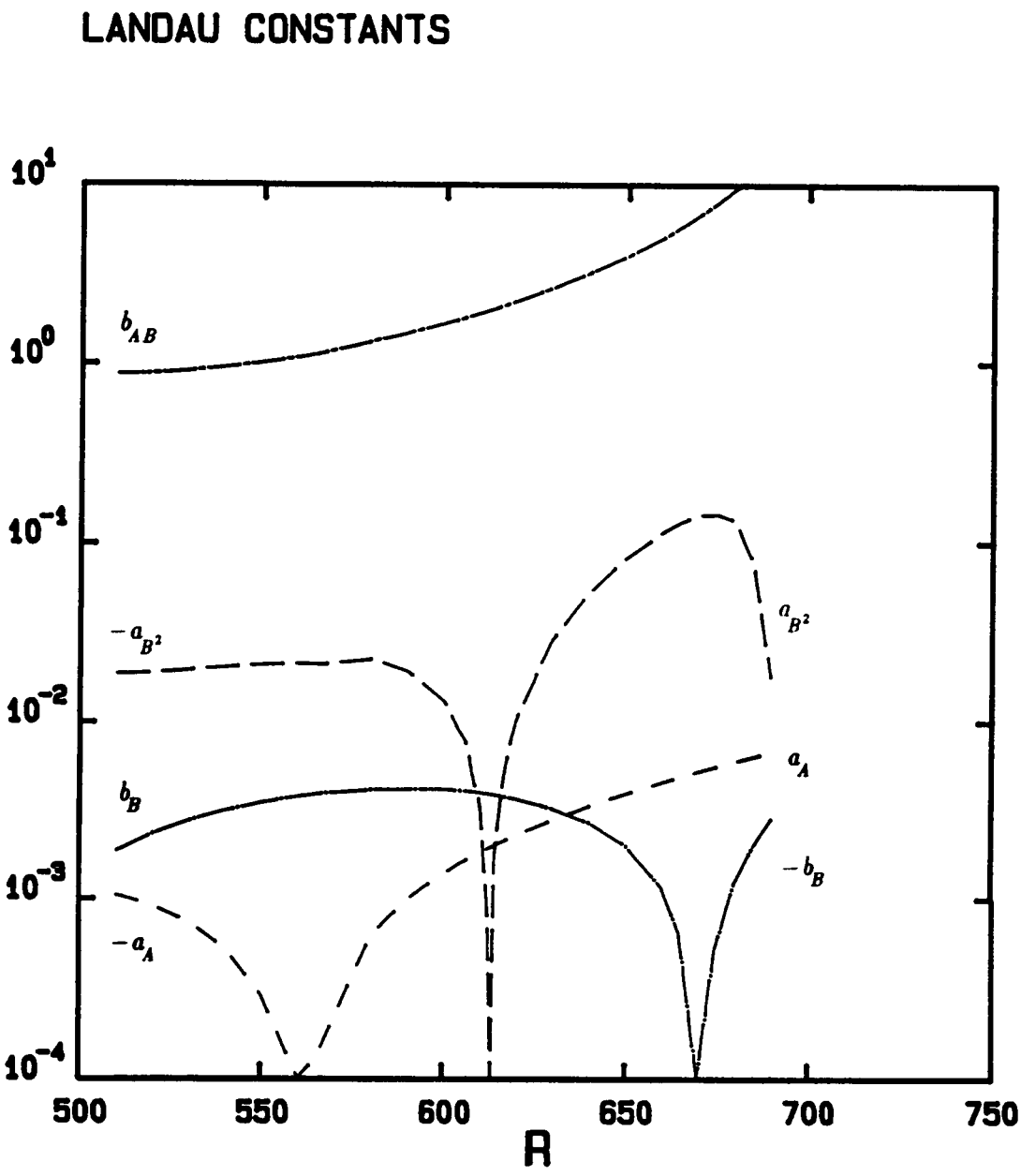

Figure 4.2 Variation of the Landau constants with Reynolds number. Results for the subharmonic mode at $F = 137$ and $b = .40$ with variable amplitudes. Initial values are $A = .004$, $\Delta = .05$, and $B = .000025$ at $R = 510$.

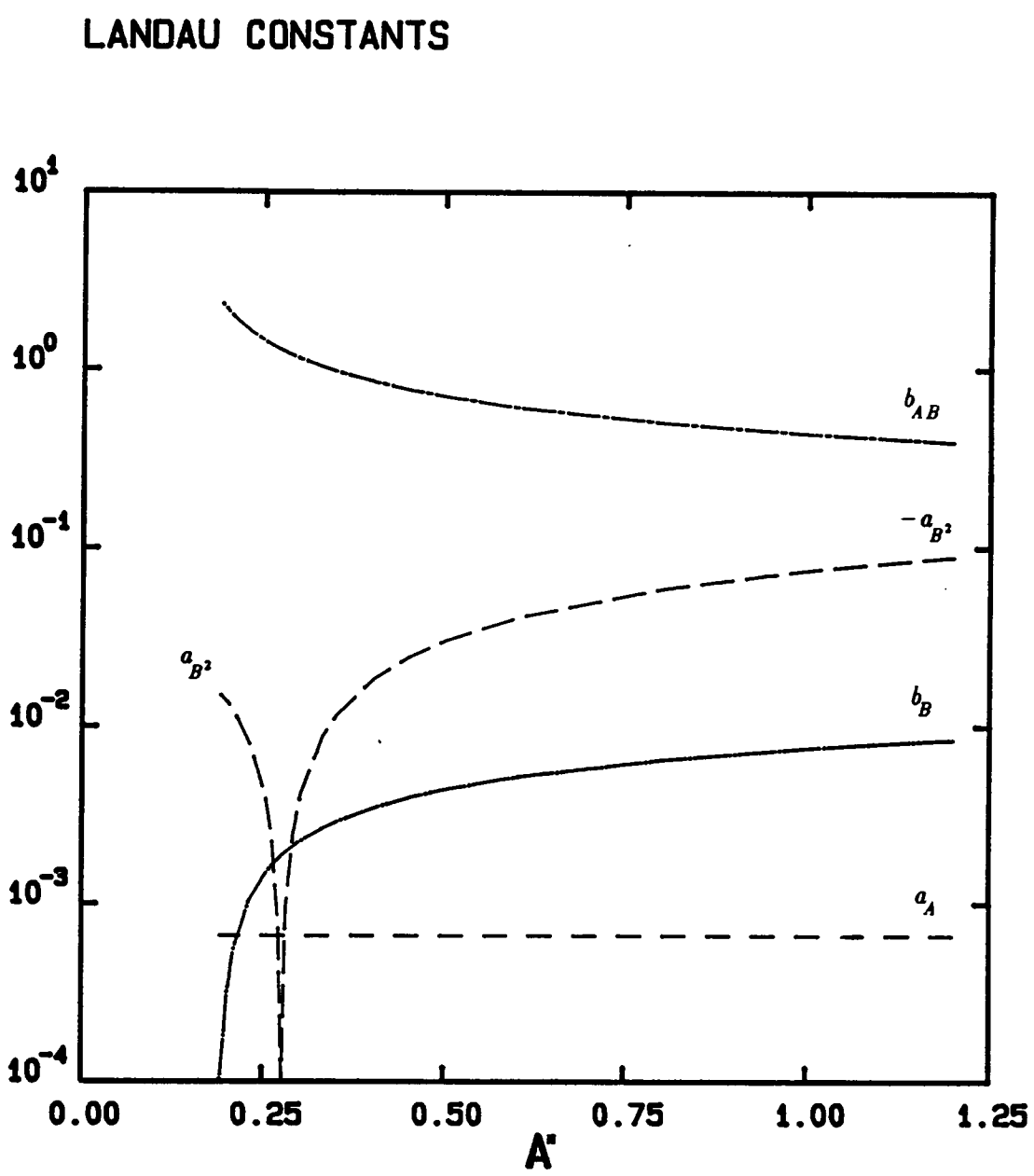

Figure 4.3 Variation of the Landau constants with amplitude, $A^*(\%)$, at fixed $R = 580$, before $R_{II} = 606$. Results for the subharmonic mode at $F = 124$, $b = .33$.

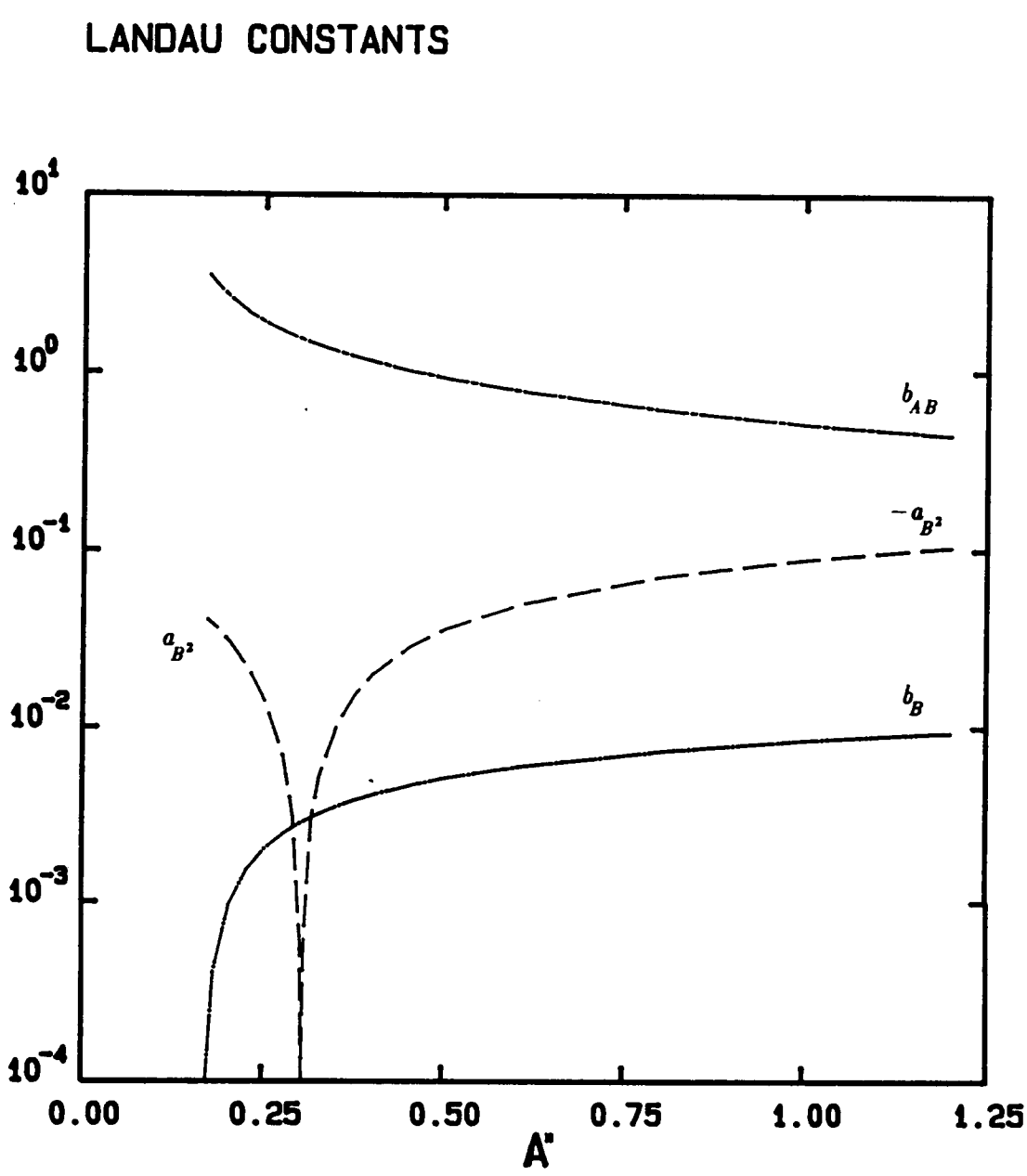

Figure 4.4 Variation of the Landau constants with amplitude, $A^*(\%)$, at fixed $R = 610$, just after $R_{II} = 606$. Results for the subharmonic mode at $F = 124$, $b = .33$

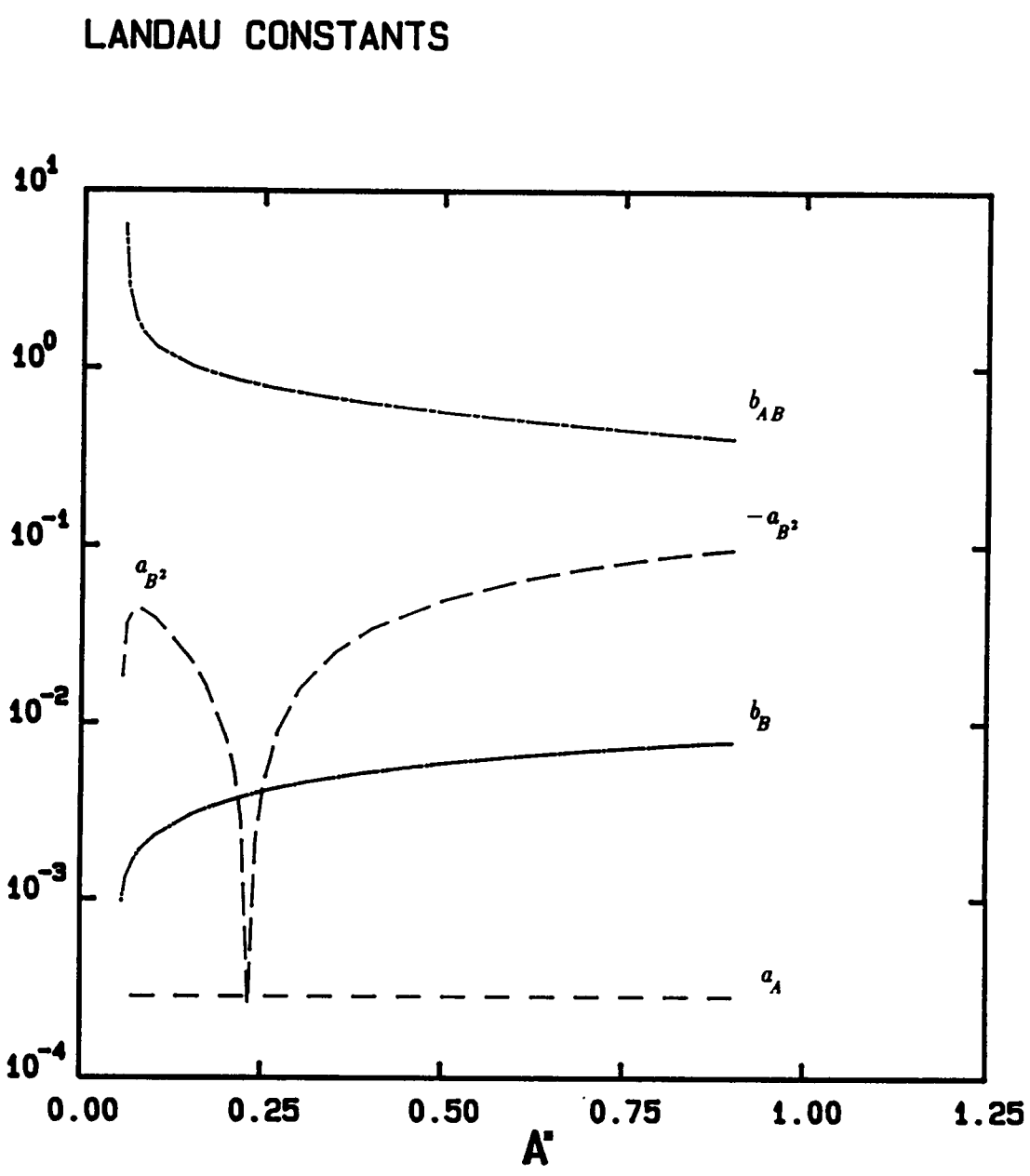

Figure 4.5 Variation of the Landau constants with amplitude, A (%), at fixed $R = 900$, before $R_{II} \approx 920$. Results for the subharmonic mode at $a = .21$, $b = .14$.

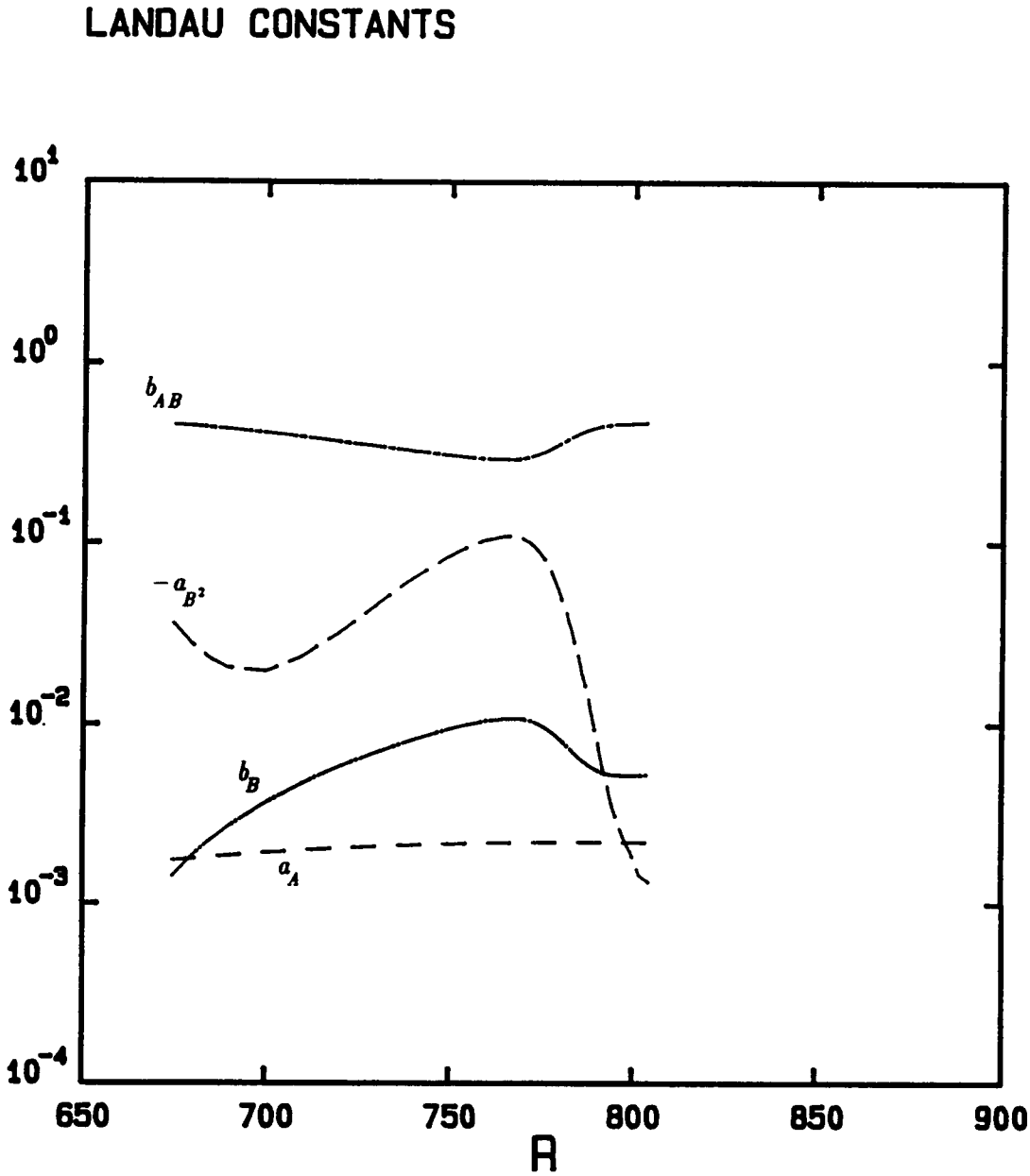

Figure 4.6 Variation of the Landau constants with Reynolds number. Results for the fundamental mode at $F = 64.4$ and $b = .44$ with variable amplitudes. Initial values are $A = .016$, $\Delta = .05$, and $B = .001$ at $R = 675$, well before R_{II}.

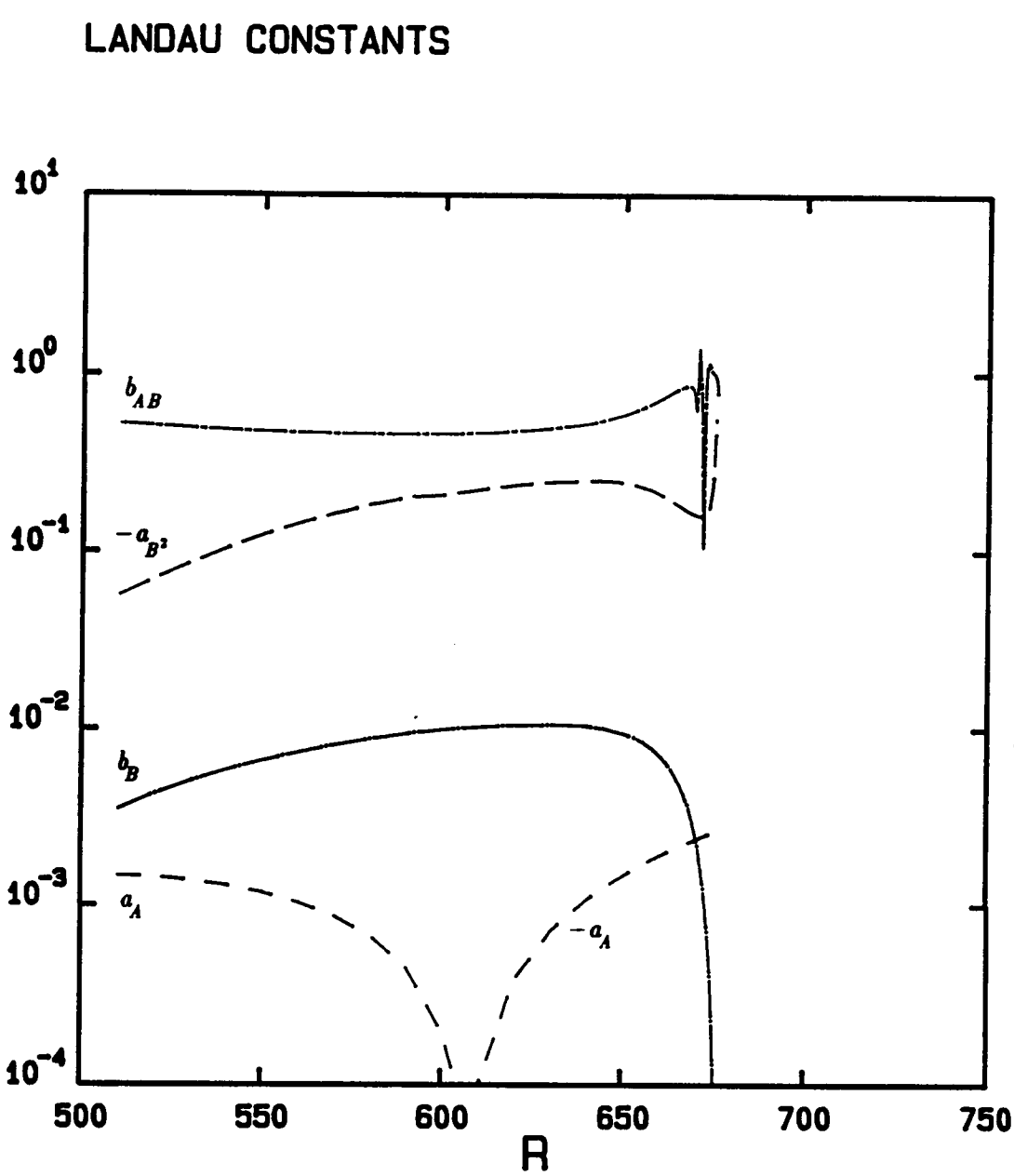

Figure 4.7 Variation of the Landau constants with Reynolds number. Results for the fundamental mode at F= 124 and b= .33 with variable amplitudes. Initial values are A= .014, Δ= .05, and B= .00002 at R= 510, before R_{II}.

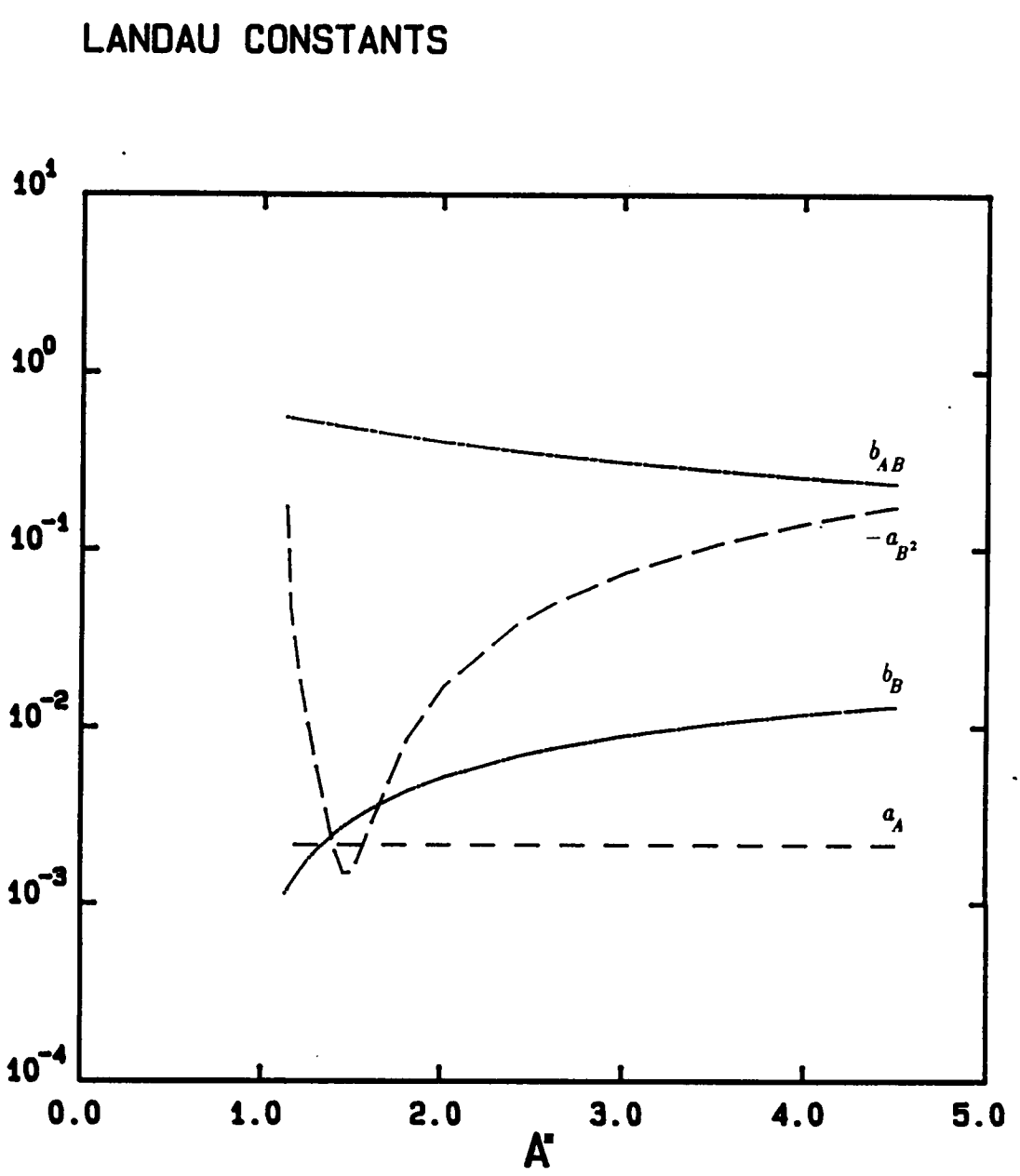

Figure 4.8 Variation of the Landau constants with amplitude, $A^*(\%)$, at fixed $R = 750$, well before R_{II}. Results for the fundamental mode at $F = 64.4$, $b = .44$.

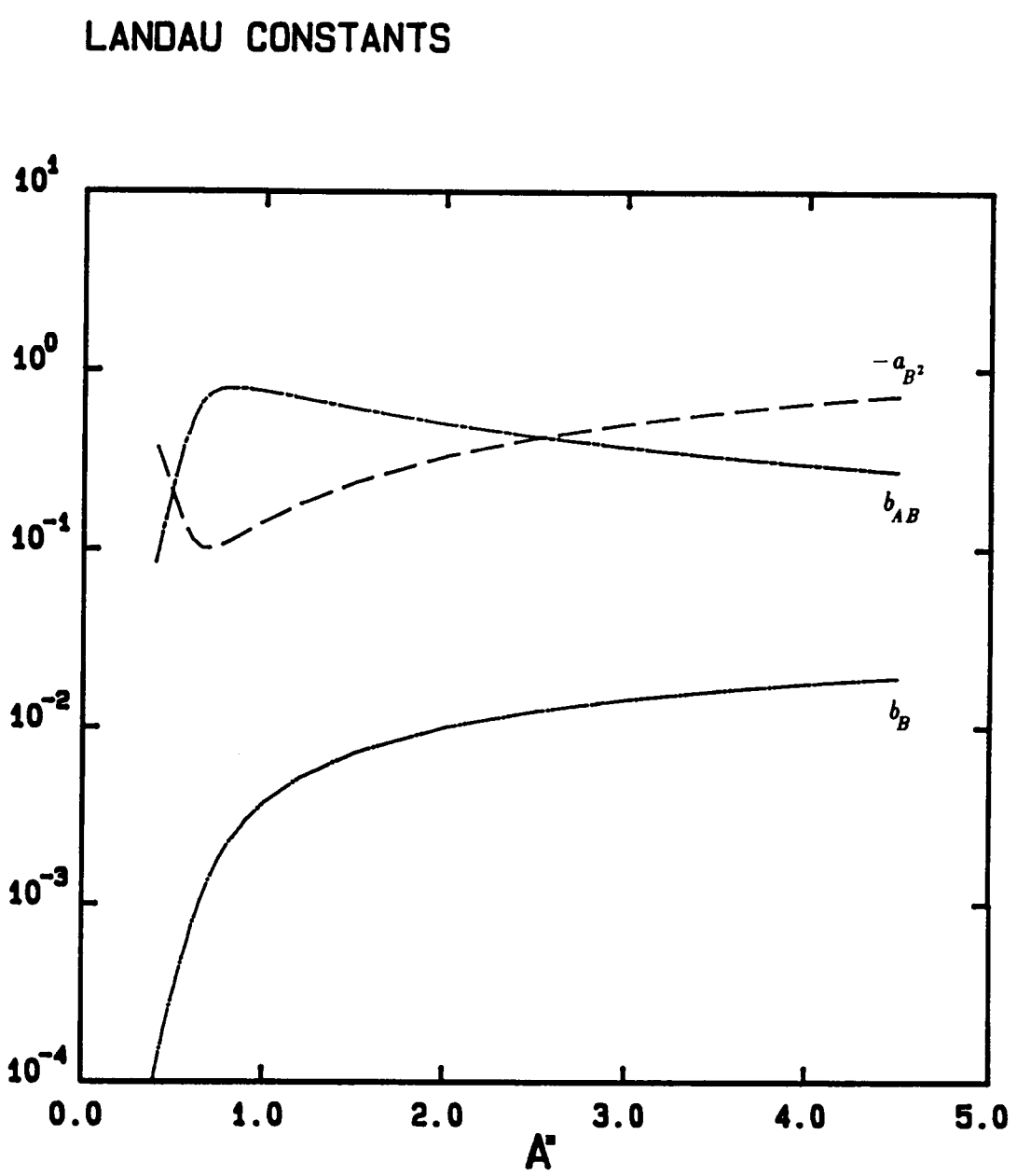

Figure 4.9 Variation of the Landau constants with amplitude, $A^*(\%)$, at fixed $R = 610$, just after $R_{II} = 606$. Results for the fundamental mode at $F = 124$, $b = .33$

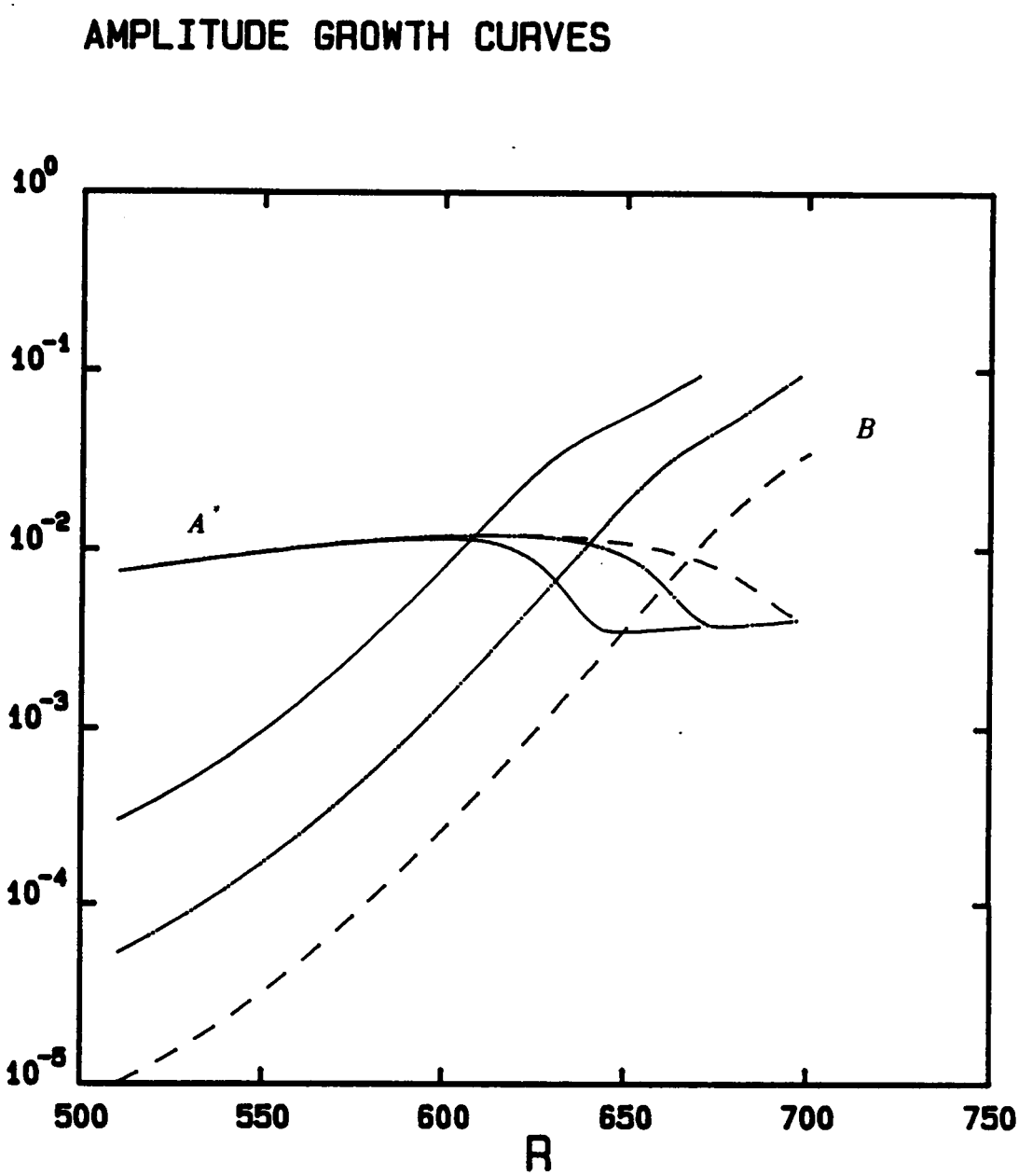

Figure 4.10 Variation of the amplitudes A^* and B, for different initial values of B, showing TS equilibrium. Results for the subharmonic mode at $F = 124$, $b = .33$, and $\Delta = .05$. Initial values are $A = .00782$ and $B = .00001, .000053, .0003$ at $R = 510$.

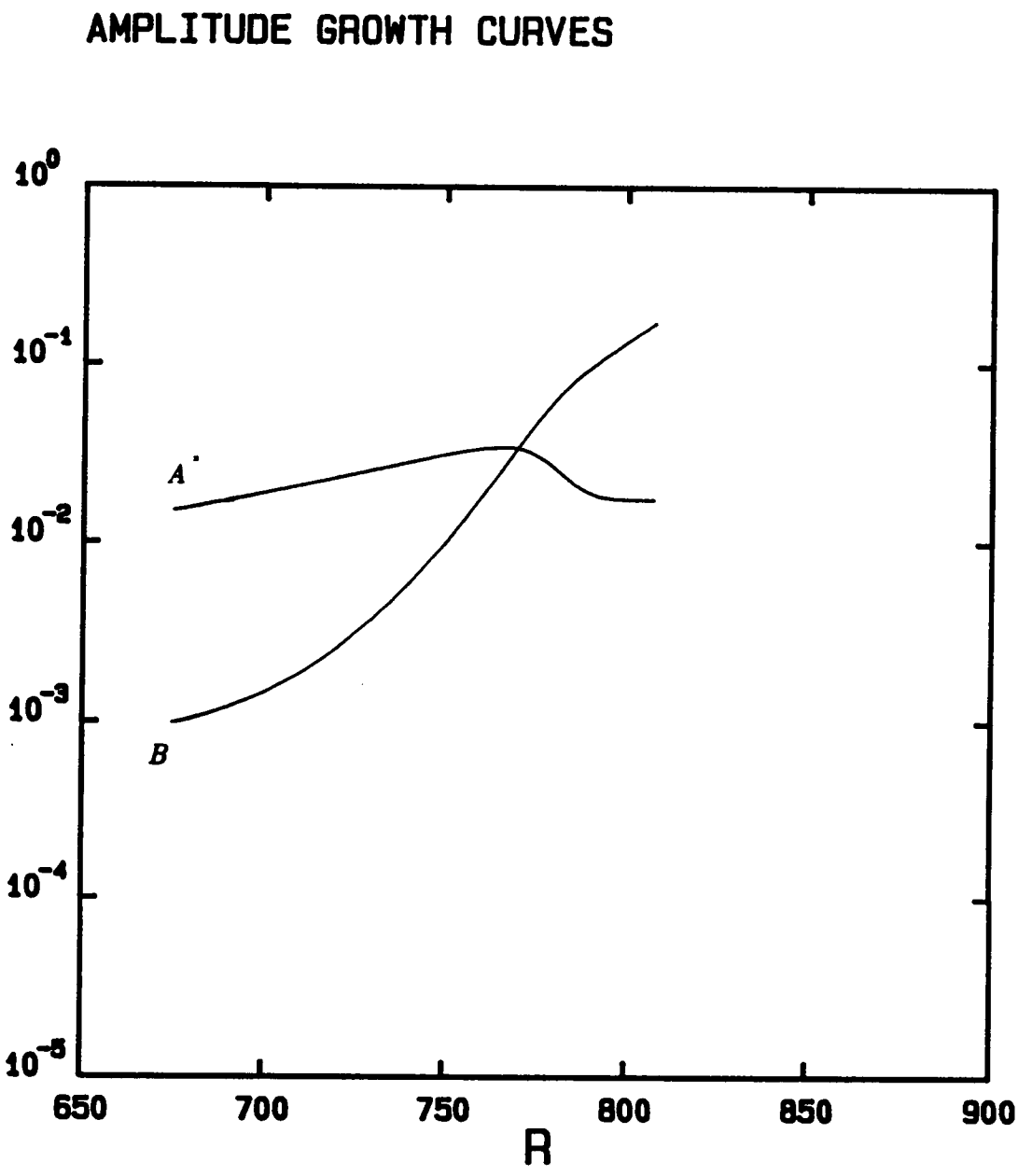

Figure 4.11 Variation of the amplitudes A and B, showing TS equilibrium. Results for the fundamental mode at $F = 64.4$, $b = .44$, and $\Delta = .05$. Initial values are $A = .016$ and $B = .001$ at $R = 675$.

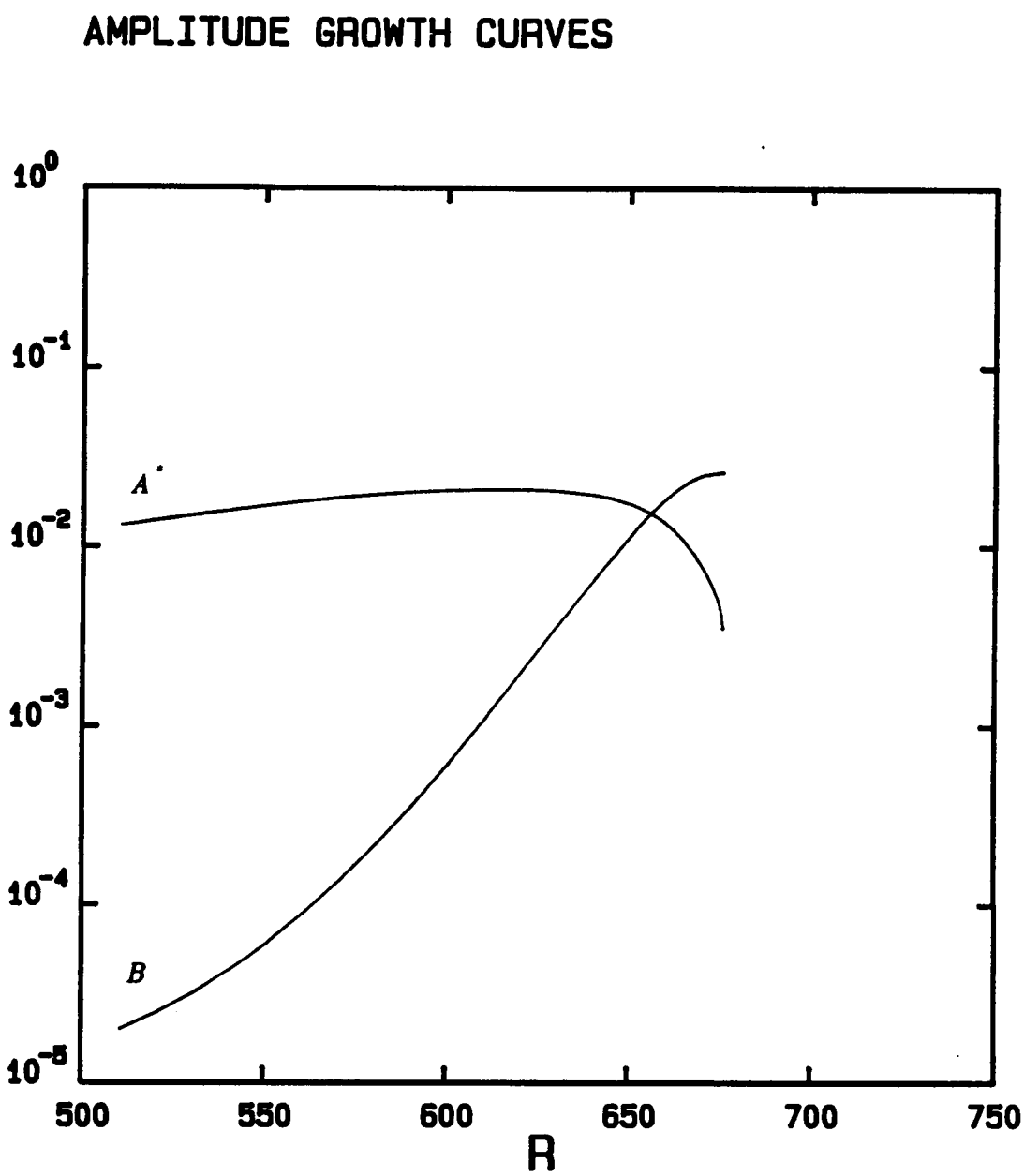

Figure 4.12 Variation of the amplitudes A and B, showing lack of TS equilibrium. Results for the fundamental mode at $F = 124$, $b = .33$, $\Delta = .05$ and $N = 2$. Initial values are $A = .014$ and $B = .00002$ at $R = 510$.

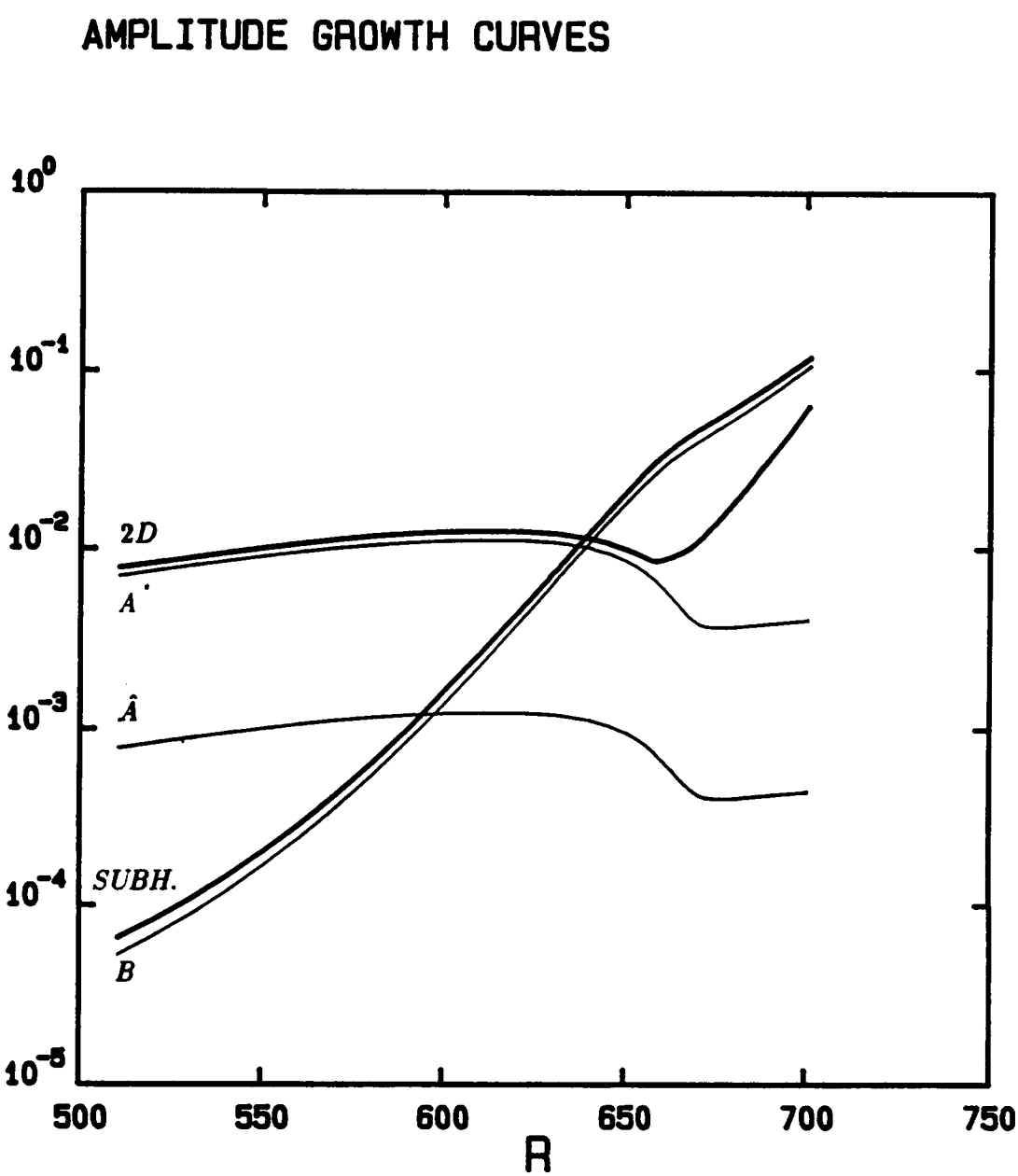

Figure 4.13 Evolution of the different amplitude components, A^*, $\hat{A}$, B, $||u_{2D}||_{max}$ and $||u_S||_{max}$. Results for the subharmonic mode at $F = 124$, $b = .33$, and $\Delta = .1$. Initial values are $A = .00782$ and $B = .000053$ at $R = 510$.

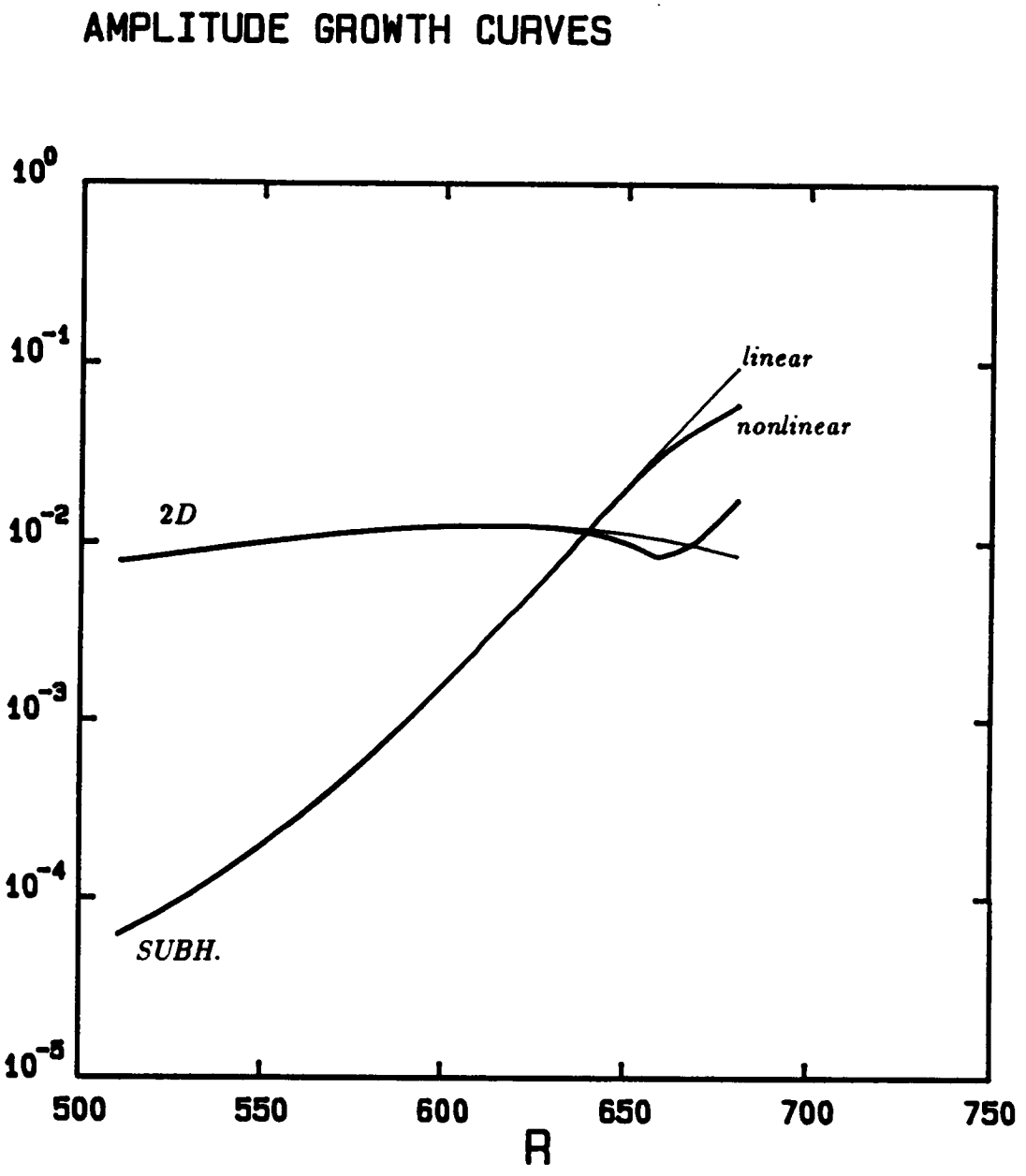

Figure 4.14 Comparison of the linear (first order) and nonlinear (second order) evolutions of $||u_{2D}||_{max}$ and $||u_S||_{max}$. Results for the subharmonic mode at $F = 124$, $b = .33$, and $\Delta = .1$. Initial values are $A = .00782$ and $B = .000053$ at $R = 510$.

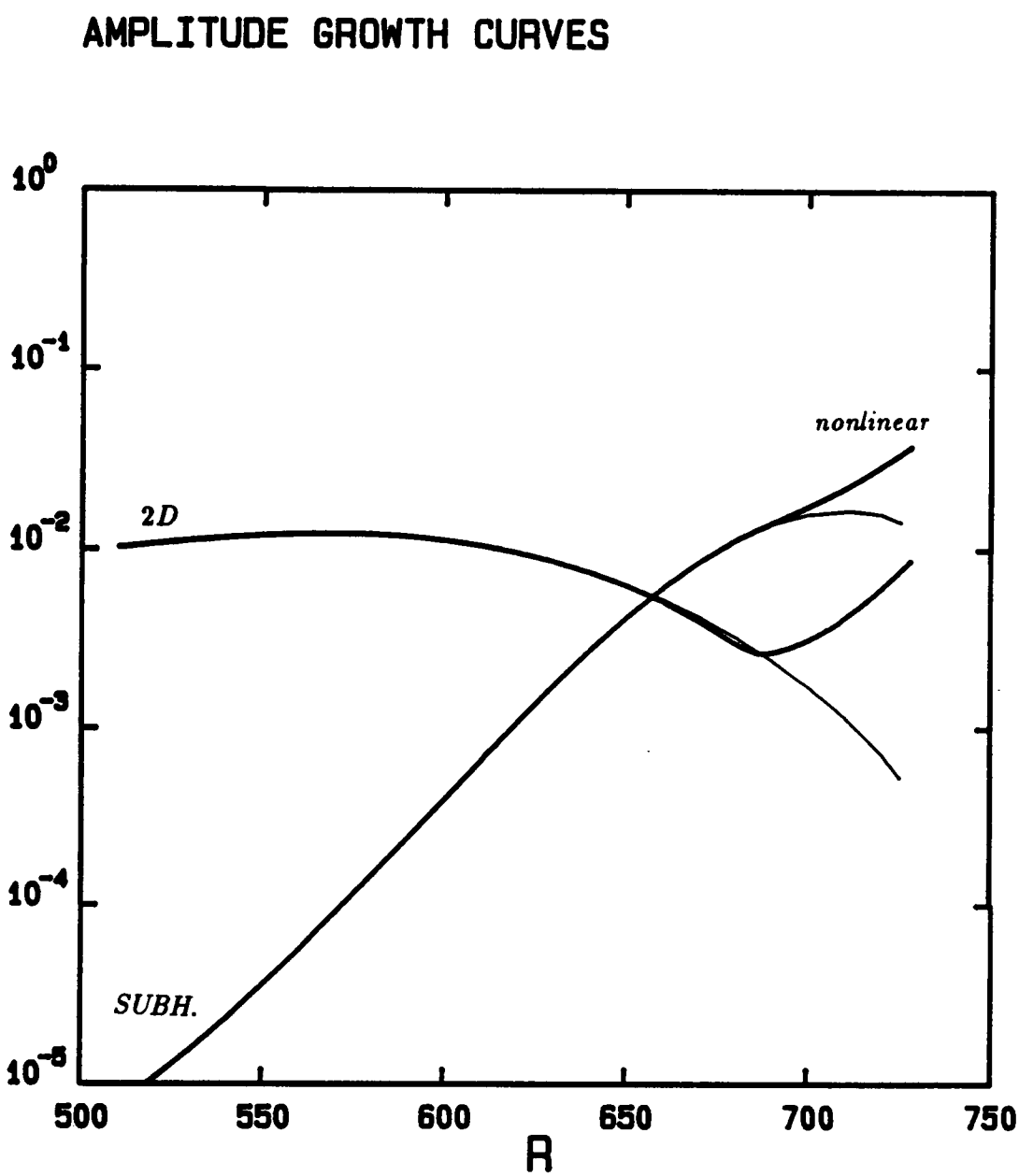

Figure 4.15 Comparison of the linear (first order) and nonlinear (second order) evolutions of $||u_{2D}||_{max}$ and $||u_S||_{max}$. Results for the subharmonic mode at $F = 137$, $b = .40$, and $\Delta = .05$. Initial values are $A = .0103$ and $B = .0000065$ at $R = 510$.

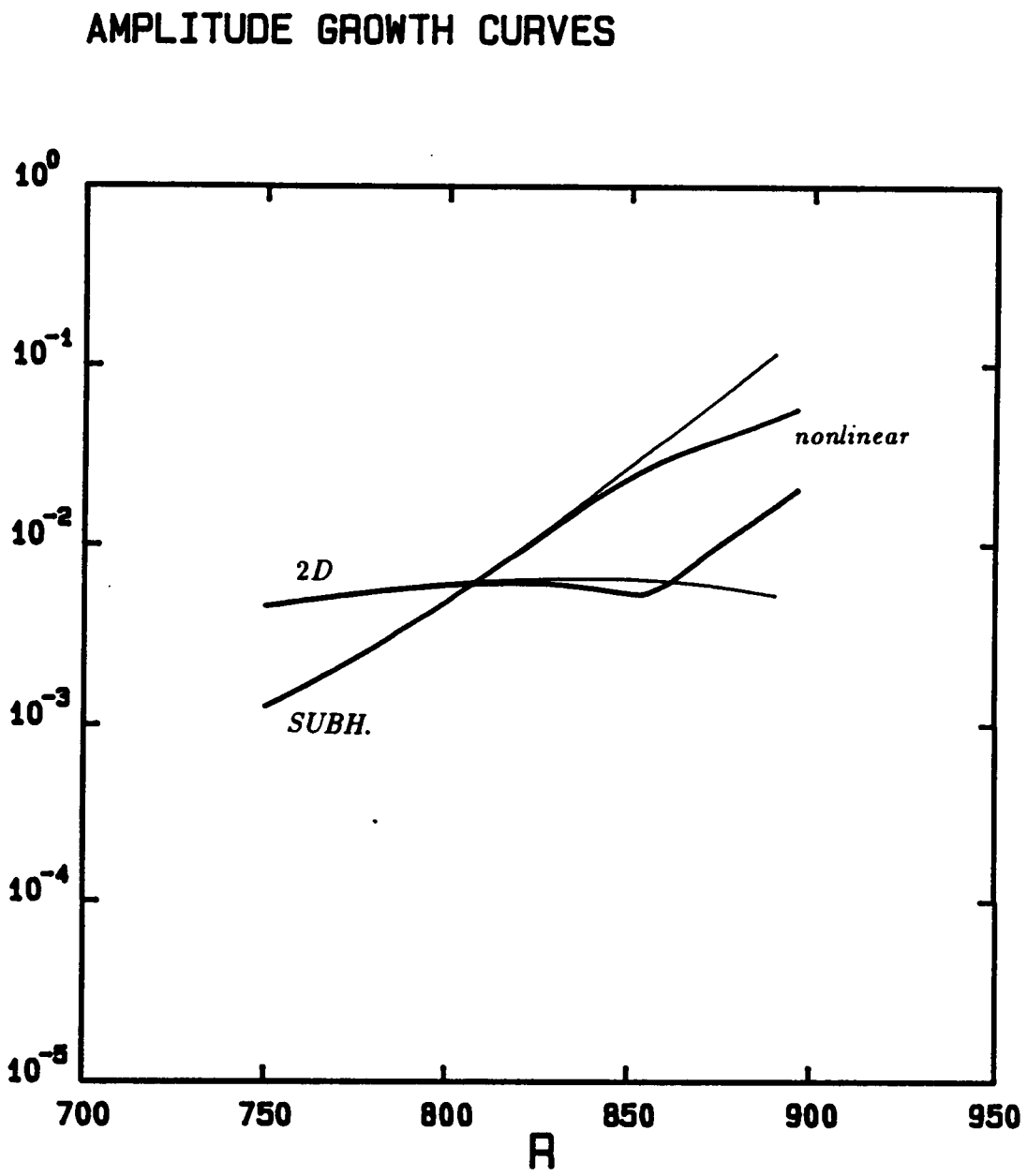

Figure 4.16 Comparison of the linear (first order) and nonlinear (second order) evolutions of $||u_{2D}||_{max}$ and $||u_S||_{max}$. Results for the subharmonic mode at $F = 82.7$, $b = .129$, and $\Delta = .05$. Initial values are $A = .0045$ and $B = .0011$ at $R = 750$.

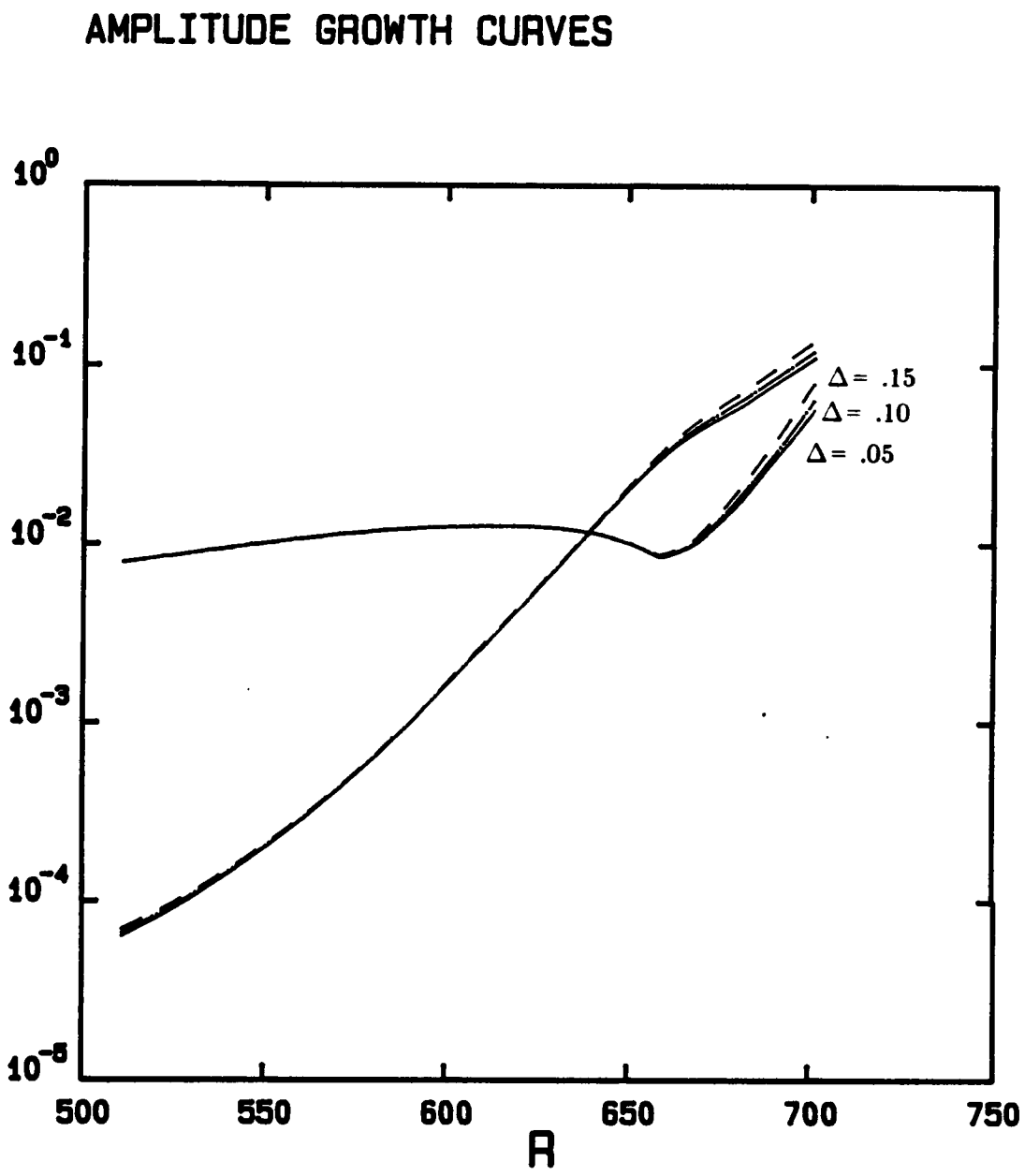

Figure 4.17 Effect of the value of Δ on the amplitude evolution of $||u_{2D}||_{max}$ and $||u_S||_{max}$. Results for the subharmonic mode at $F = 124$, $b = .33$, and $\Delta = .05$ .1, .15. Initial values are $A = .00782$ and $B = .000053$ at $R = 510$.

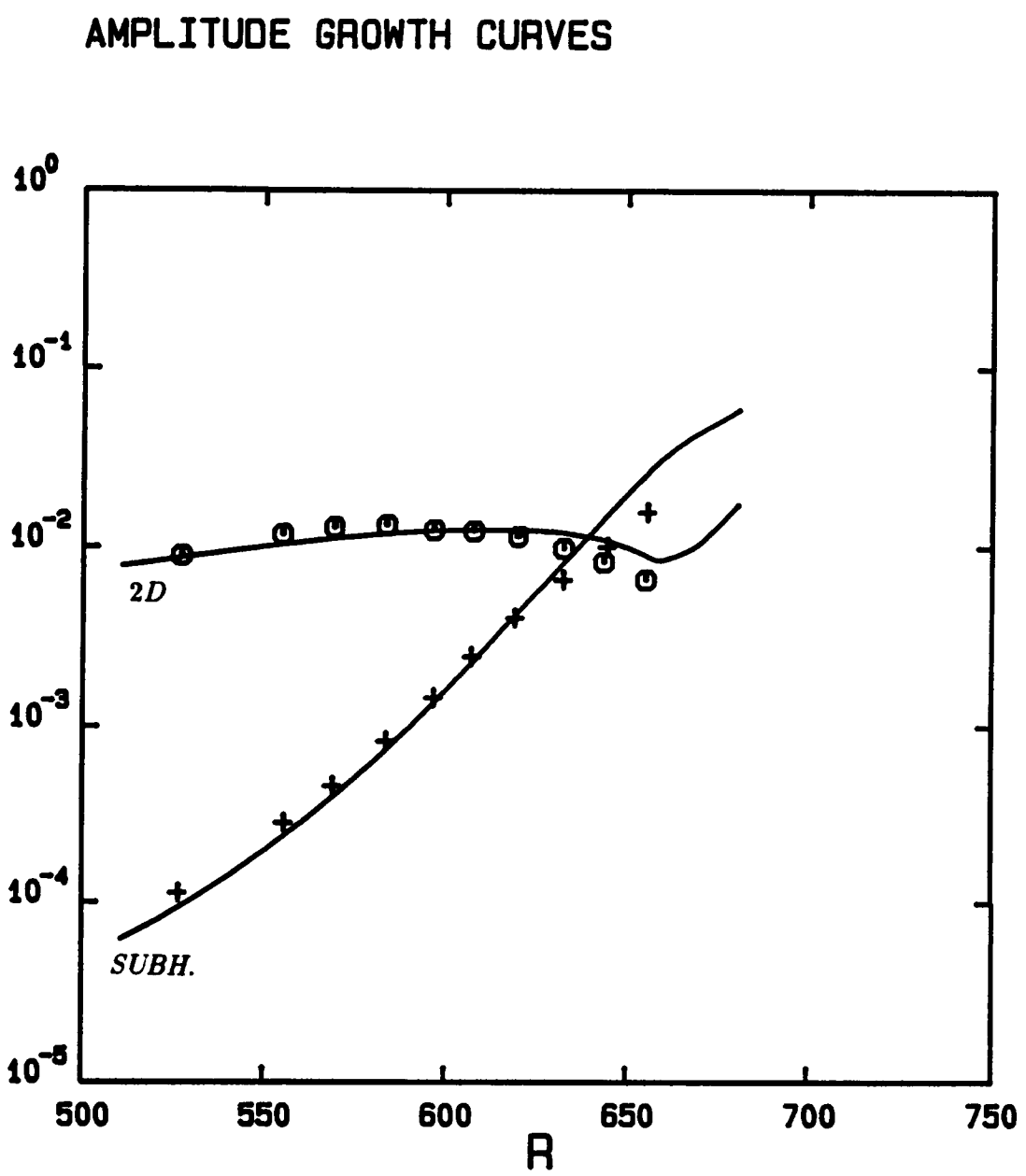

Figure 4.18 Comparison of the evolution of $||u_{2D}||_{max}$ and $||u_S||_{max}$ with the experiments of Kachanov and Levchenko (1984), figure 23(a). Results for the subharmonic mode at $F = 124$, $b = .33$, and $\Delta = .05$. Initial values are $A = .00782$ and $B = .000053$ at $R = 510$.

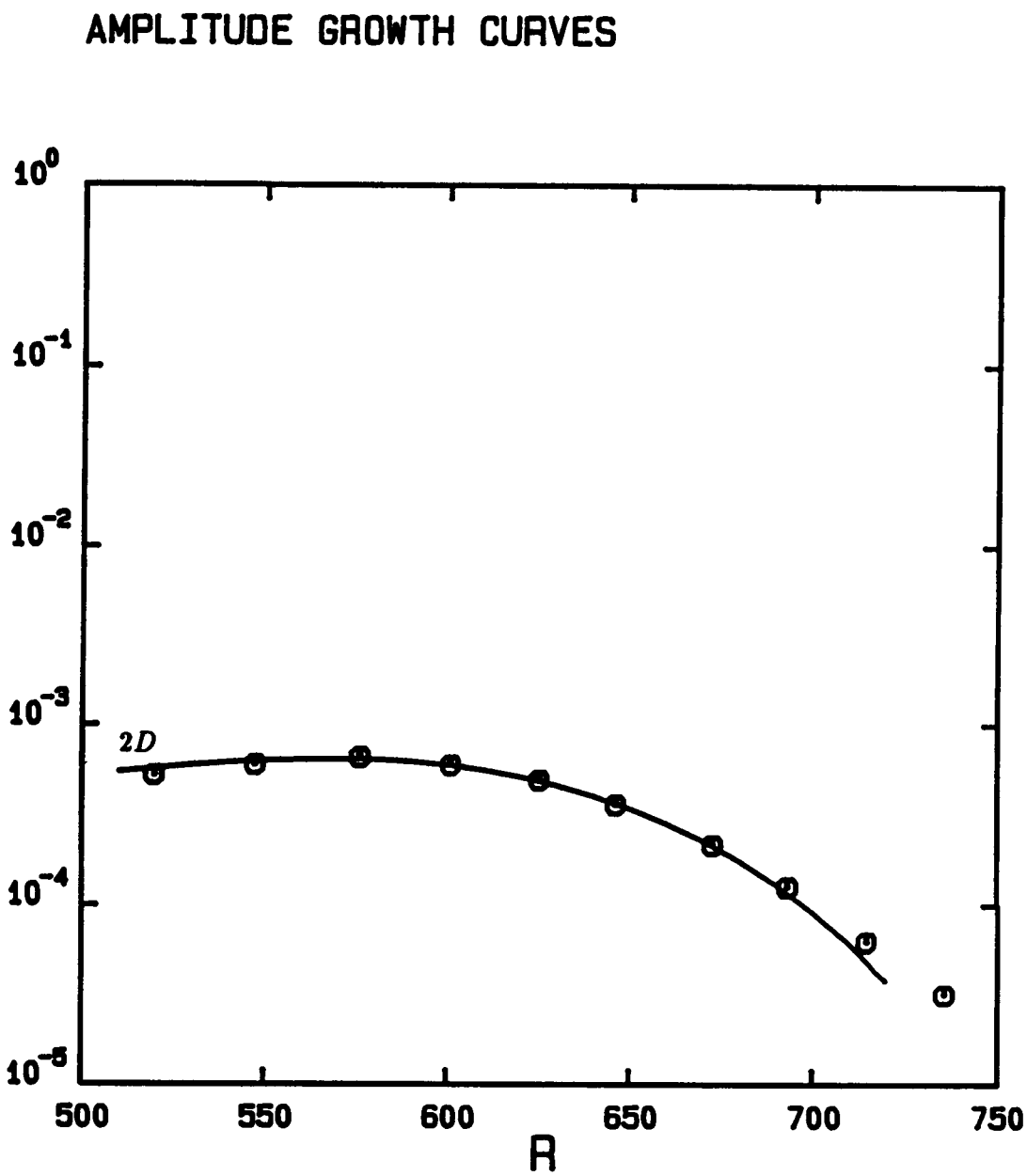

Figure 4.19 Comparison of the evolution of $||u_{2D}||_{max}$ with the experiments of Kachanov and Levchenko (1984), figure 2 (A_0= .00022). Results for the TS wave, in the absence of the secondary, at F= 137. Initial values are A= .00052 at R= 500. Experimental data are shifted by R= −10.

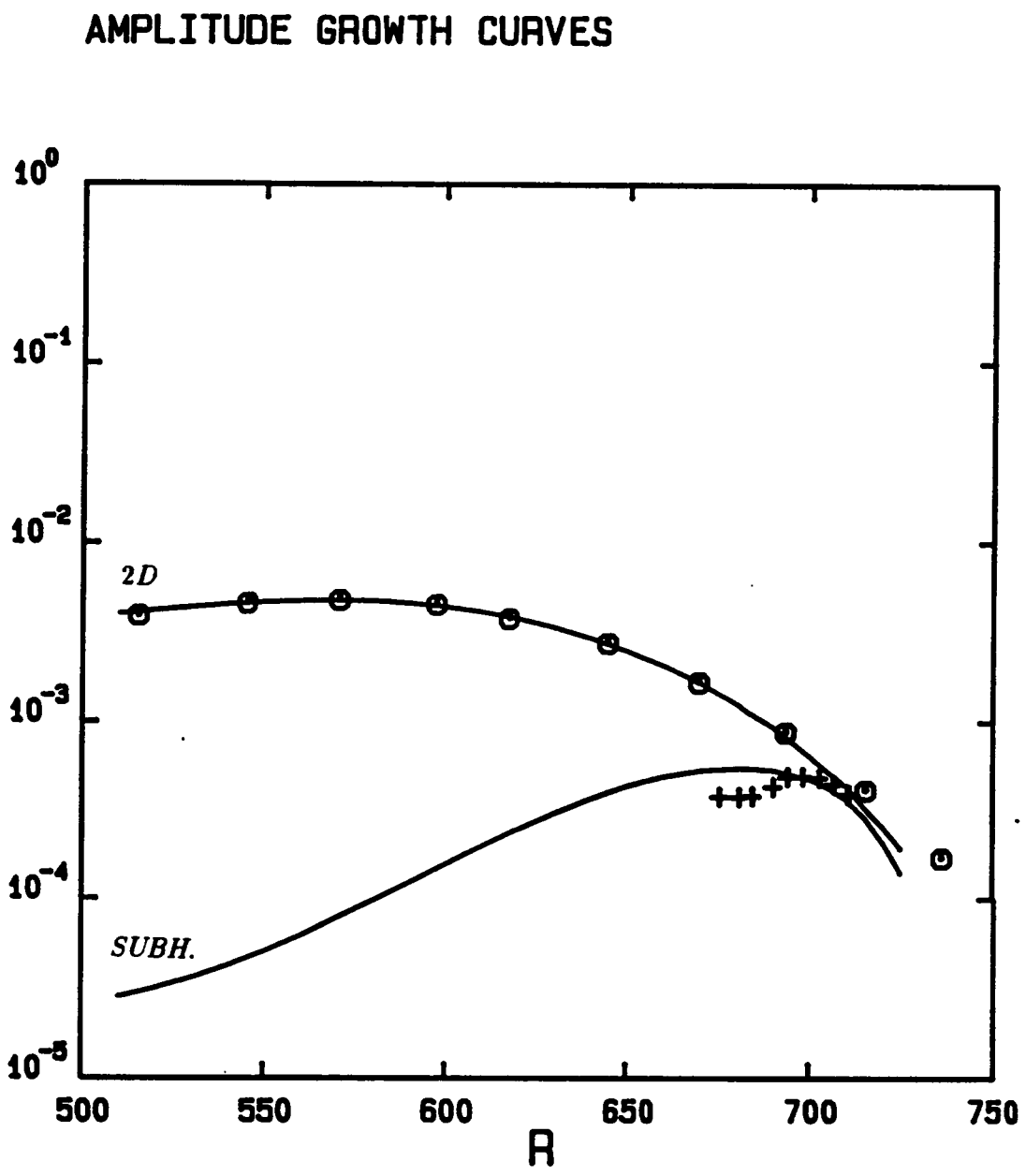

Figure 4.20 Comparison of the evolution of $||u_{2D}||_{max}$ and $||u_S||_{max}$ with the experiments of Kachanov and Levchenko (1984), figure 2 ($A_0 = .00163$). Results for the subharmonic mode at $F = 137$, $b = .40$, and $\Delta = .05$. Initial values are $A = .004$ and $B = .000025$ at $R = 510$. Experimental data are shifted by $R = -10$.

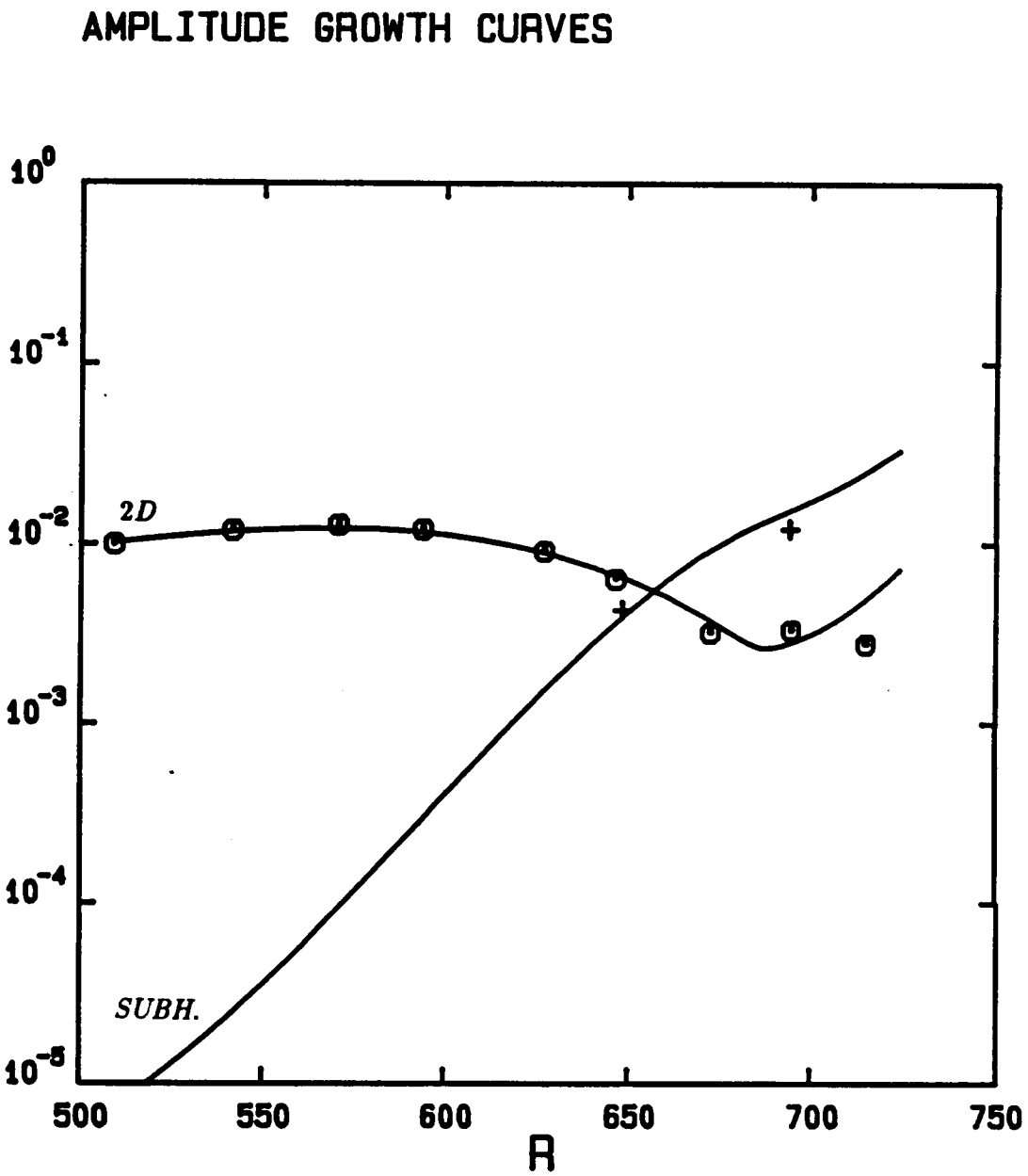

Figure 4.21 Comparison of the evolution of $||u_{2D}||_{max}$ and $||u_S||_{max}$ with the experiments of Kachanov and Levchenko (1984), figure 2 ($A_0 = .00436$). Results for the subharmonic mode at $F = 137$, $b = .40$, and $\Delta = .05$. Initial values are $A = .0103$ and $B = .0000065$ at $R = 510$. Experimental data are shifted by $R = -10$.

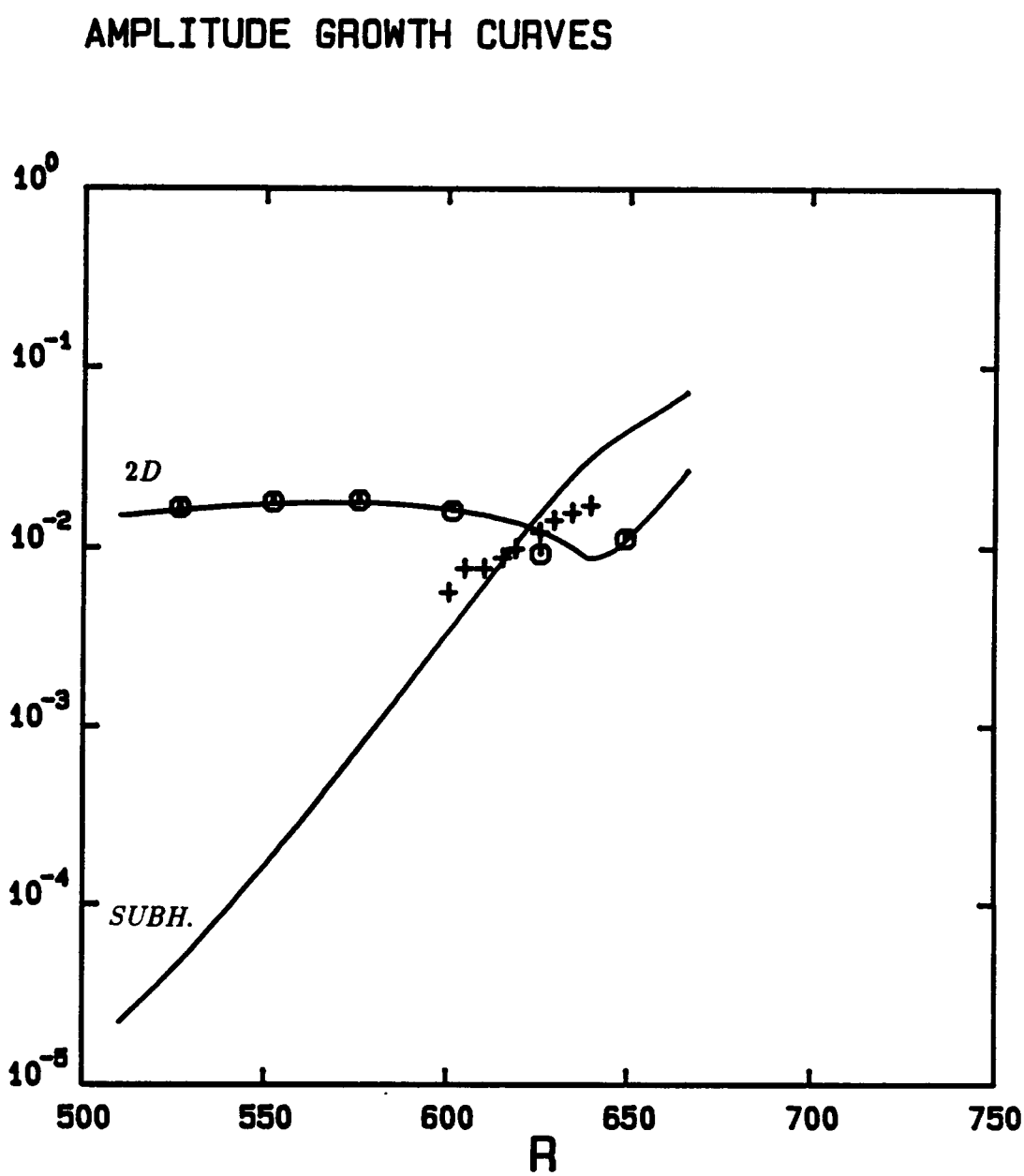

Figure 4.22 Comparison of the evolution of $||u_{2D}||_{max}$ and $||u_S||_{max}$ with the experiments of Kachanov and Levchenko (1984), figure 2 ($A_0 = .00654$). Results for the subharmonic mode at $F = 137$, $b = .40$, and $\Delta = .05$. Initial values are $A = .015$ and $B = .000019$ at $R = 510$. Experimental data are shifted by $R = -10$.

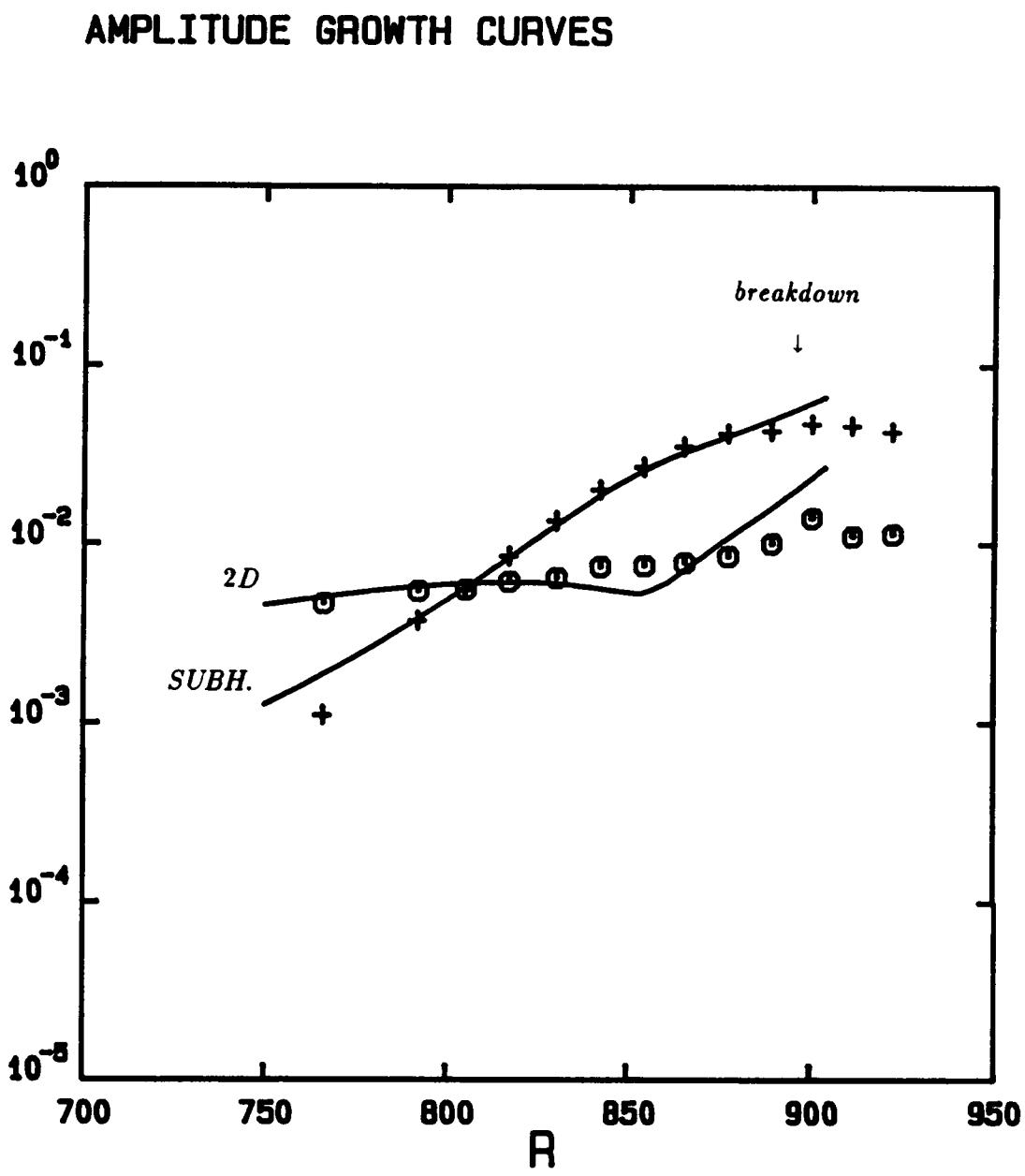

Figure 4.23 Comparison of the evolution of $||u_{2D}||_{max}$ and $||u_S||_{max}$ with the experiments of Corke and Mangano (1987). figure 65. Results for the subharmonic mode at $F = 82.7$, $b = .129$, and $\Delta = .05$. Initial values are $A = .0045$ and $B = .0011$ at $R = 750$.

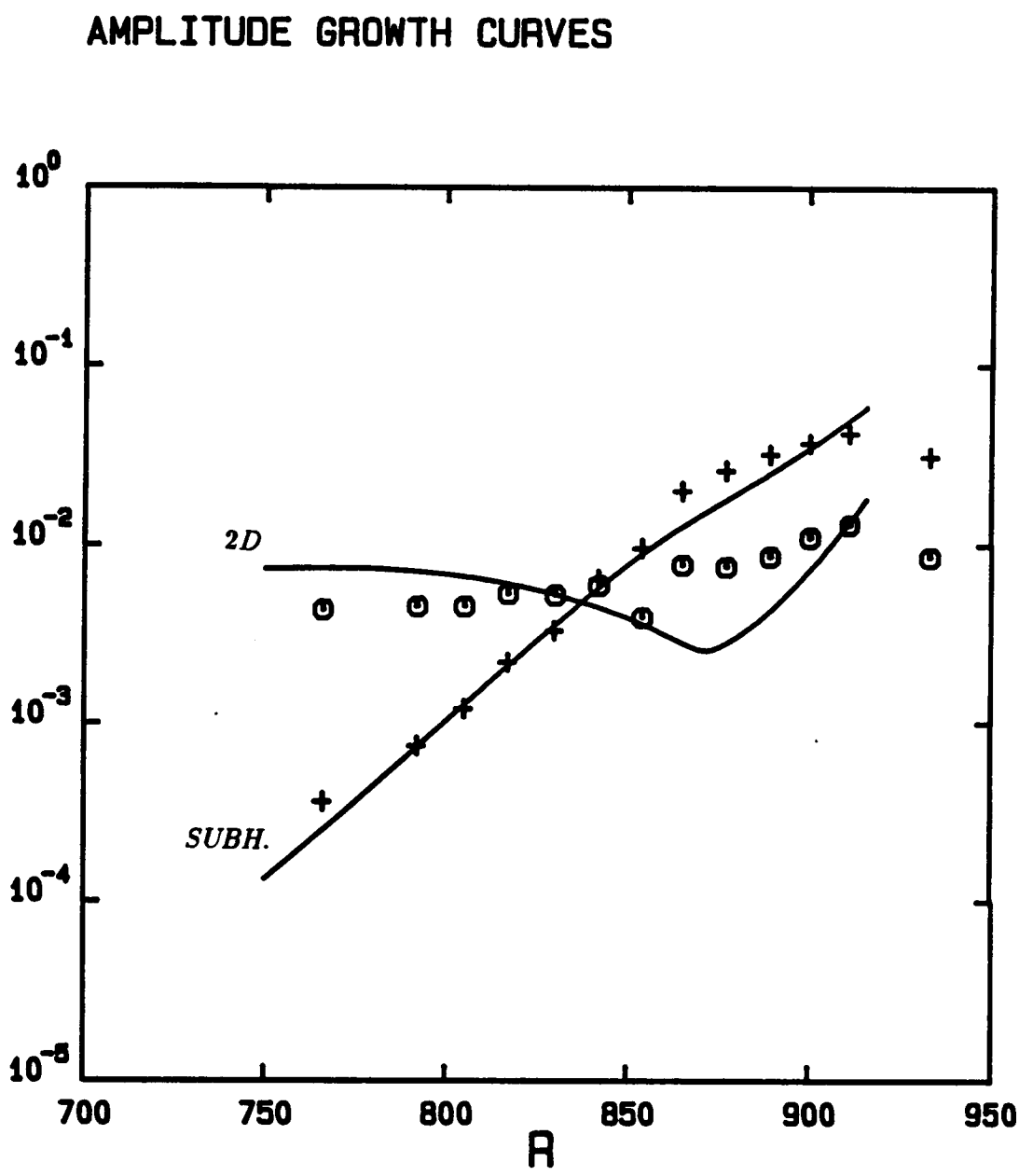

Figure 4.24 Comparison of the evolution of $||u_{2D}||_{max}$ and $||u_S||_{max}$ with the experiments of Corke and Mangano (1987). figure 66. Results for the subharmonic mode at $F = 93$. $b = .174$, and $\Delta = .05$. Initial values are $A = .0073$ and $B = .00012$ at $R = 750$.

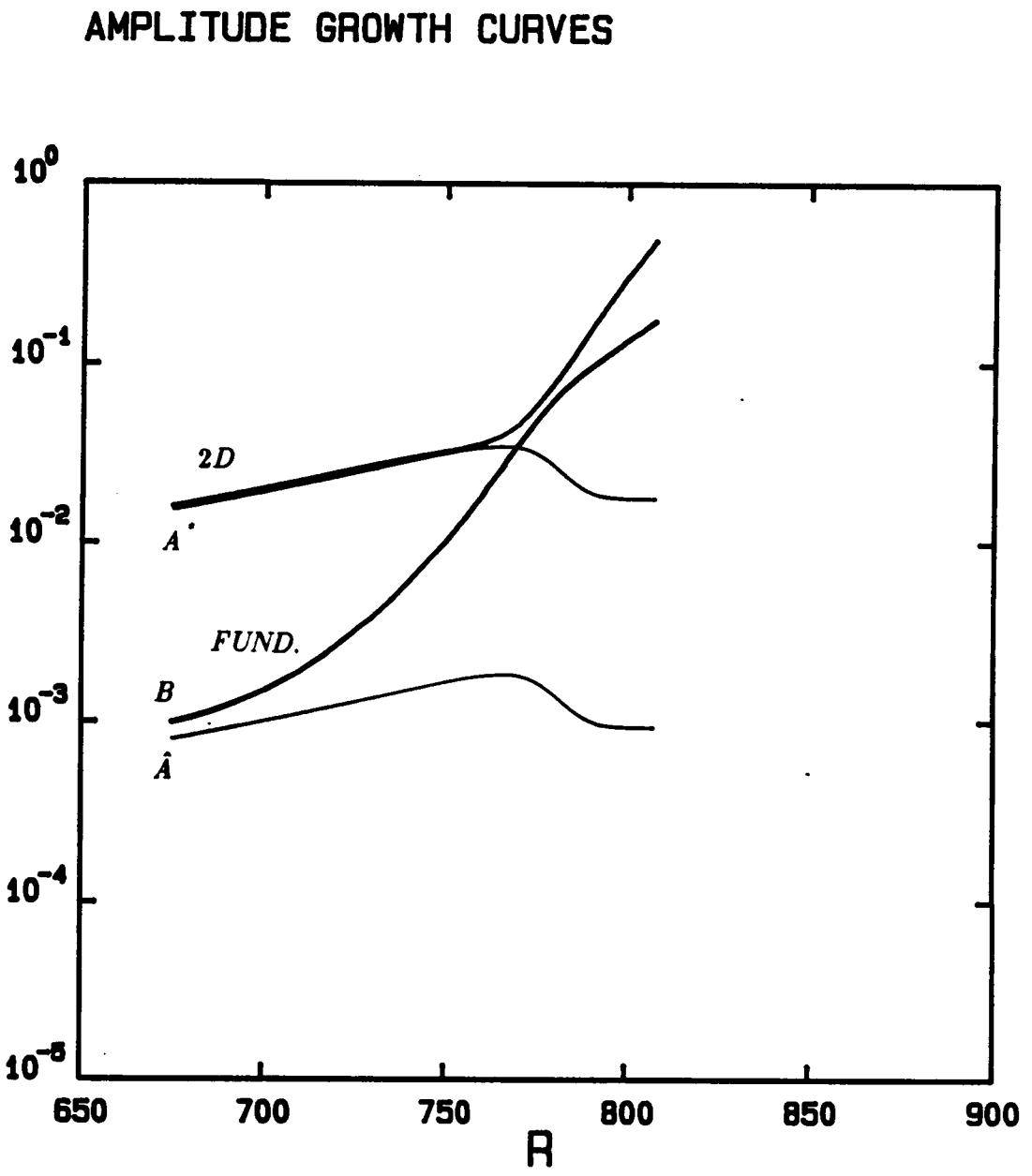

Figure 4.25 Evolution of the different amplitude components, $A^{\cdot}$, $\hat{A}$, B, $||u_{2D}||_{max}$ and $||u_F||_{max}$. Results for the fundamental mode at $F = 64.4$, $b = .44$, and $\Delta = .05$. Initial values are $A = .016$ and $B = .001$ at $R = 675$.

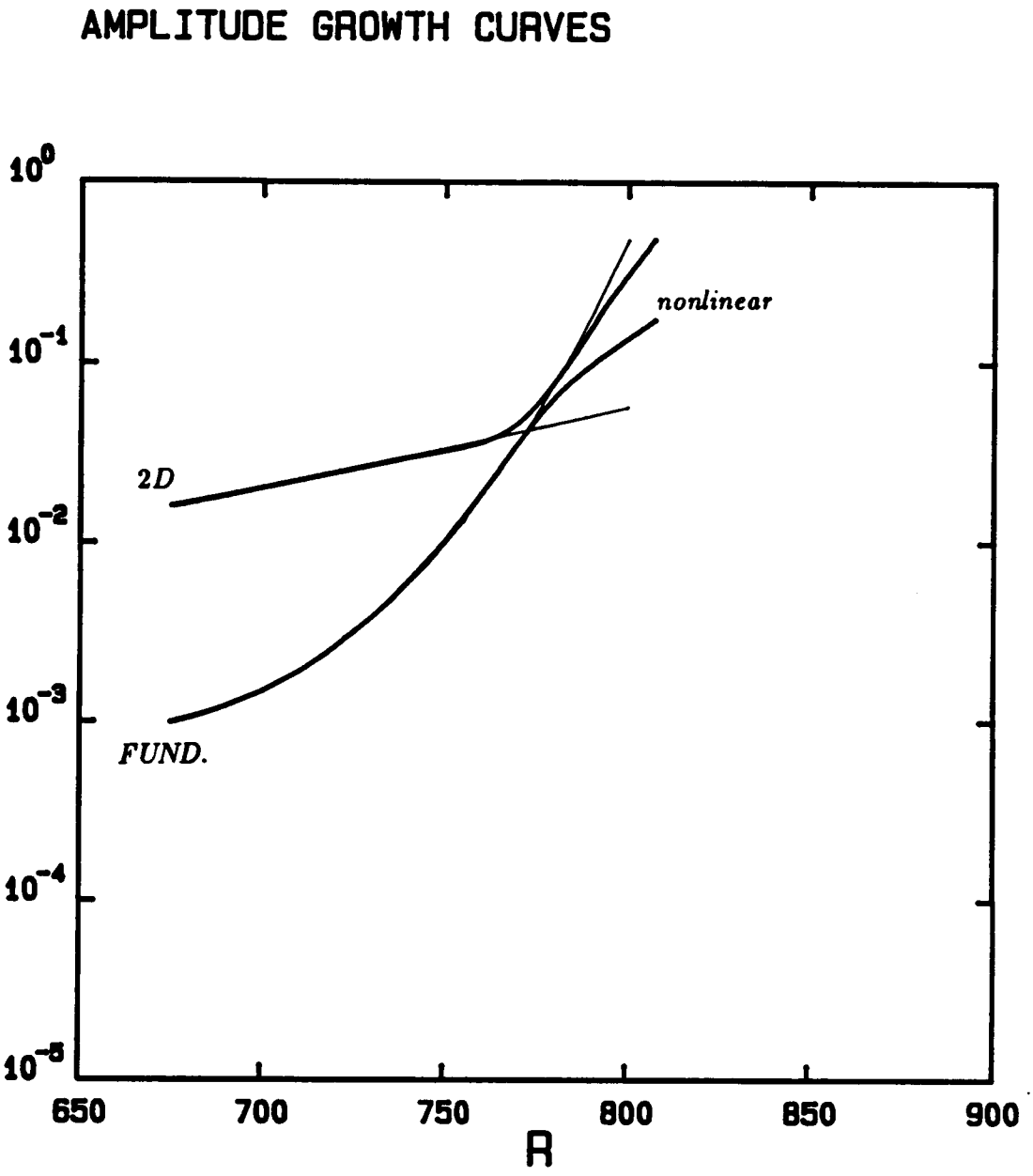

Figure 4.26 Comparison of the linear (first order) and nonlinear (second order) evolutions of $||u_{2D}||_{max}$ and $||u_F||_{max}$. Results for the fundamental mode at $F = 64.4$, $b = .44$, and $\Delta = .05$. Initial values are $A = .016$ and $B = .001$ at $R = 675$.

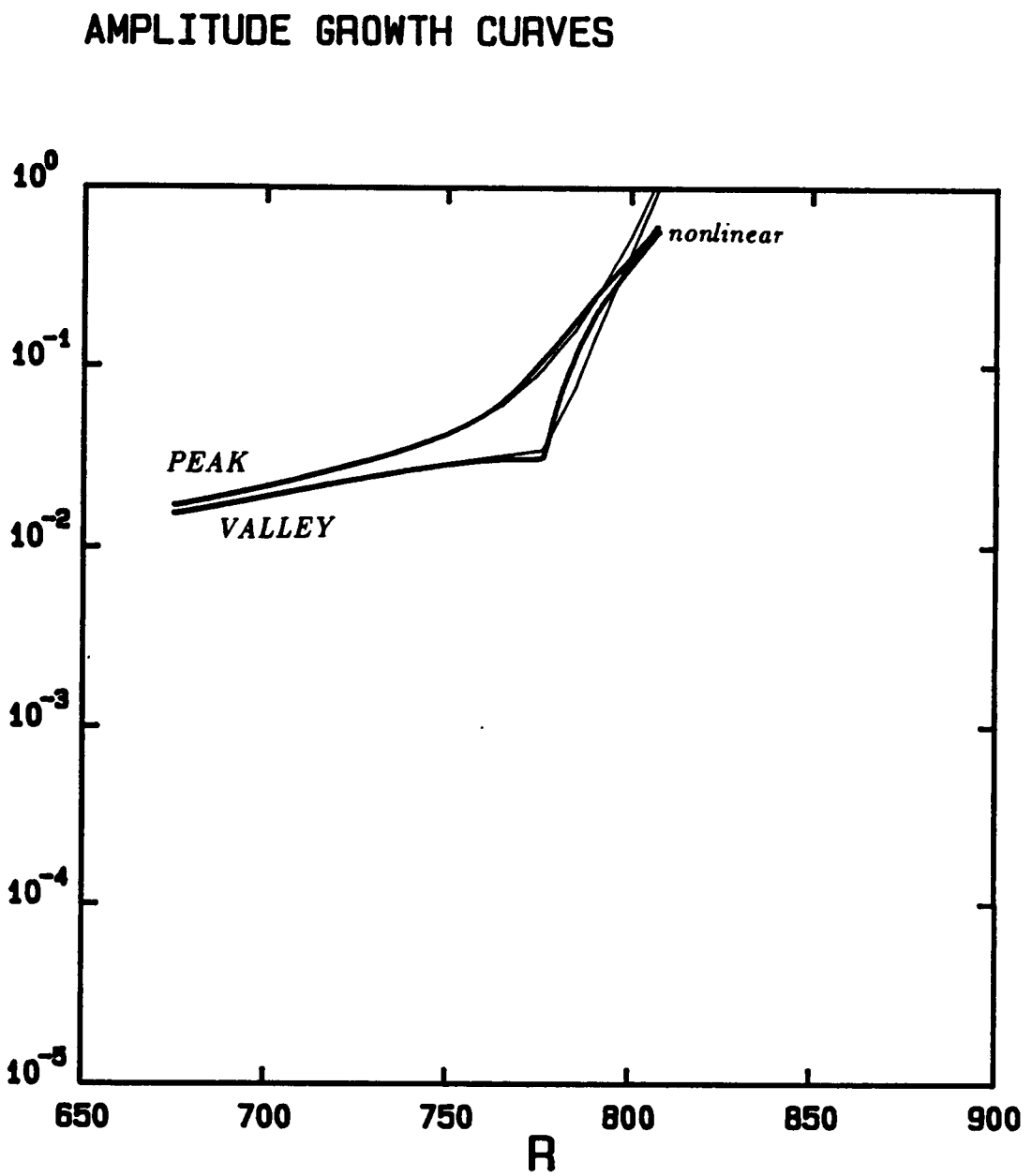

Figure 4.27 Comparison of the linear (first order) and nonlinear (second order) evolutions of the peak $||u_P||_{max}$, and the valley, $||u_V||_{max}$. Results for the fundamental mode at $F = 64.4$, $b = .44$, and $\Delta = .05$. Initial values are $A = .016$ and $B = .001$ at $R = 675$.

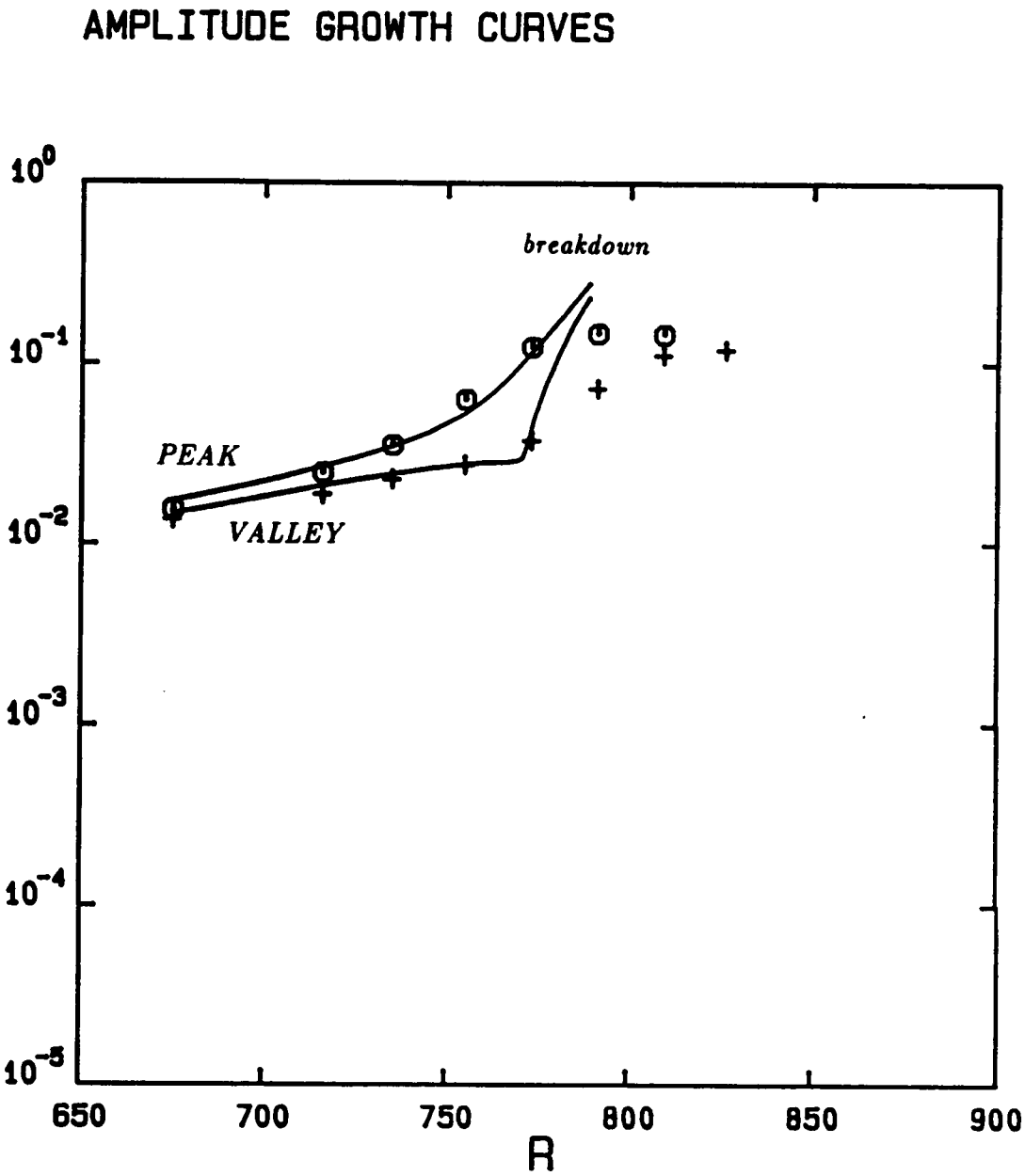

Figure 4.28 Comparison of the evolution of $||u_p||_{max}$ and $||u_v||_{max}$ with the profile maximums of Cornelius (1985), figures 16 and 17. Results for the fundamental mode at $F = 64.4$, $b = .44$, and $\Delta = .05$. Initial values are $A = .016$ and $B = .0015$ at $R = 675$.

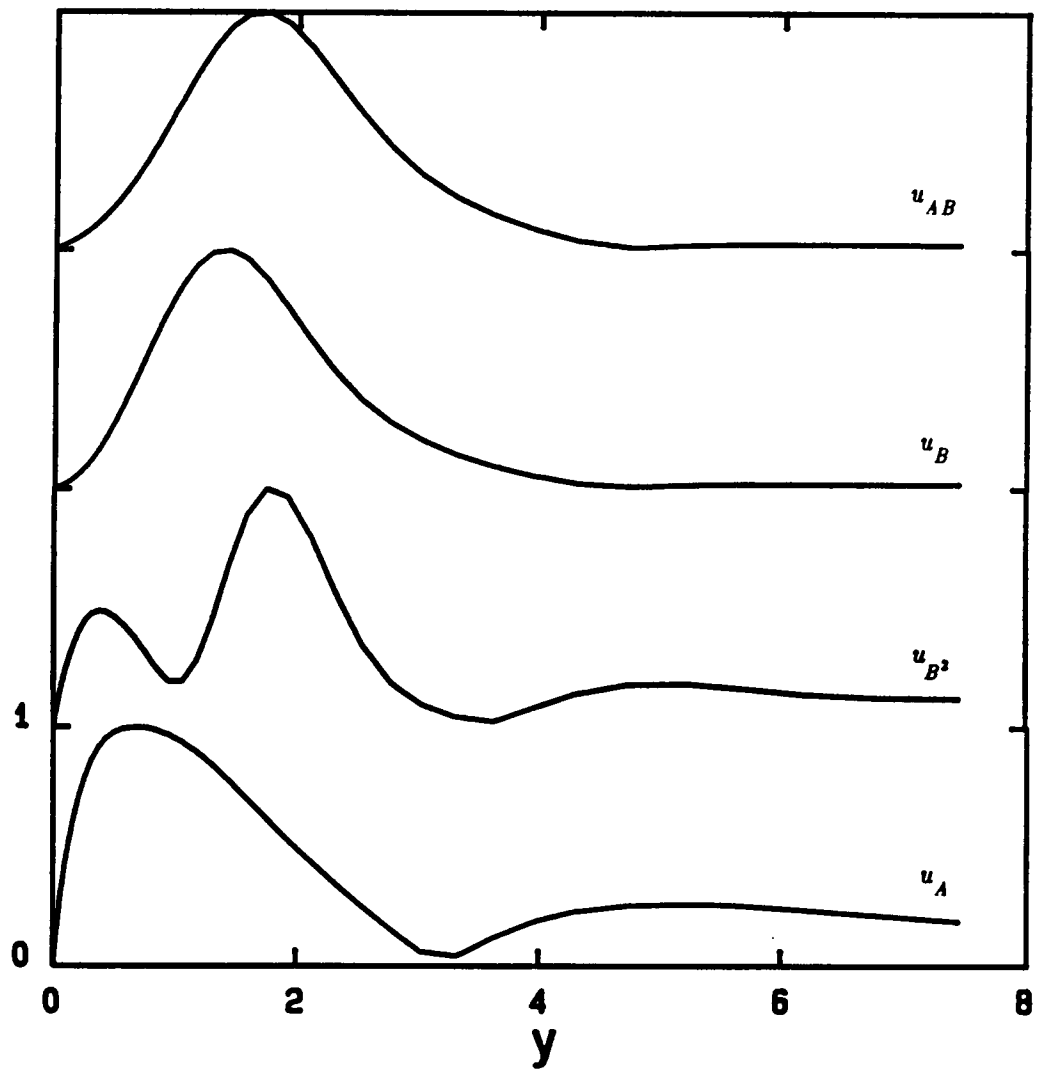

Figure 4.29 Normalized velocity functions u_A, u_{B^2}, u_B, and u_{AB} at fixed $R = 580$. Results for the subharmonic mode at $F = 124$, $b = .33$, and $\Delta = .05$, with initial values $A = .00782$ and $B = .000053$ at $R = 510$.

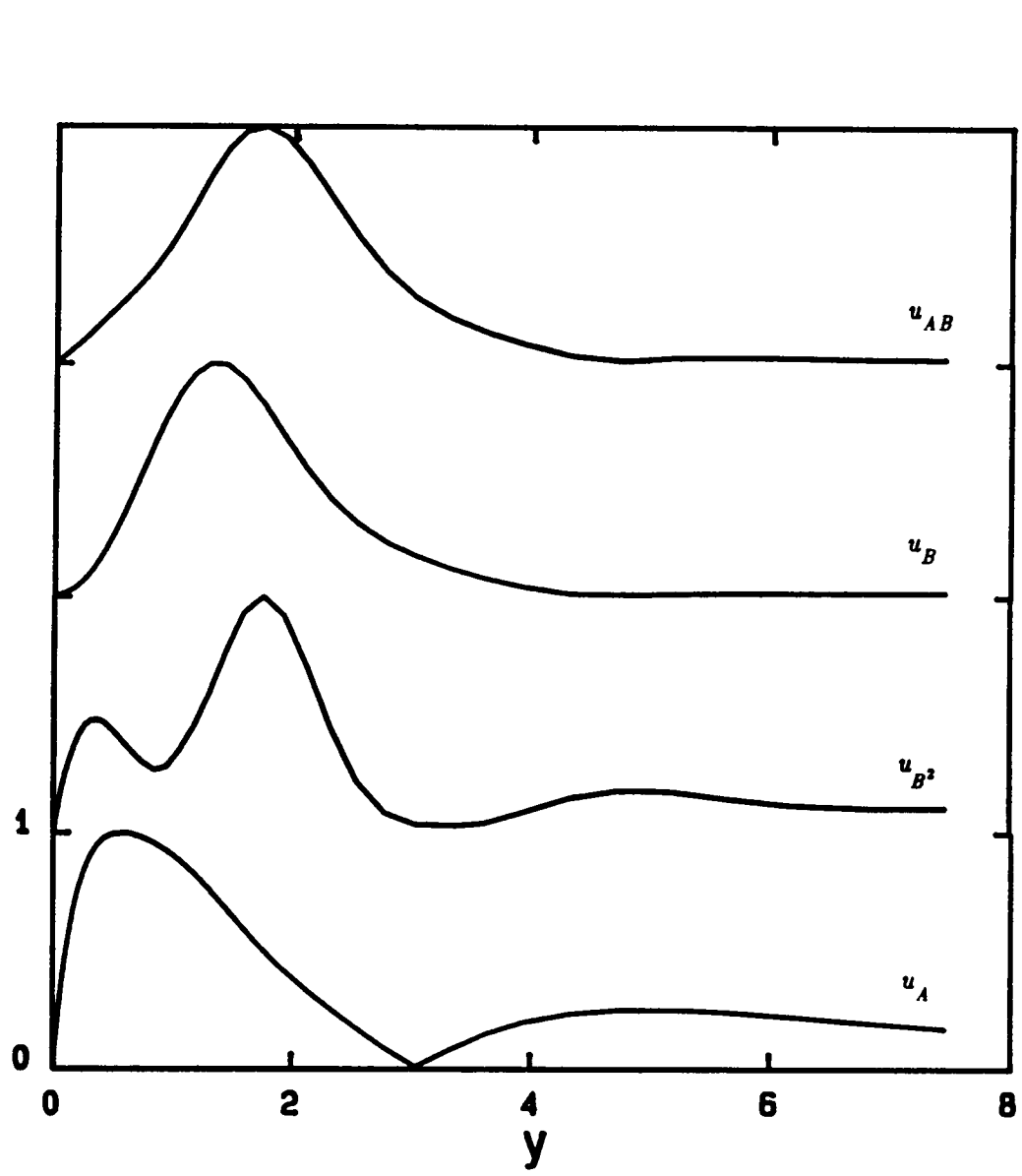

Figure 4.30 Normalized velocity functions u_A, u_{B^2}, u_B, and u_{AB} at fixed $R = 650$. Results for the subharmonic mode at $F = 124$, $b = .33$, and $\Delta = .05$, with initial values $A = .00782$ and $B = .000053$ at $R = 510$.

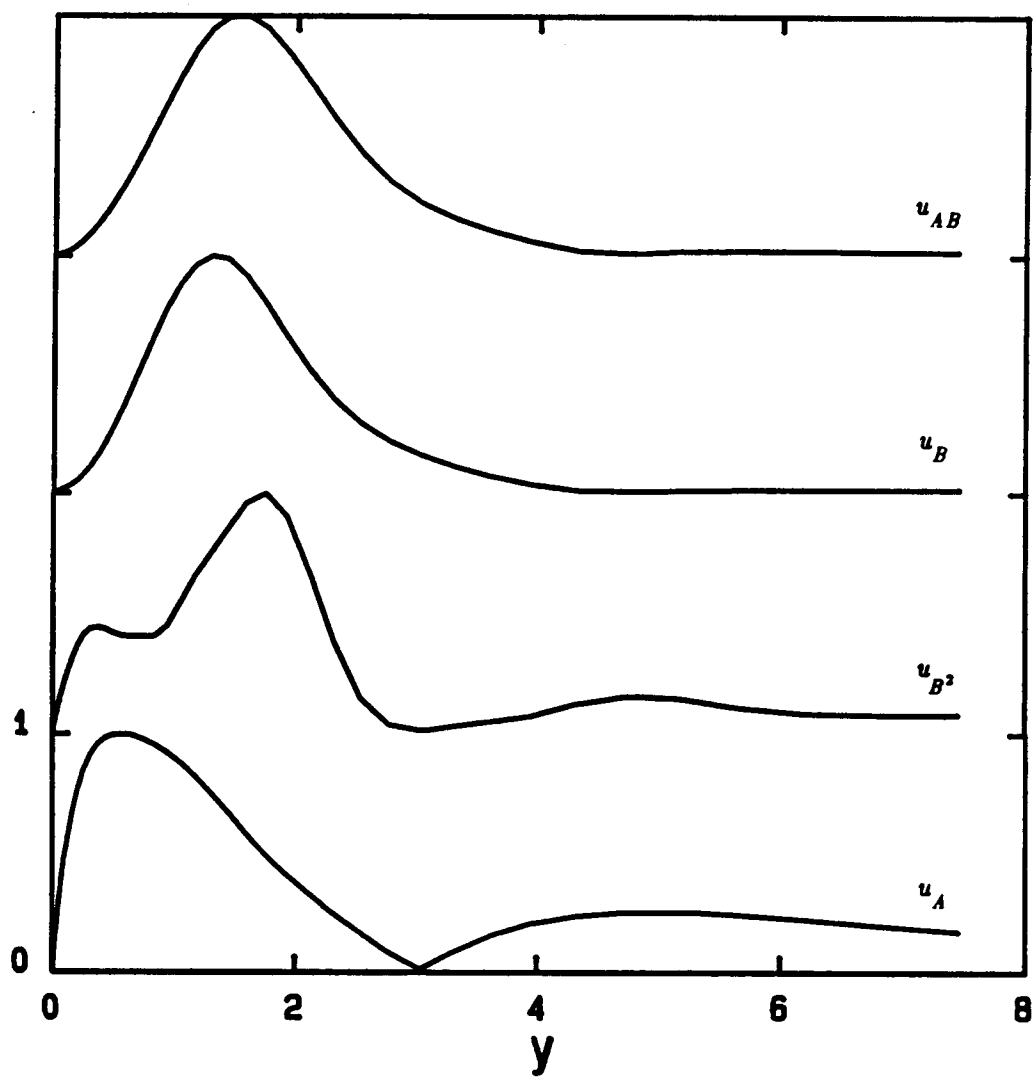

Figure 4.31 Normalized velocity functions u_A, u_{B^2}, u_B, and u_{AB} at fixed $R = 660$. Results for the subharmonic mode at $F = 124$, $b = .33$, and $\Delta = .05$, with initial values $A = .00782$ and $B = .000053$ at $R = 510$.

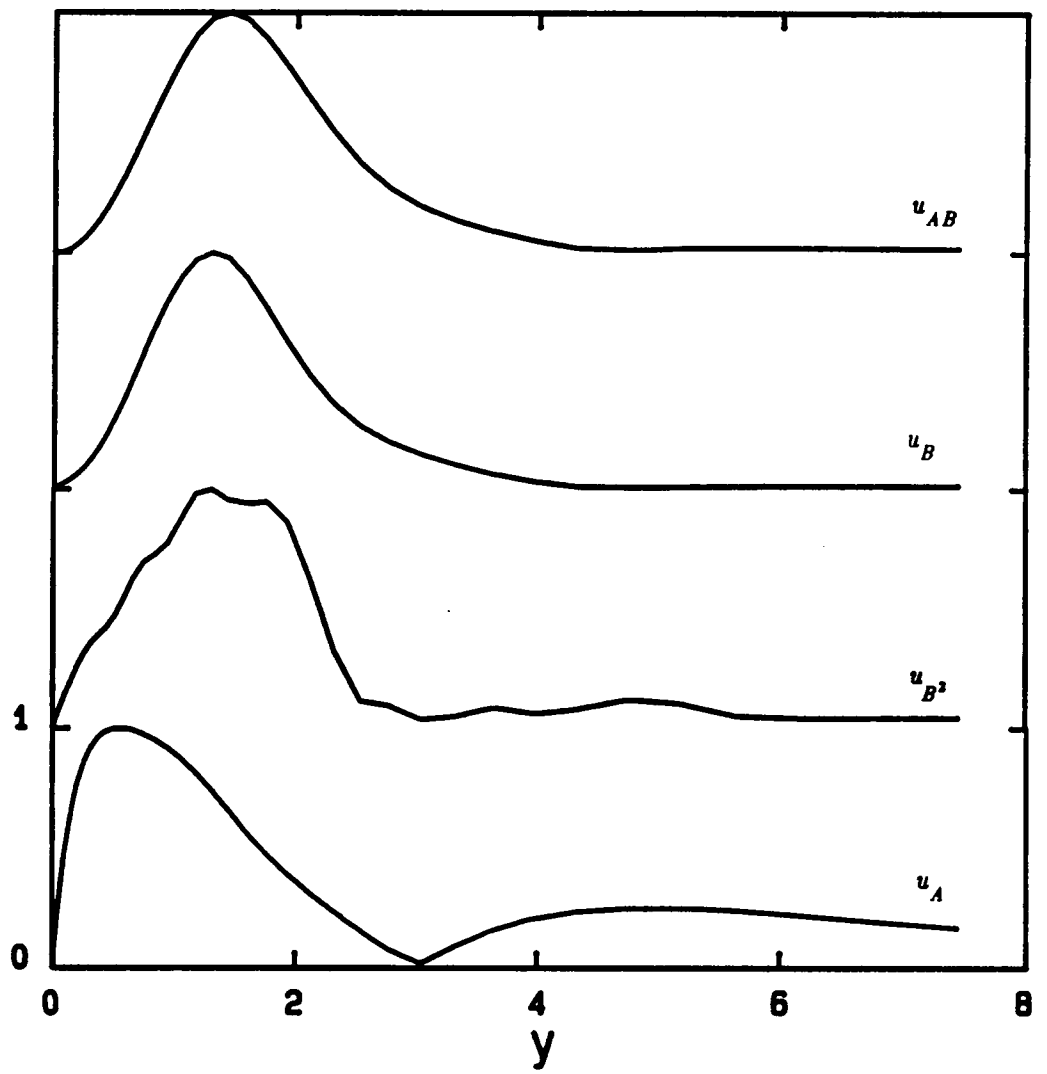

Figure 4.32 Normalized velocity functions u_A, u_{B^2}, u_B, and u_{AB} at fixed $R = 670$. Results for the subharmonic mode at $F = 124$, $b = .33$. and $\Delta = .05$, with initial values $A = .00782$ and $B = .000053$ at $R = 510$.

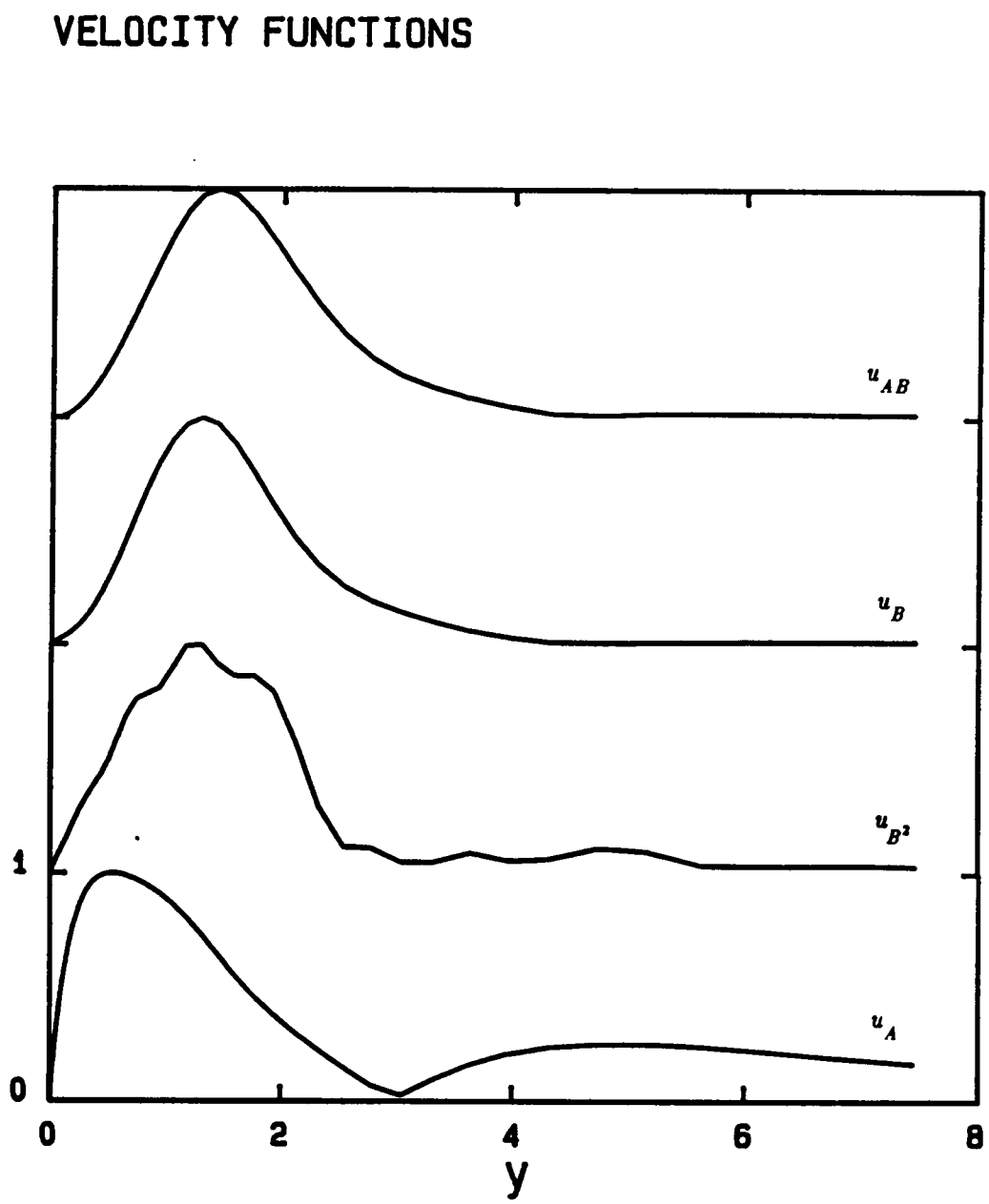

Figure 4.33 Normalized velocity functions u_A, u_{B^2}, u_B, and u_{AB} at fixed $R = 680$. Results for the subharmonic mode at $F = 124$, $b = .33$. and $\Delta = .05$, with initial values $A = .00782$ and $B = .000053$ at $R = 510$.

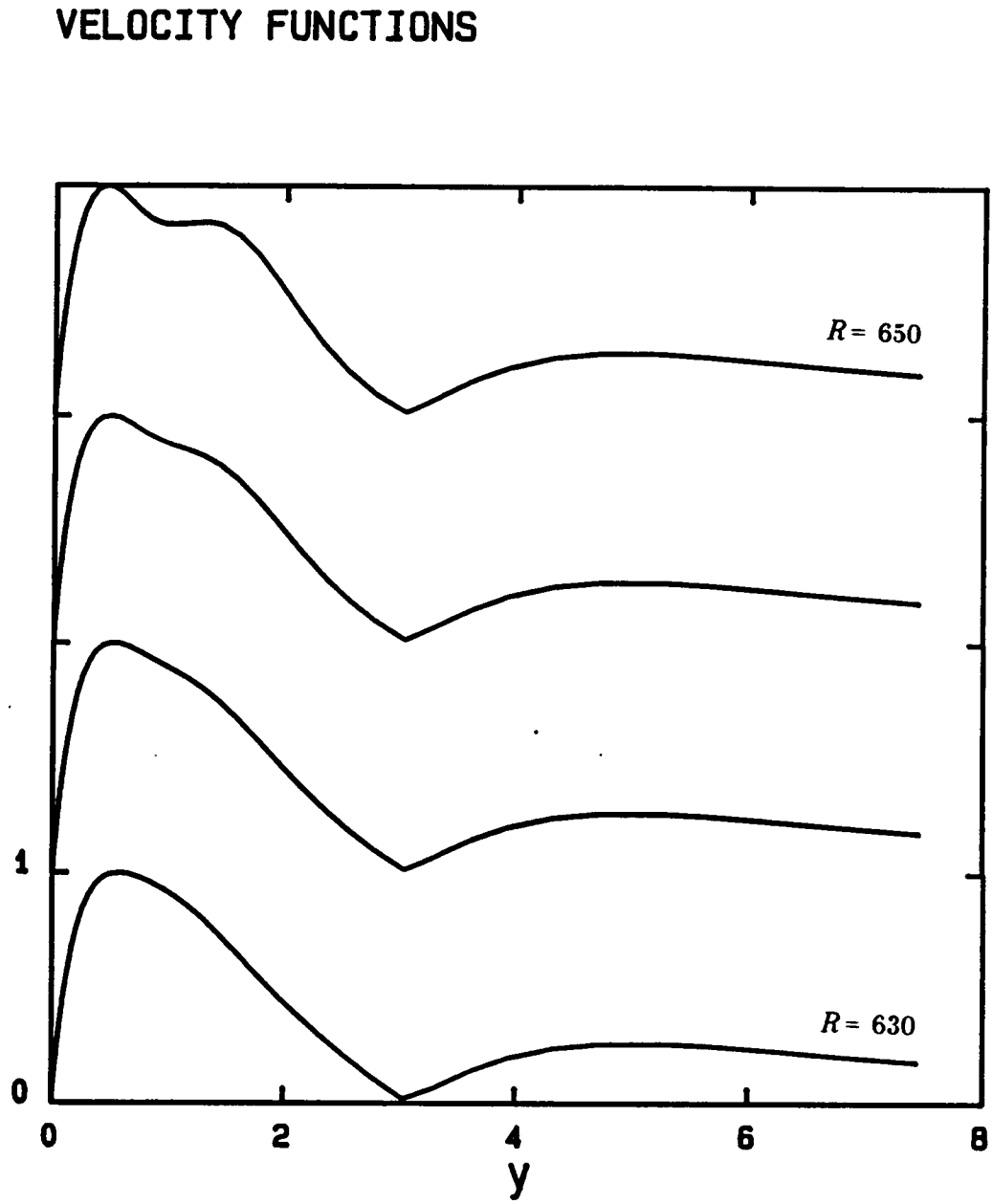

Figure 4.34 Evolution of the total two-dimensional velocity function, u_{2D}. Normalized functions at $R = 630, 640, 645, 650$. Results for the subharmonic mode at $F = 124$, $b = .33$, and $\Delta = .05$, with initial values $A = .00782$ and $B = .000053$ at $R = 510$.

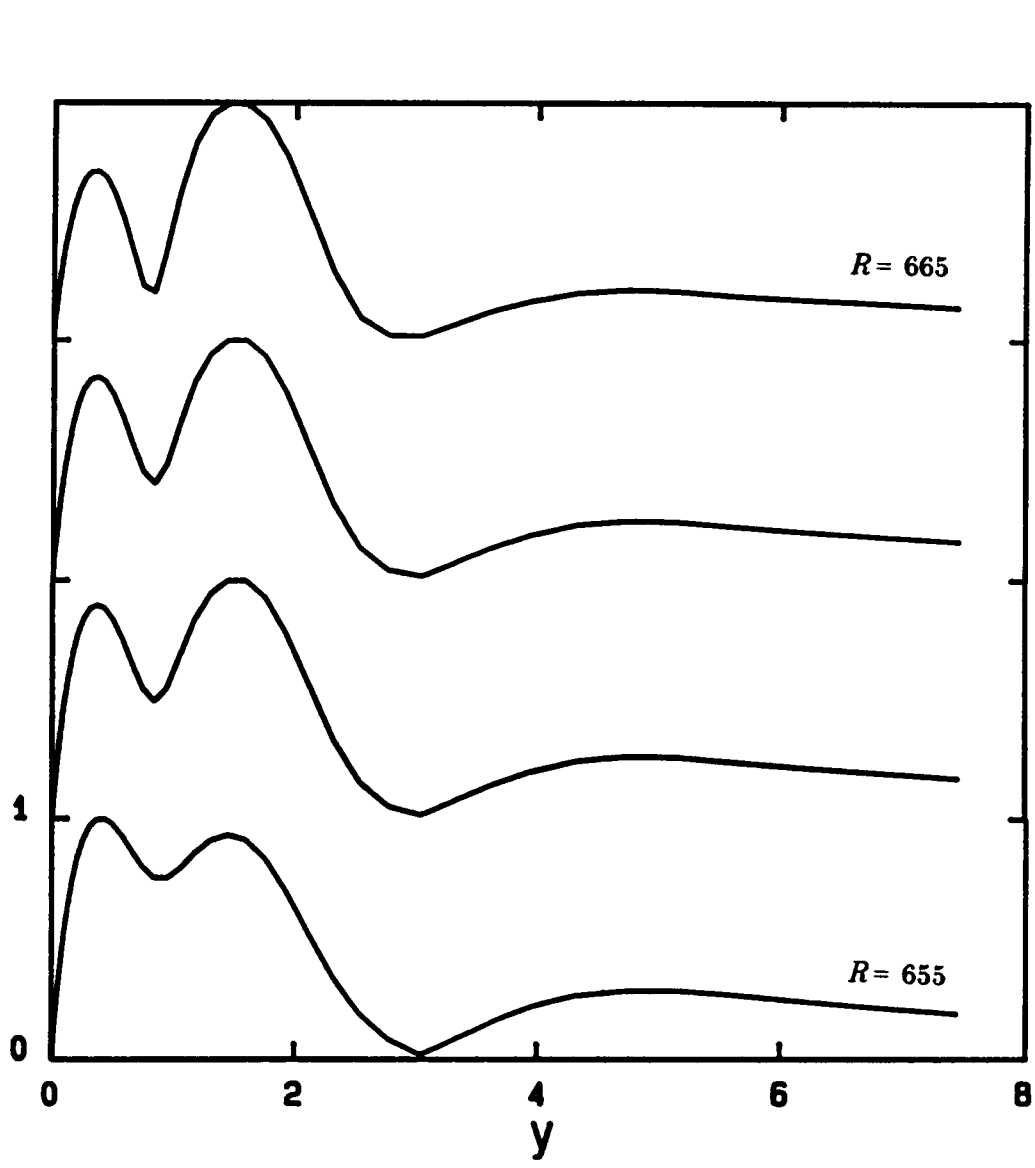

Figure 4.35 Evolution of the total two-dimensional velocity function, u_{2D}. Normalized functions at $R = 655, 660, 662, 665$. Results for the subharmonic mode at $F = 124$, $b = .33$, and $\Delta = .05$, with initial values $A = .00782$ and $B = .000053$ at $R = 510$.

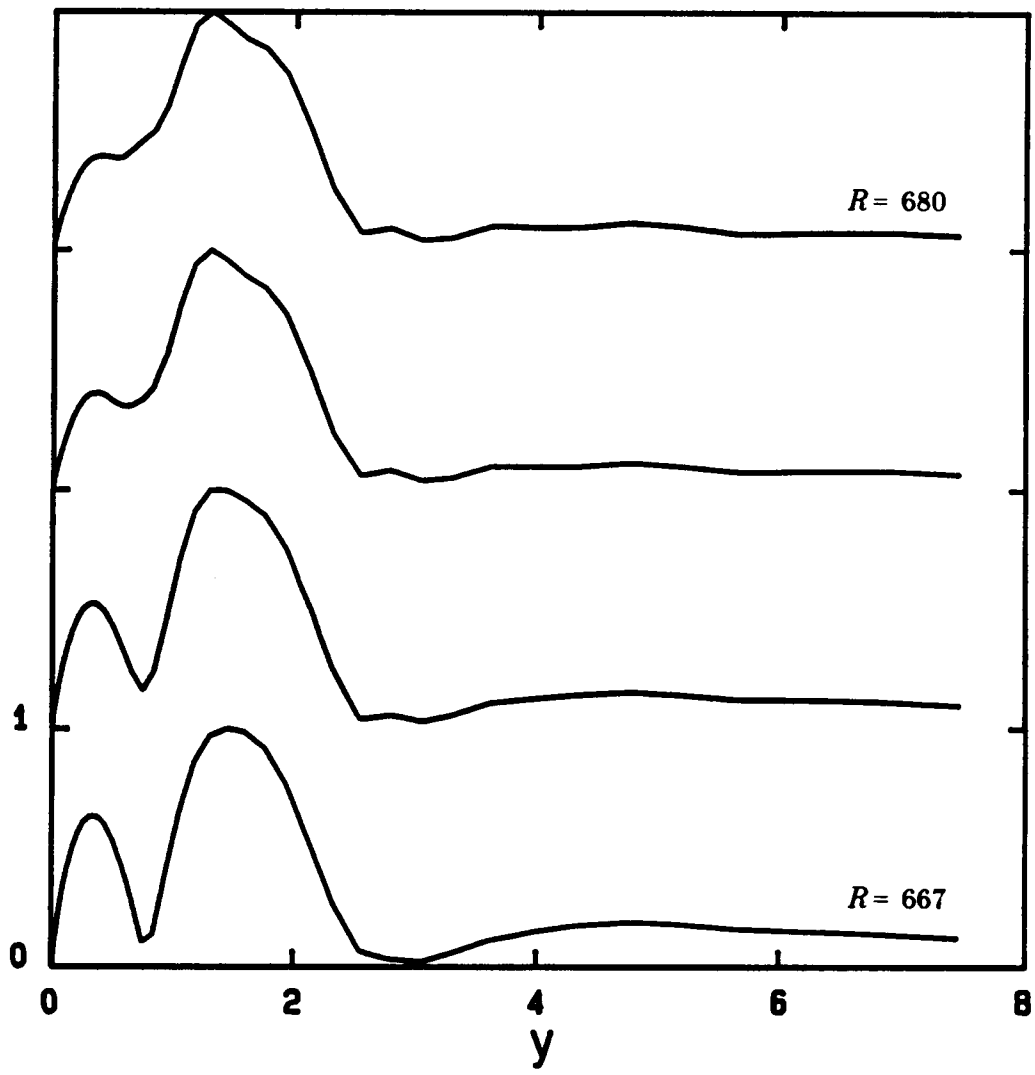

Figure 4.36 Evolution of the total two-dimensional velocity function, u_{2D}. Normalized functions at $R = 667, 670, 675, 680$. Results for the subharmonic mode at $F = 124$, $b = .33$, and $\Delta = .05$, with initial values $A = .00782$ and $B = .000053$ at $R = 510$.

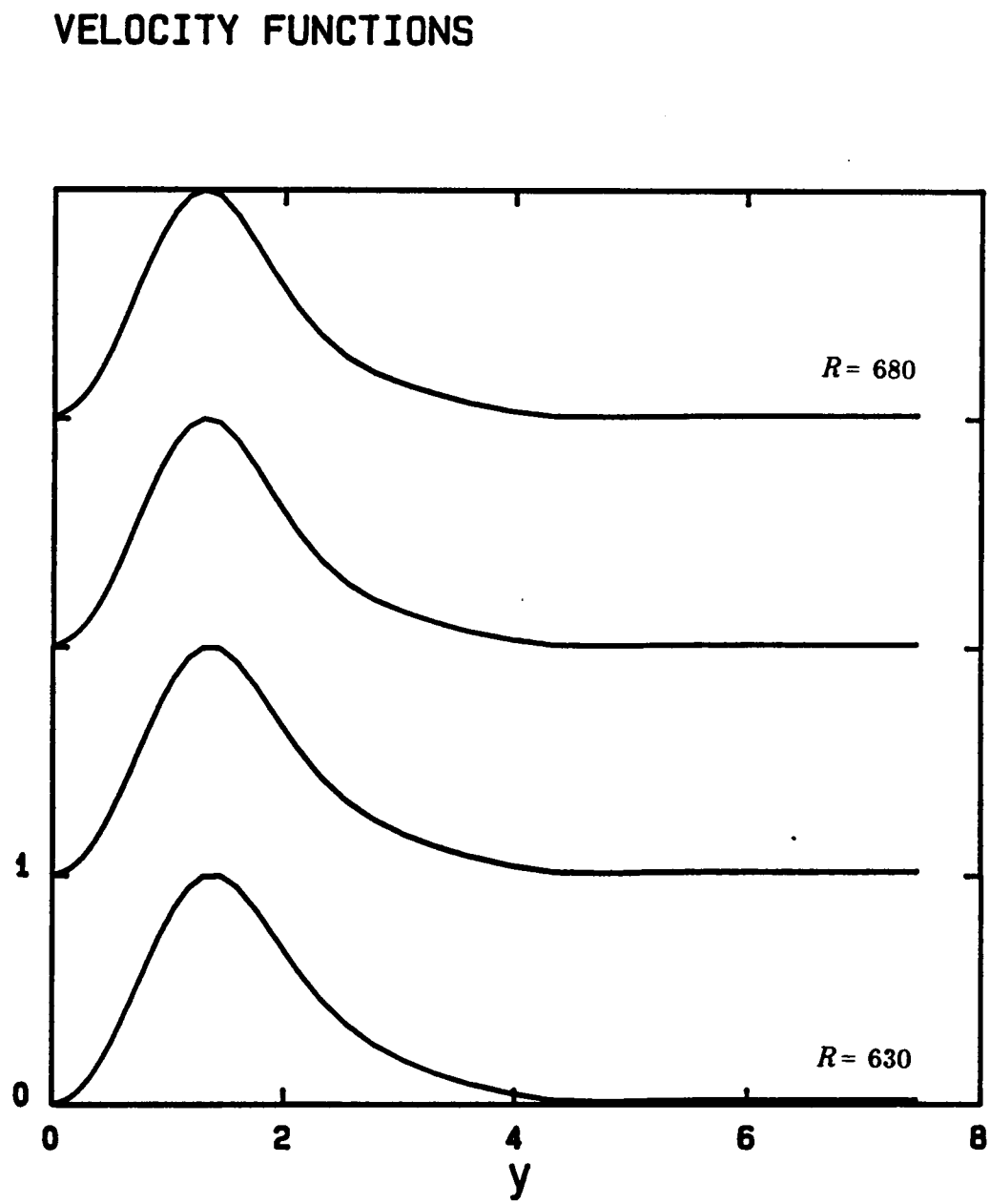

Figure 4.37 Evolution of the total subharmonic velocity function, u_s. Normalized functions at $R = 630, 650, 665, 680$. Results for the subharmonic mode at $F = 124$, $b = .33$, and $\Delta = .05$, with initial values $A = .00782$ and $B = .000053$ at $R = 510$.

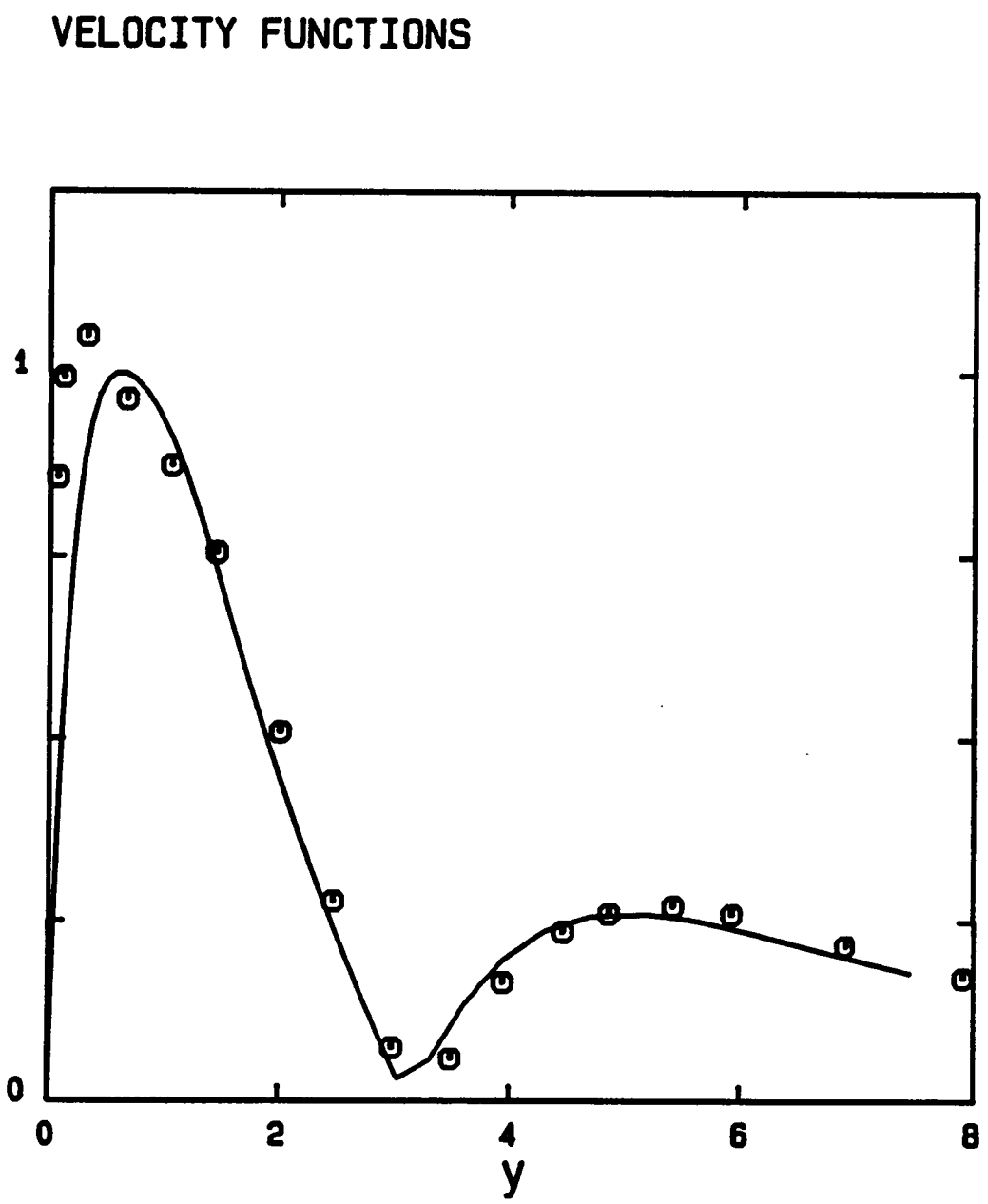

Figure 4.38 Comparison of the total two-dimensional velocity function, u_{2D}, with the experiments of Kachanov and Levchenko (1984). figure 22. Normalized function at $R = 608$. Results for the subharmonic mode at $F = 124$, $b = .33$, and $\Delta = .05$, with initial values $A = .00782$ and $B = .000053$ at $R = 510$.

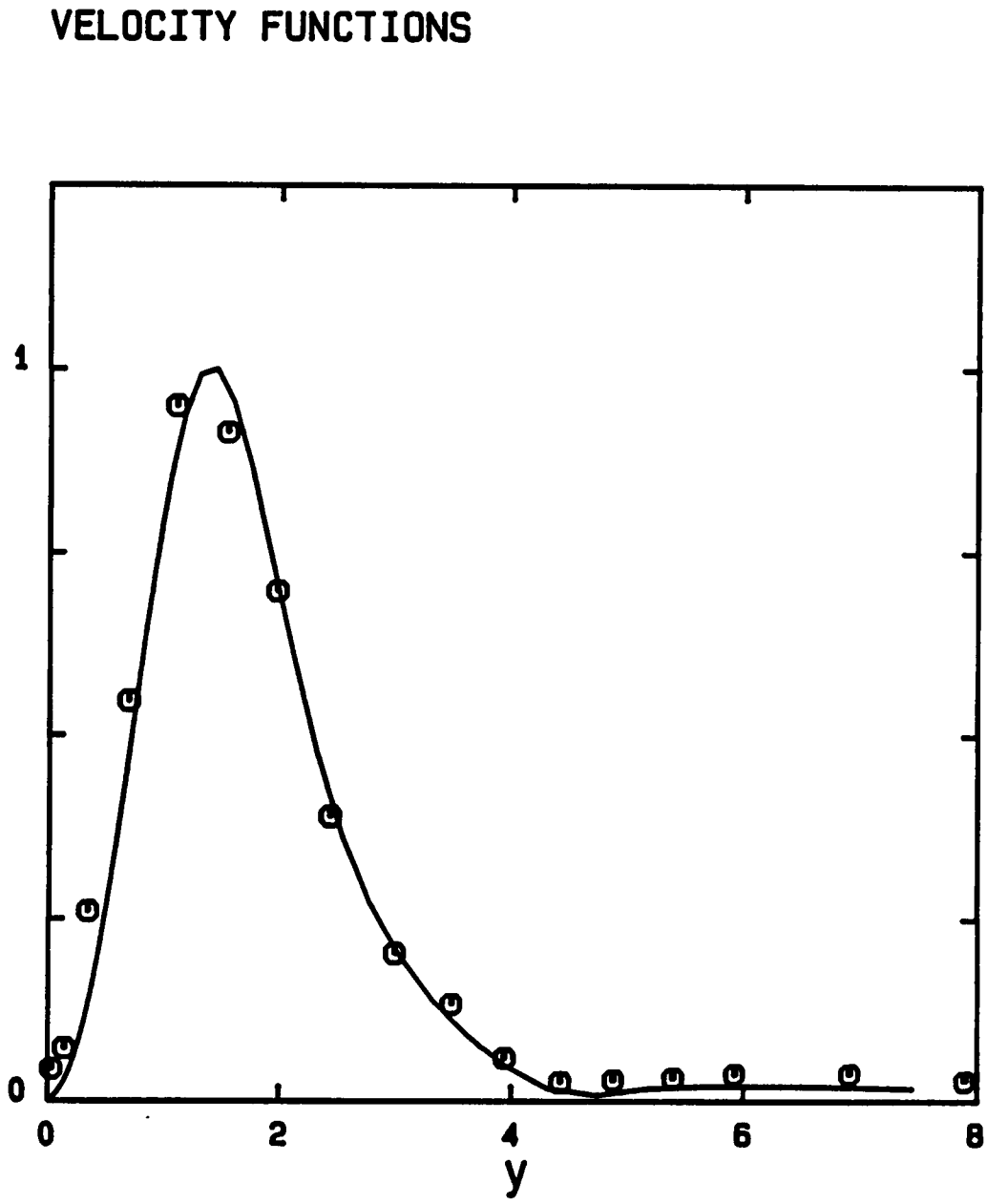

Figure 4.39 Comparison of the total subharmonic velocity function, u_S, with the experiments of Kachanov and Levchenko (1984), figure 22. Normalized function at $R = 608$. Results for the subharmonic mode at $F = 124$, $b = .33$, and $\Delta = .05$, with initial values $A = .00782$ and $B = .000053$ at $R = 510$.

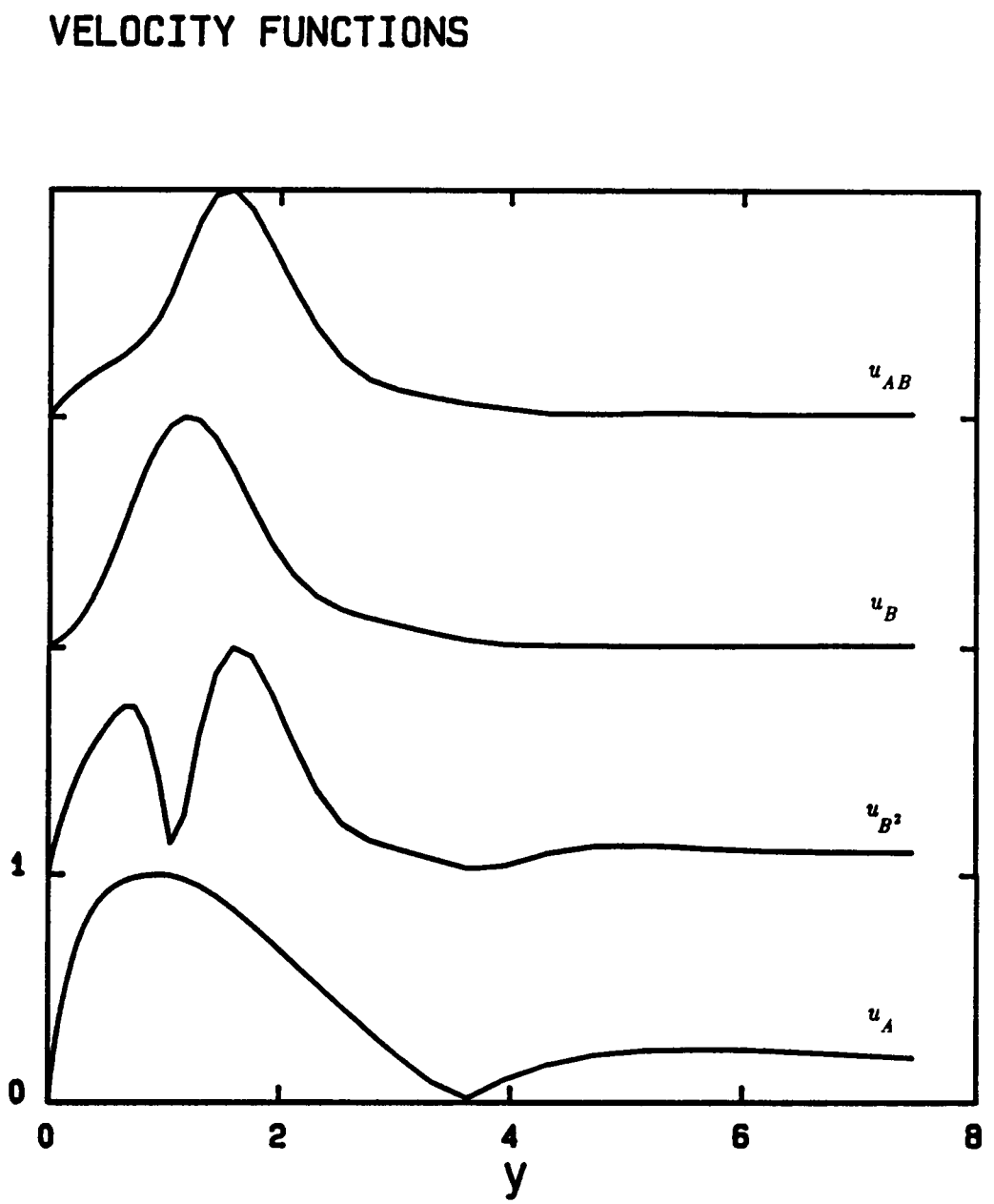

Figure 4.40 Normalized velocity functions u_A, u_{B^2}, u_B, and u_{AB} at fixed $R = 725$. Results for the fundamental mode at $F = 64.4$, $b = .44$, and $\Delta = .05$, with initial values $A = .016$ and $B = .0015$ at $R = 675$.

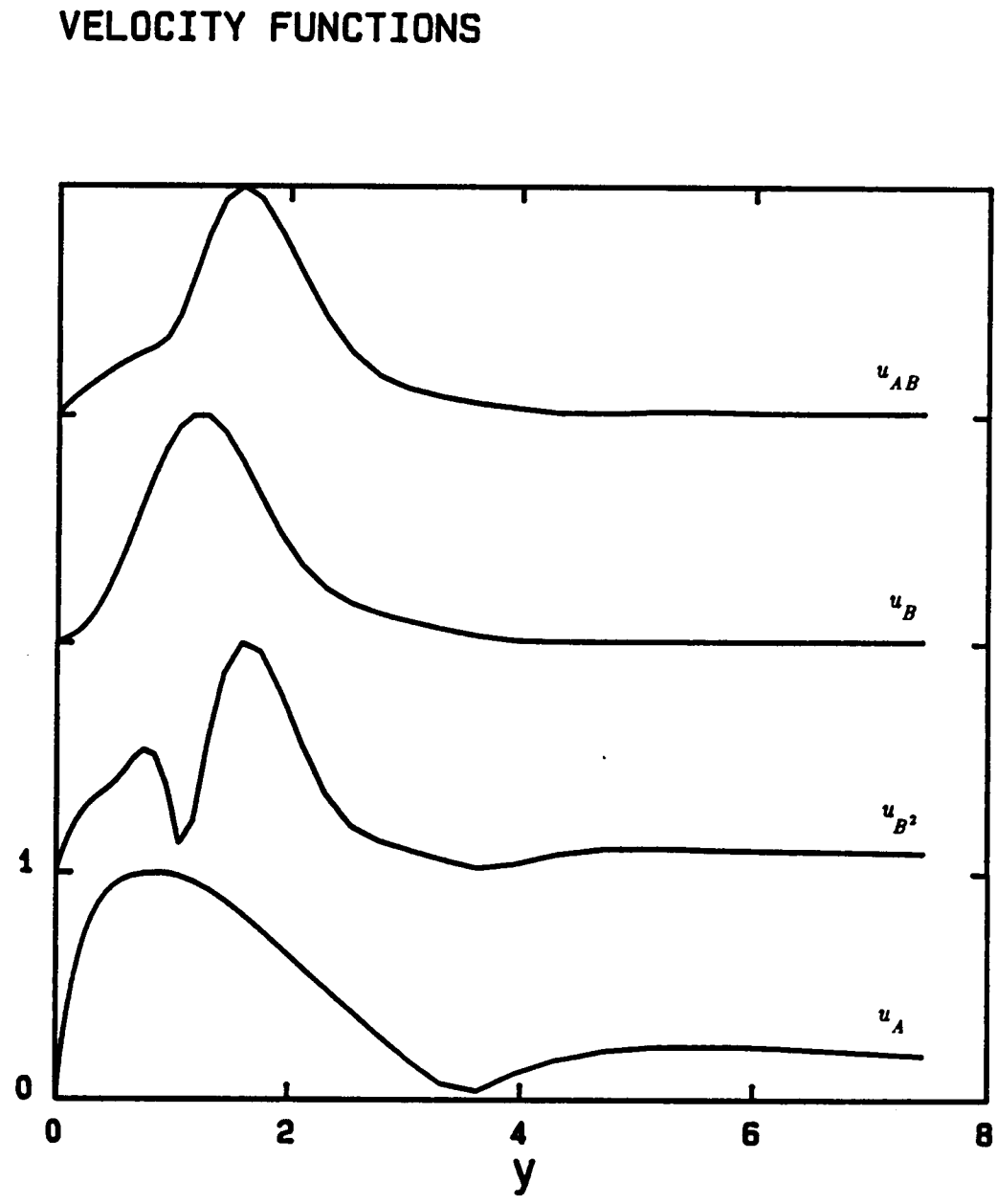

Figure 4.41 Normalized velocity functions u_A, u_{B^2}, u_B, and u_{AB} at fixed $R = 765$. Results for the fundamental mode at $F = 64.4$, $b = .44$, and $\Delta = .05$, with initial values $A = .016$ and $B = .0015$ at $R = 675$.

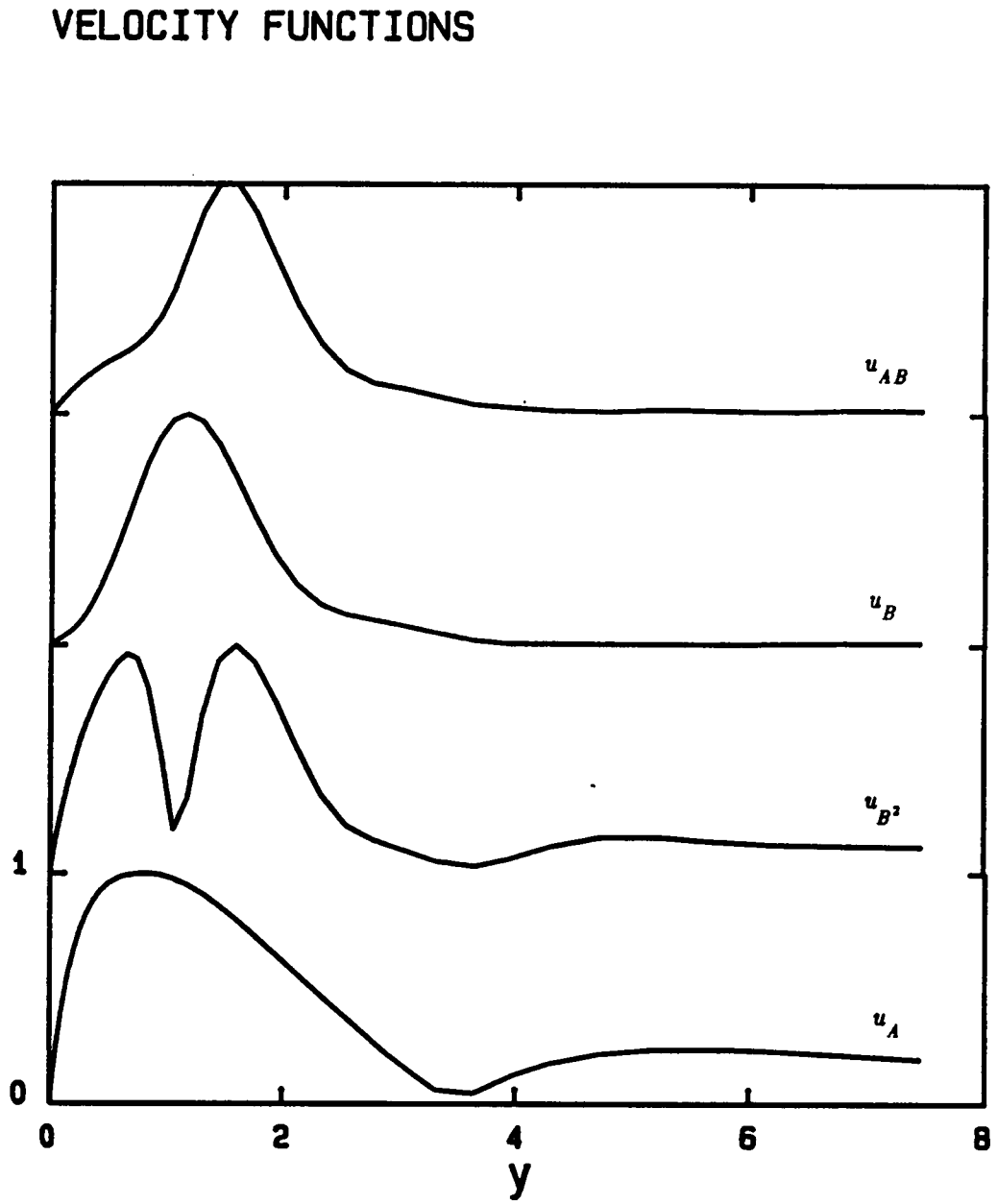

Figure 4.42 Normalized velocity functions u_A, u_{B^2}, u_B, and u_{AB} at fixed $R = 785$. Results for the fundamental mode at $F = 64.4$, $b = .44$, and $\Delta = .05$, with initial values $A = .016$ and $B = .0015$ at $R = 675$.

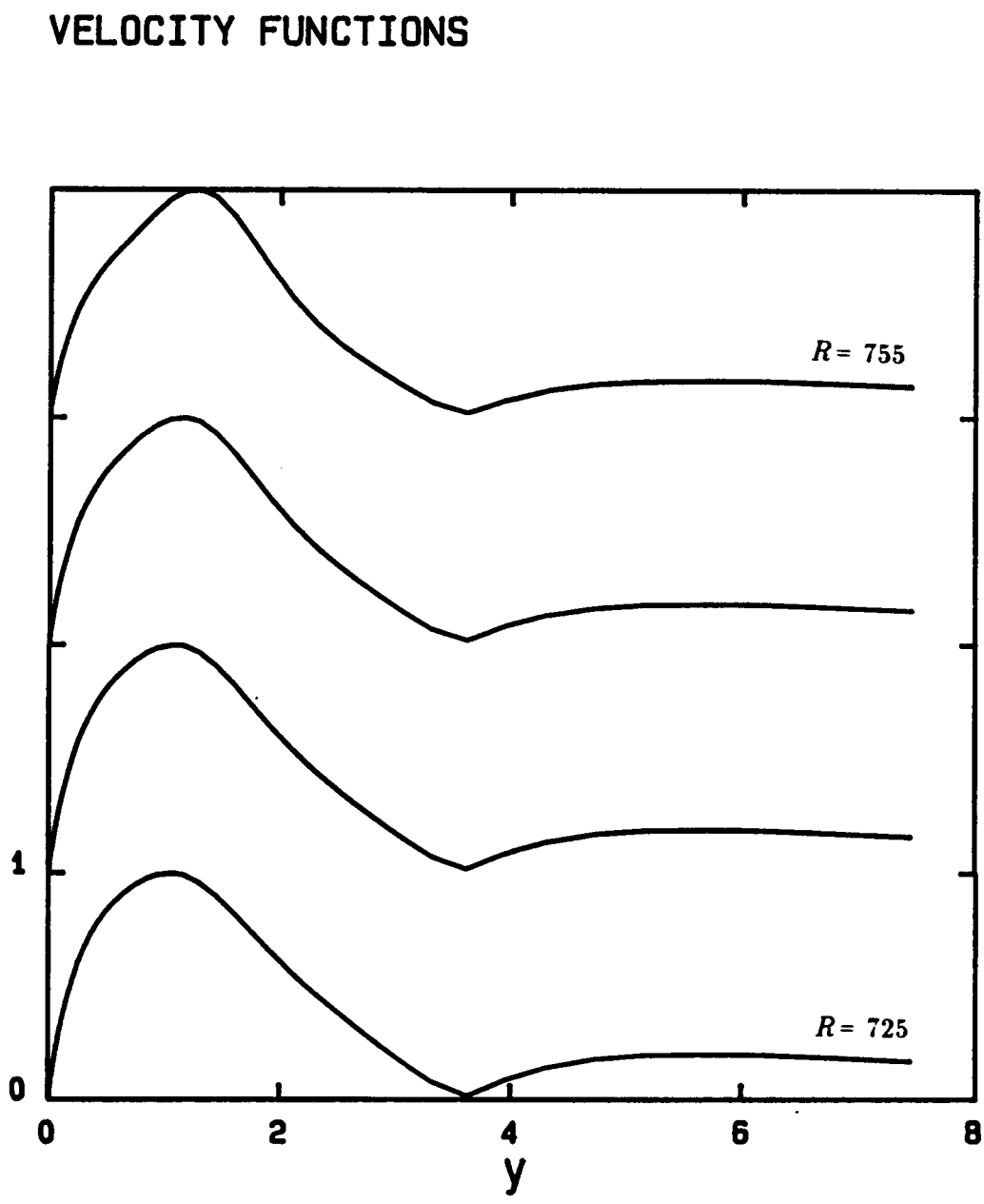

Figure 4.43 Evolution of the total peak velocity function, u_p. Normalized functions at R= 725, 735, 745, 755. Results for the fundamental mode at F= 64.4, b= .44, and Δ= .05, with initial values A= .016 and B= .0015 at R= 675.

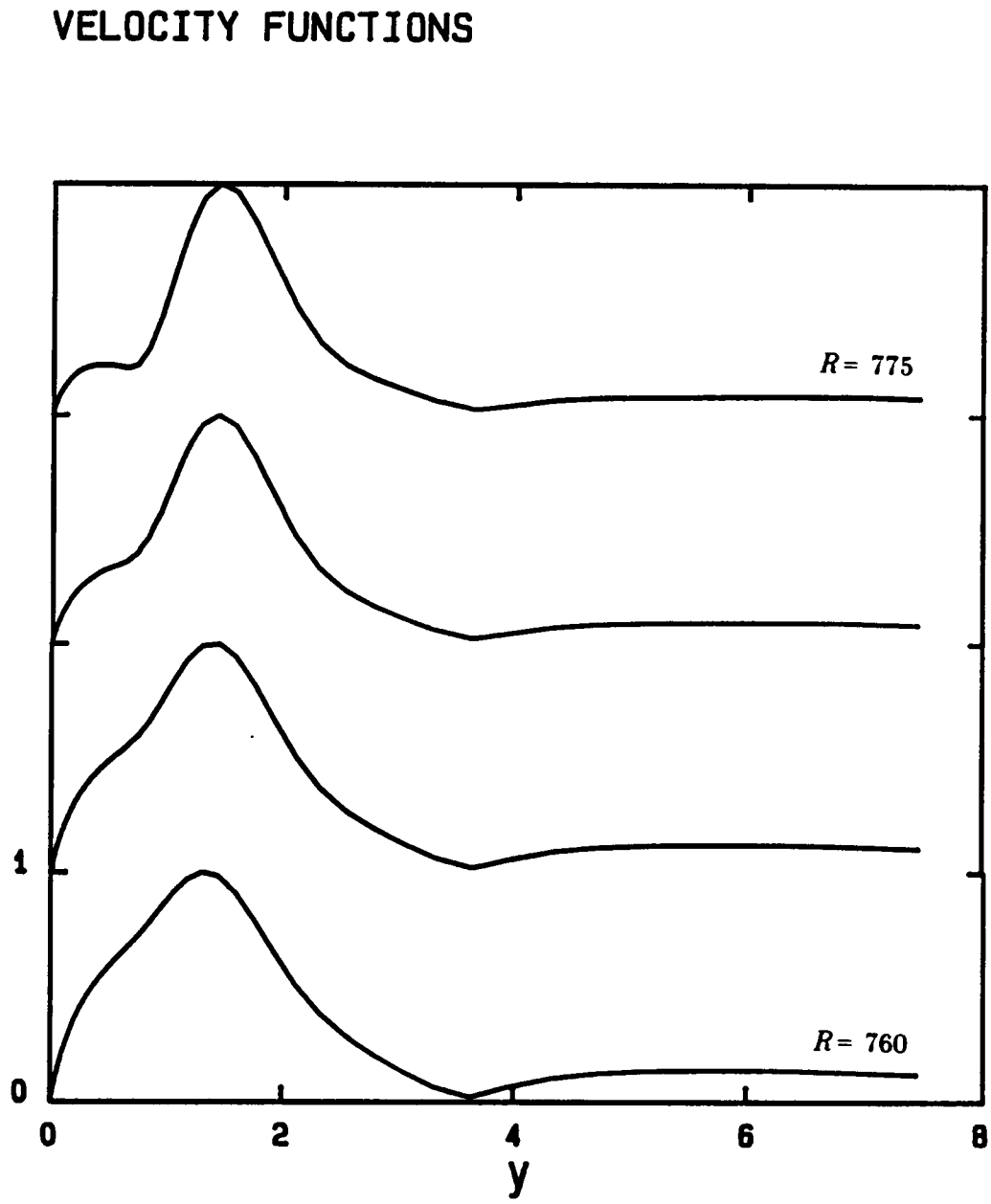

Figure 4.44 Evolution of the total peak velocity function, u_p. Normalized functions at R= 760, 765, 770, 775. Results for the fundamental mode at F= 64.4, b= .44, and Δ= .05, with initial values A= .016 and B= .0015 at R= 675.

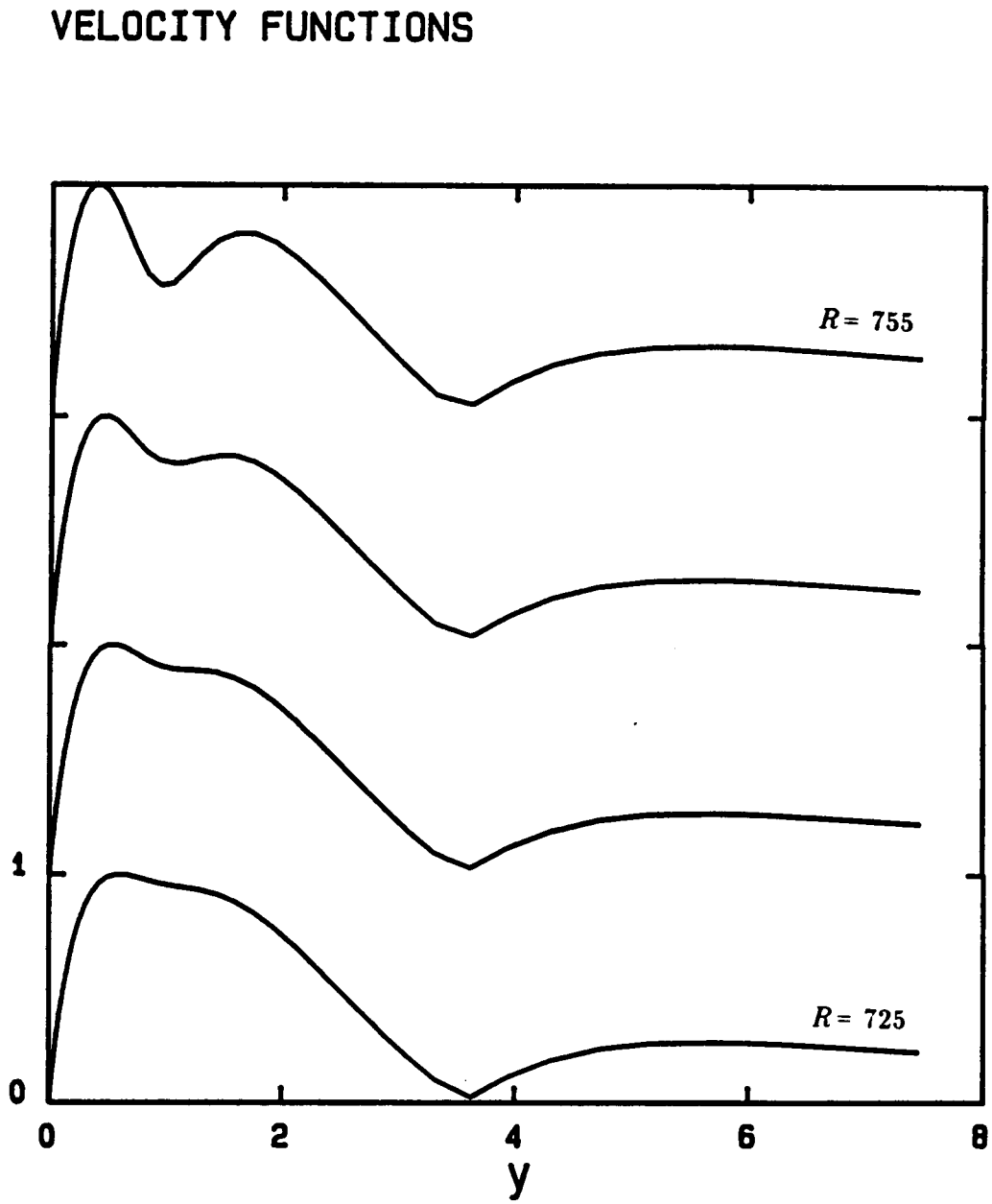

Figure 4.45 Evolution of the total valley velocity function, u_V. Normalized functions at R= 725, 735, 745, 755. Results for the fundamental mode at F= 64.4, b= .44, and Δ= .05, with initial values A= .016 and B= .0015 at R= 675.

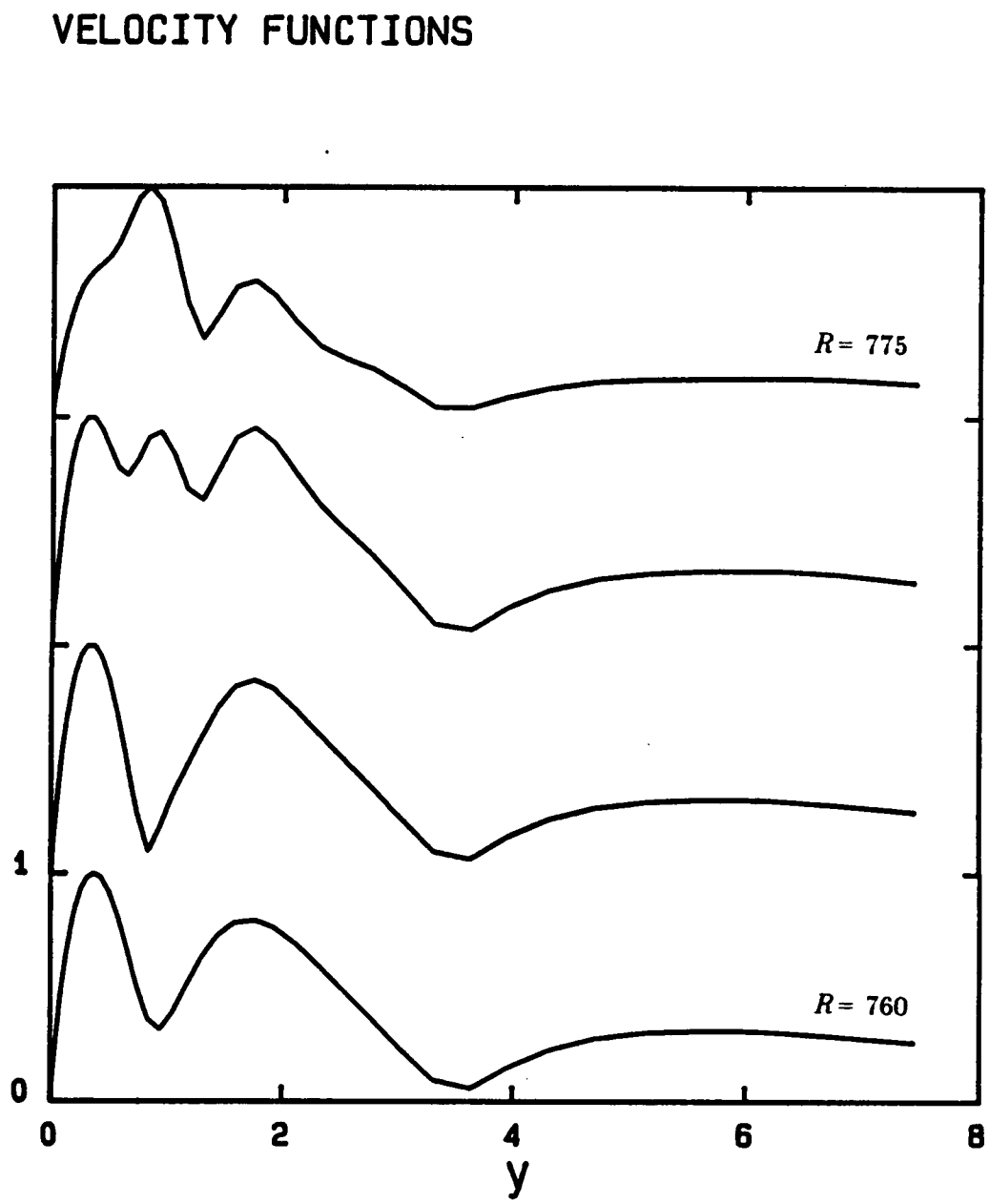

Figure 4.46 Evolution of the total valley velocity function, u_V. Normalized functions at R= 760, 765, 770, 775. Results for the fundamental mode at F= 64.4, b= .44, and Δ= .05, with initial values A= .016 and B= .0015 at R= 675.

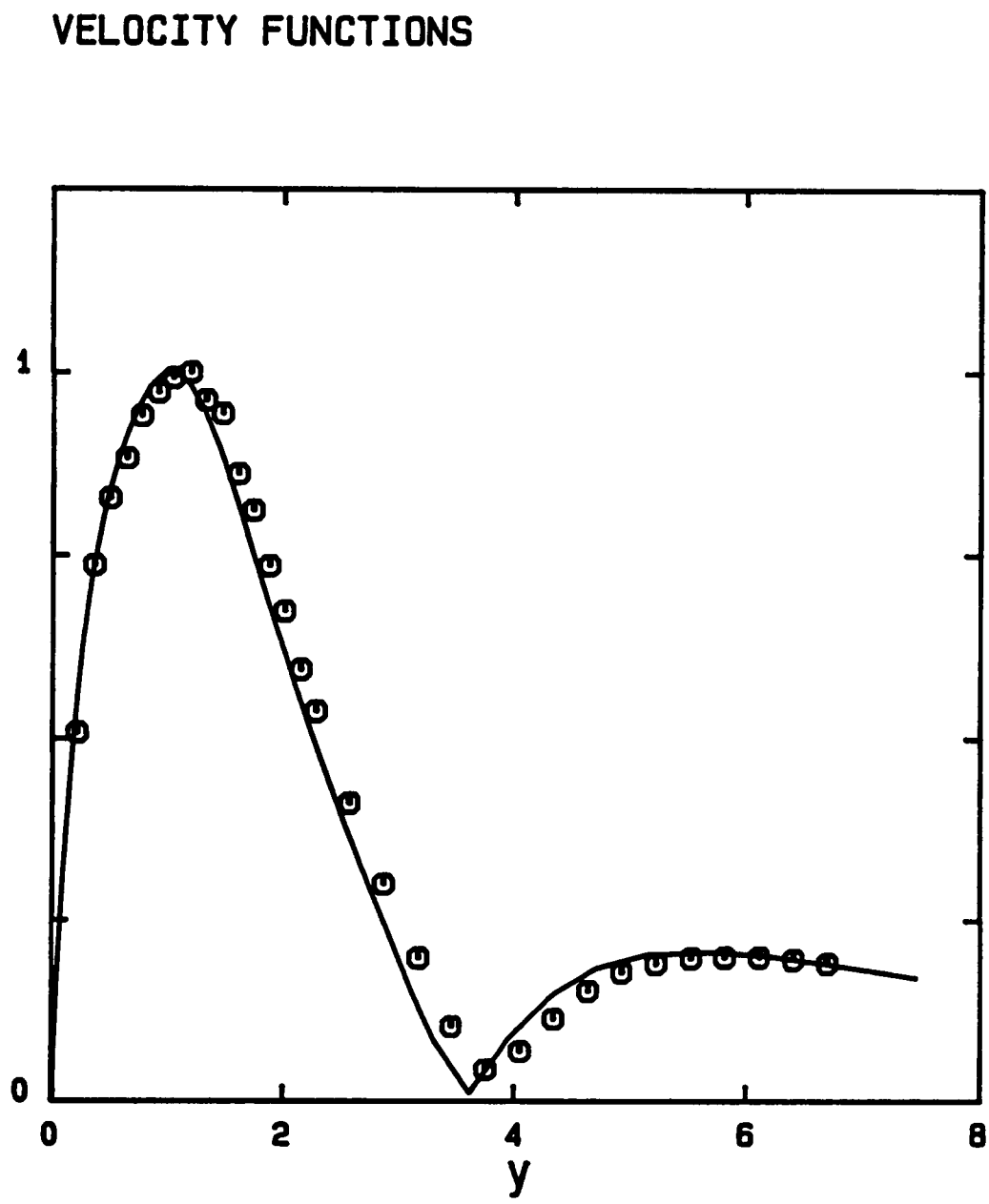

Figure 4.47 Comparison of the total peak velocity function, u_p, with the experiments of Cornelius (1985), figure 16a. Normalized function at $R = 716$. Results for the fundamental mode at $F = 64.4$, $b = .44$, and $\Delta = .05$, with initial values $A = .016$ and $B = .0015$ at $R = 675$.

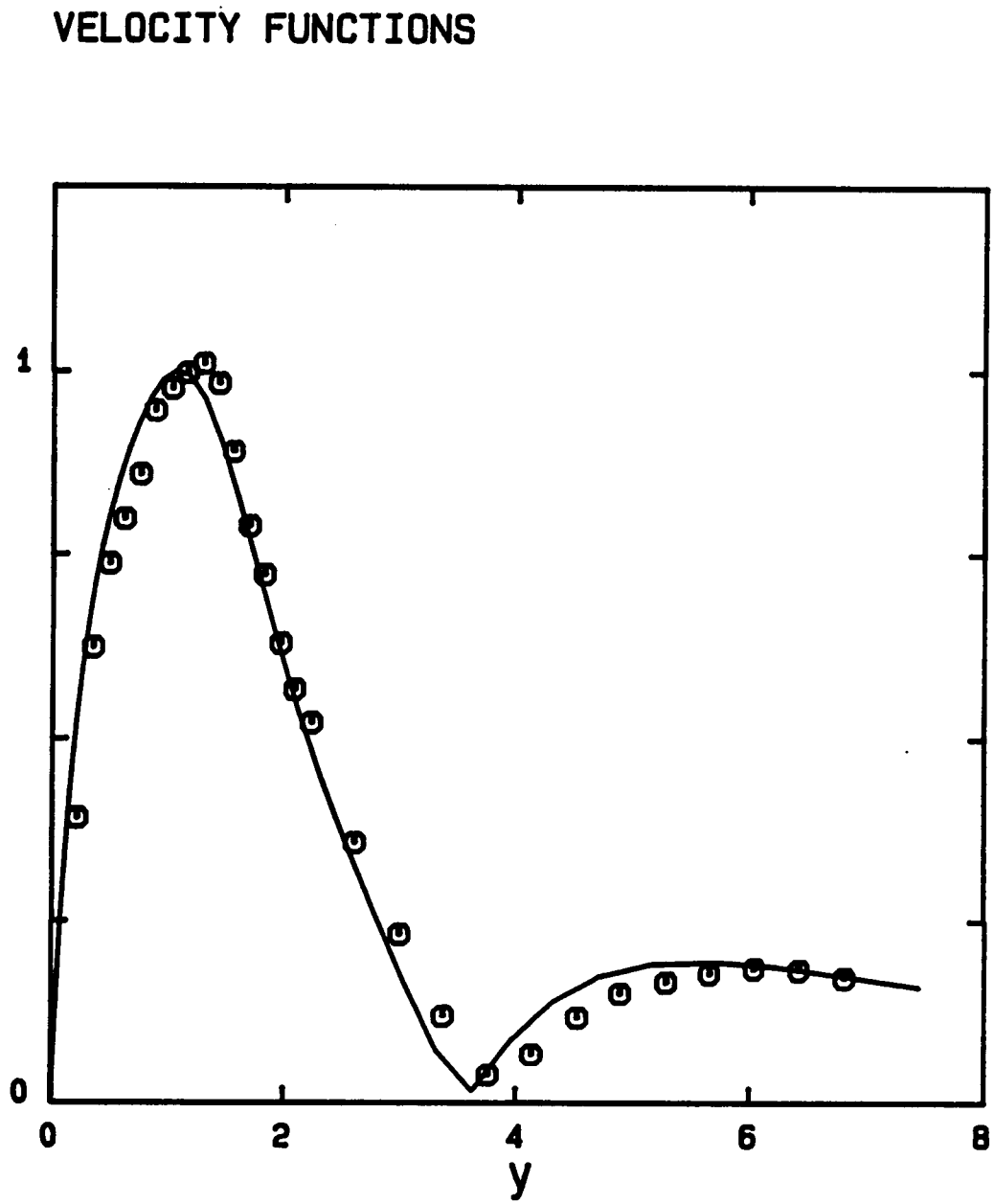

Figure 4.48 Comparison of the total peak velocity function, u_p, with the experiments of Cornelius (1985), figure 16b. Normalized function at $R = 735$. Results for the fundamental mode at $F = 64.4$, $b = .44$, and $\Delta = .05$, with initial values $A = .016$ and $B = .0015$ at $R = 675$.

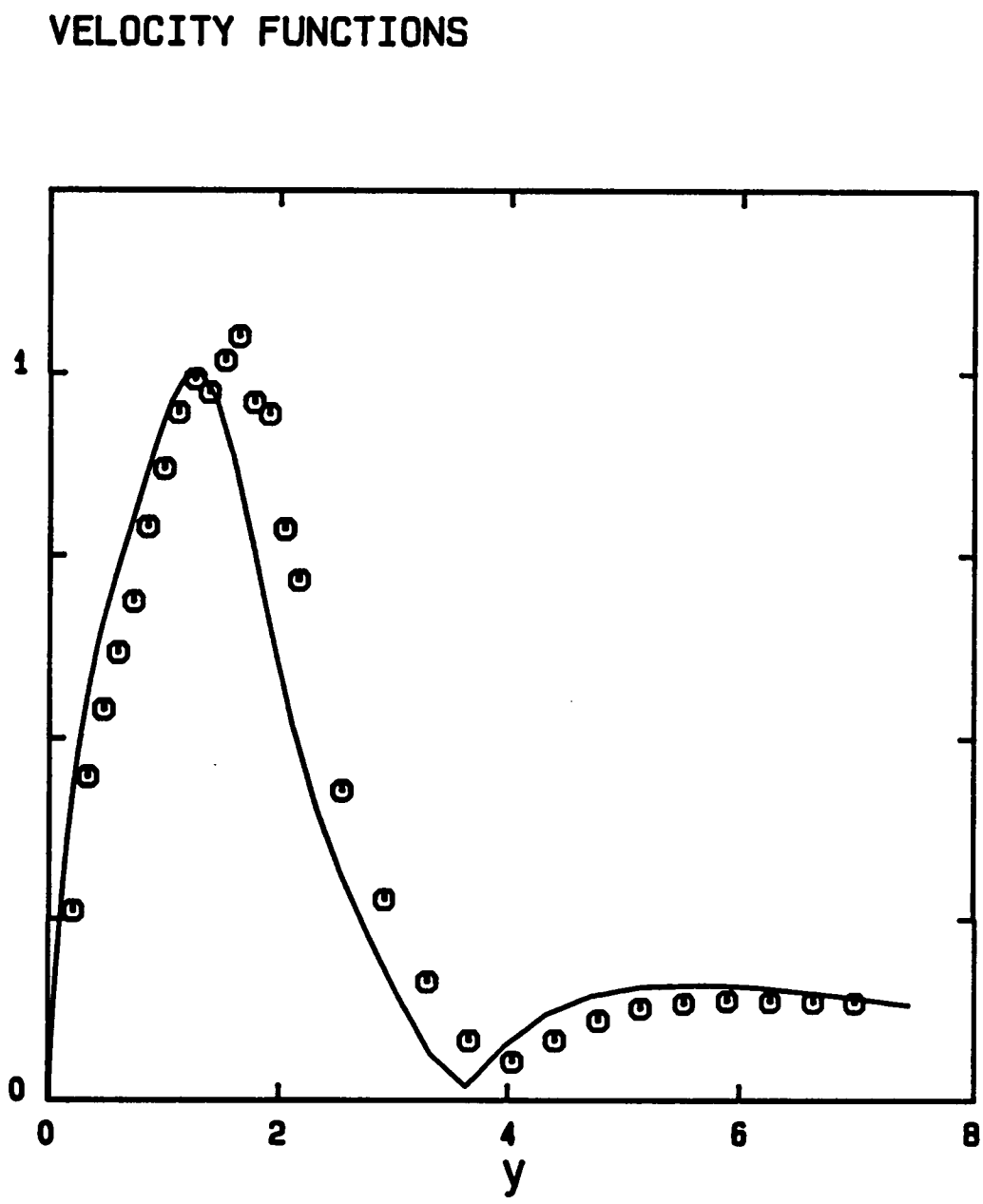

Figure 4.49 Comparison of the total peak velocity function, u_p, with the experiments of Cornelius (1985), figure 16b. Normalized function at $R = 755$. Results for the fundamental mode at $F = 64.4$, $b = .44$, and $\Delta = .05$, with initial values $A = .016$ and $B = .0015$ at $R = 675$.

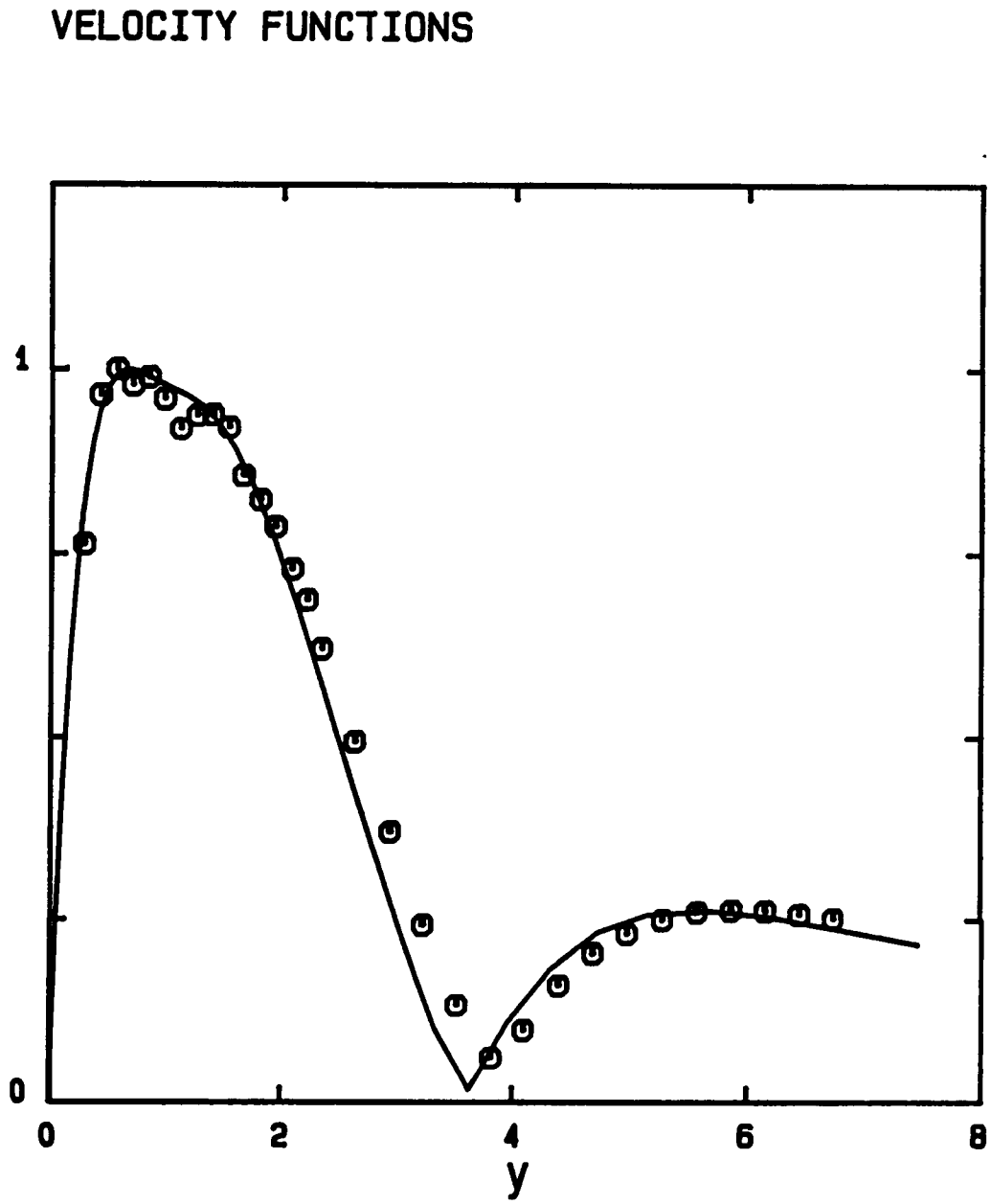

Figure 4.50 Comparison of the total valley velocity function. u_V, with the experiments of Cornelius (1985), figure 17a. Normalized function at $R = 716$. Results for the fundamental mode at $F = 64.4$, $b = .44$, and $\Delta = .05$, with initial values $A = .016$ and $B = .0015$ at $R = 675$.

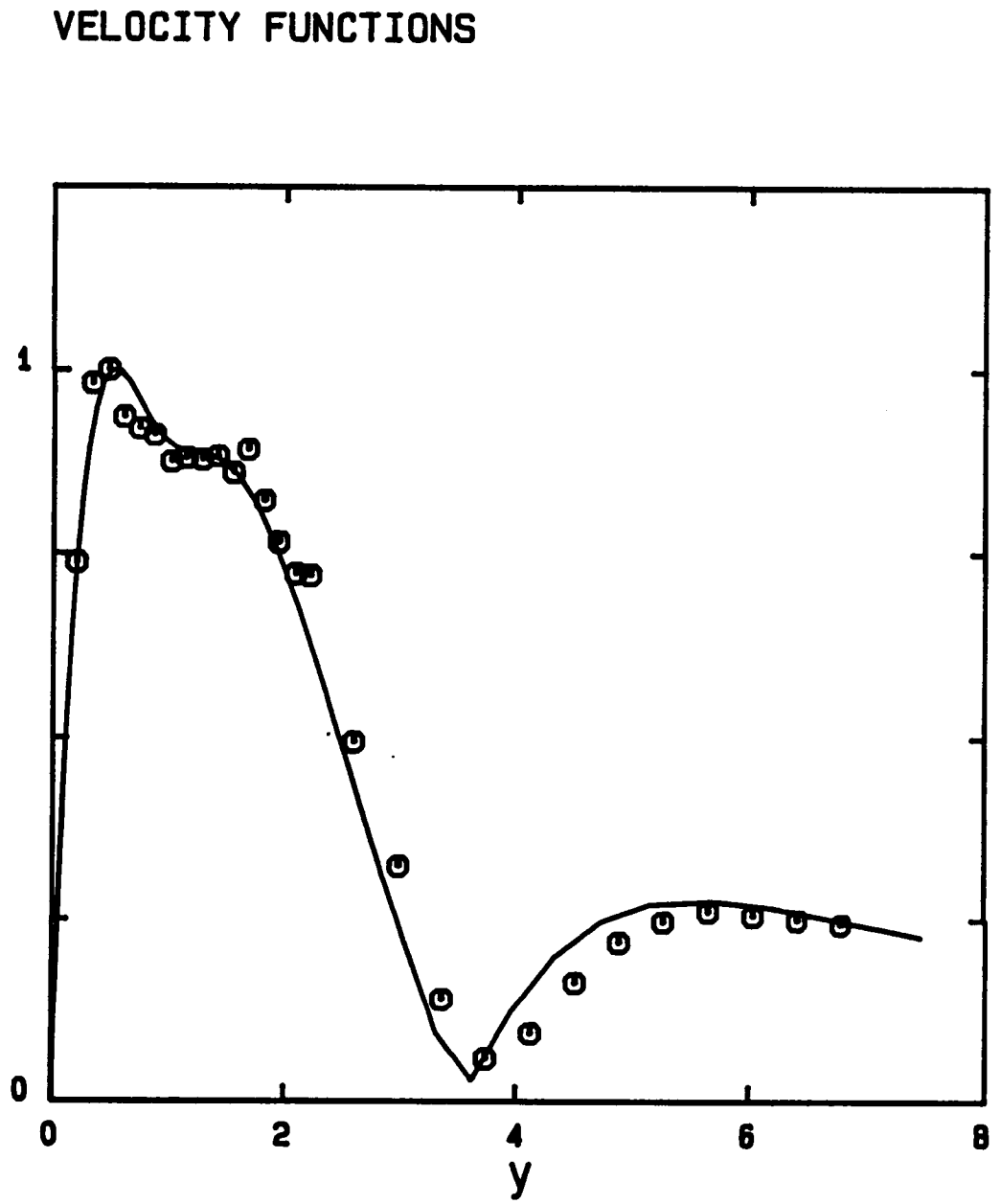

Figure 4.51 Comparison of the total valley velocity function, u_V, with the experiments of Cornelius (1985), figure 17b. Normalized function at $R = 735$. Results for the fundamental mode at $F = 64.4$, $b = .44$, and $\Delta = .05$, with initial values $A = .016$ and $B = .0015$ at $R = 675$.

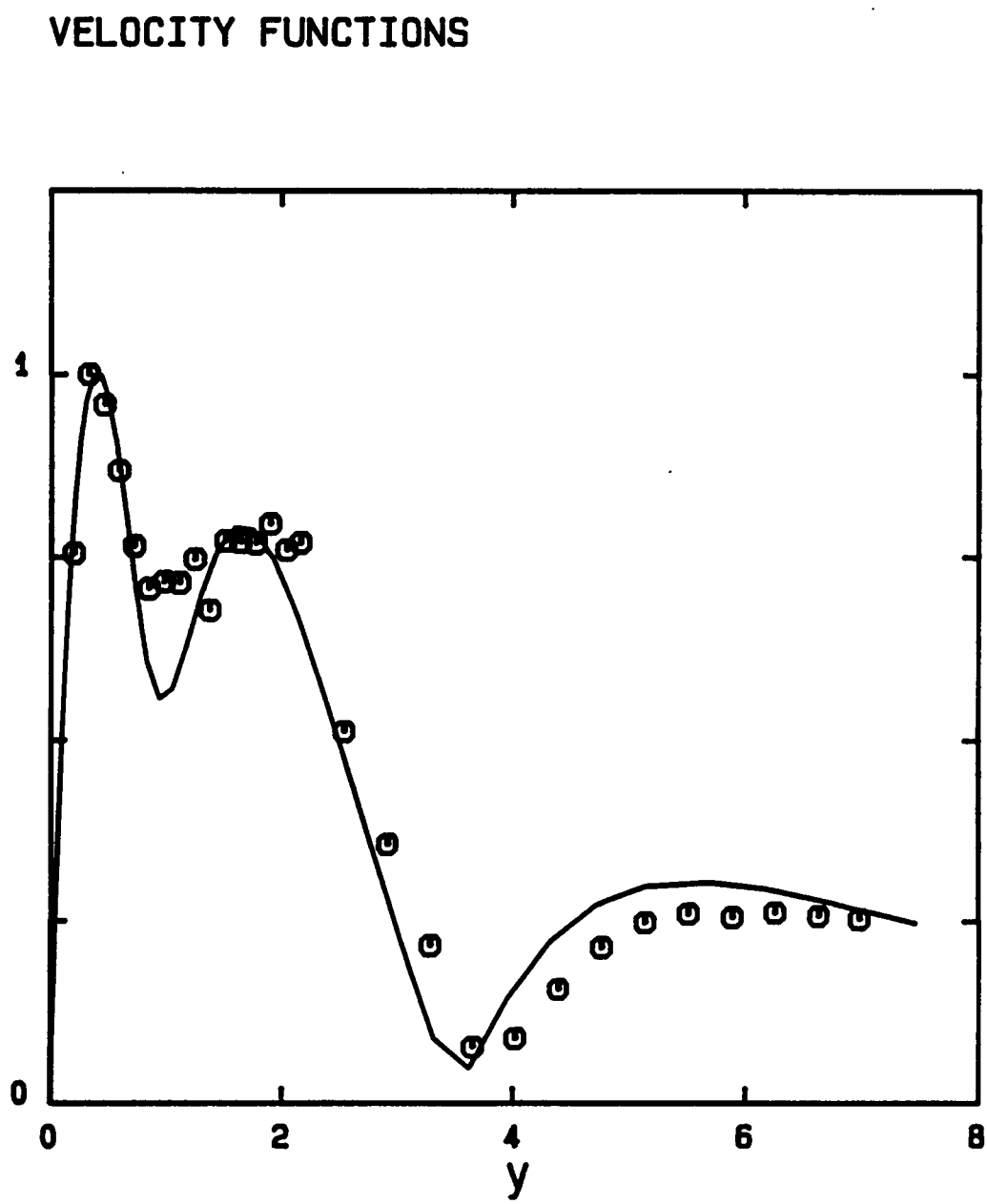

Figure 4.52 Comparison of the total valley velocity function, u_V, with the experiments of Cornelius (1985), figure 17b. Normalized function at $R = 755$. Results for the fundamental mode at $F = 64.4$, $b = .44$. and $\Delta = .05$, with initial values $A = .016$ and $B = .0015$ at $R = 675$.

References

F. P. Bertolotti 1985 "Temporal and spatial growth of subharmonic disturbances in Falkner-Skan flows," VPI & SU, M.S. thesis.

T. C. Corke and R. A. Mangano 1987 "Transition of a boundary layer: controlled fundamental-subharmonic interactions," Fluid Dynamics Center Rep. No. 87-1, Illinois Institute of Technology, Chicago, Illinois.

K. C. Cornelius 1985 "Three dimensional wave development during boundary layer transition," Lockheed Georgia Res. Rep. LG85RR0004, Marietta, Georgia.

A. D. D. Craik 1971 "Nonlinear resonant instability in boundary layers." *J. Fluid Mech.* **50**, pp. 393-413.

J. W. Croswell 1985 "On the energetics of primary and secondary instabilities in plane Poiseuille flow," VPI & SU, M.S. thesis.

A. Davey and H. P. F. Nguyen 1971 "Finite-amplitude stability of pipe flow," *J. Fluid Mech.* **45**, pp. 701-720.

H. F. Fasel, U. Rist, and U. Konzelmann 1987 "Numerical investigation of the three-dimensional development in boundary layer transition," AIAA Paper No. 87-1203.

M. Gaster 1962 "A note on the relation between temporally-increasing and spatially-increasing disturbances in hydrodynamic stability," *J. Fluid Mech.* **14**, pp. 222-224.

M. Gaster 1974 "On the effects of boundary-layer growth on flow stability," *J. Fluid Mech.* **66**, pp. 465-480.

Th. Herbert 1975 "On finite amplitudes of periodic disturbances of the

boundary layer along a flat plate," in *Proc. 4th Int. Conf. Numer. Meth. Fluid Dyn., Boulder, CO*, Lecture Notes in Physics, vol. 35, pp. 212-217, Springer-Verlag.

Th. Herbert 1983 "On perturbation methods in nonlinear stability theory," *J. Fluid Mech.* **126**, pp. 167-186.

Th. Herbert 1984a "Analysis of the subharmonic route to transition in boundary layers," AIAA Paper No. 84-0009.

Th. Herbert 1984b "Secondary Instability of Shear Flows," in *Special Course on Stability and Transition of Laminar Flow*, AGARD Report No. 709.

Th. Herbert 1985 "Three-dimensional phenomena in the transitional flat-plate boundary layer," AIAA Paper No. 85-0489.

Th. Herbert 1986 "Vortical mechanisms in shear flow transition," in *Direct and Large Eddy Simulation of Turbulence*, ed. U. Schumann and R. Friedrich, pp. 19-36, Vieweg-Verlag.

Th. Herbert 1988a "Secondary instability of boundary layers," *Ann. Rev. Fluid Mech.* **20**, pp. 487-526.

Th. Herbert 1988b "Onset of Transition in Boundary Layers," *Int. J. Num. Meth. Fluids* , In press.

Yu. S. Kachanov, V. V. Kozlov, and V. Ya. Levchenko 1977 "Nonlinear development of a wave in a boundary layer," *Izv. AN USSR, Mekh. Zhidk. i Gaza* **3**, pp. 49-53. (In Russian)

Yu. S. Kachanov and V. Ya. Levchenko 1982 "Resonant interactions of disturbances in transition to turbulence in a boundary layer," Preprint No. 10-82, I.T.A.M., USSR Acad. Sci., Novosibirsk.(In Russian)

Yu. S. Kachanov and V. Ya. Levchenko 1984 "The resonant interaction of disturbances at laminar-turbulent transition in a boundary layer," *J. Fluid Mech.* **138**, pp. 209-247.

P. S. Klebanoff, K. D. Tidstrom, and L. M. Sargent 1962 "The three-dimensional nature of boundary-layer instability," *J. Fluid Mech.* **12**, pp. 1-34.

C. F. Knapp and P. J. Roache 1968 "A combined visual and hot-wire anamometer investigation of boundary-layer transition," *AIAA J.* **6**, pp. 29-36.

R. Li 1986 "Analysis for Taylor-Vortex Flow," Ph. D. Thesis, Virginia Polytechnic Institute and State University, Blacksburg, Virginia.

A. H. Nayfeh 1981 *Introduction to Perturbation Techniques*, Wiley-Interscience.

A. H. Nayfeh 1985 "Three-dimensional spatial secondary instability in boundary-layer flows," AIAA Paper No. 85-1697.

A. H. Nayfeh 1987 "Nonlinear stability of boundary layers," AIAA Paper No. 87-0044.

A. H. Nayfeh and D. T. Mook 1979 *Nonlinear Oscillations*, Wiley.

S. A. Orszag and A. T. Patera 1983 "Secondary instability of wall-bounded shear flows," *J. Fluid Mech.* **128**, pp. 347-385.

G. R. Santos 1987 "Studies on secondary instabilities," Ph. D. Thesis, Virginia Polytechnic Institute and State University, Blacksburg, Virginia.

W. S. Saric and A. H. Nayfeh 1977 "Nonparallel stability of boundary layers with pressure gradients and suction," in *Laminar-Turbulent Transition*, pp. 6/1-21. AGARD CP-224.

G. B. Schubauer and H. K. Skramstad 1948 "Laminar boundary-layer oscillations and transition on a flat plate," N.A.C.A. Rep. No. 909.

P. R. Spalart and K.-S. Yang 1987 "Numerical study of ribbon-induced transition in Blasius flow," *J. Fluid Mech.* **178**, pp. 345-365.

J. T. Stuart 1960 "On the non-linear mechanics of wave disturbances in stable and unstable parallel flows. Part 1.," *J. Fluid Mech.* **9**, pp. 353-370.

J. Watson 1960 "On the non-linear mechanics of wave disturbances in stable and unstable parallel flows. Part 2.," *J. Fluid Mech.* **9**, pp. 371-389.

T. A. Zang and M. Y. Hussaini 1985 "Numerical experiments on subcritical transition mechanism," AIAA Paper No. 85-0296.

Appendix. Nonlinear dynamics example

In order to see the basic features of the perturbation approach given in chapter 2, a similar approach is taken to solve a simple nonlinear dynamics problem. Consider the two degree of freedom system

$$\ddot{u} + u + v^2 = 0 \ , \tag{A.1}$$

$$\ddot{v} + v + uv = 0 \ , \tag{A.2}$$

where u and v are functions of time. This provides an interaction analogous to the primary/secondary interaction. Namely, through the v^2 effect on u and the uv effect on v. Unlike the equations for the primary, however, the u equation is linear in u. This is not a major shortcoming since the resulting variations are easily recognizable.

To justify the use of this perturbation approach for (A.1) and (A.2), assumptions are made on relative sizes of u and v. In particular, it is assumed that the magnitude of u is considerably larger than that of v when nonlinear effects become significant. This could result from initial conditions or some kind of internal or external forcing not here considered. As long as v is small, nonlinear effects can be neglected even though u is larger.

For simplicity the straight forward expansion is used, which neglects modifications to the frequency (Nayfeh 1981). These modifications could be included with little difficulty but they do not alter the basic approach. There are three different forms of expansion which could be used to address (A.1) and (A.2).

The first of these is

$$u = \hat{a}u_1 + b^2u_2 + \cdots , \tag{A.3}$$

$$v = bv_1 + \hat{a}bv_2 + \cdots , \tag{A.4}$$

where u_1, v_1, u_2, and v_2 are functions and $\hat{a}$ and b are ordering parameters related to amplitudes. The particular arrangement of the ordering parameters is drawn from the structure of the nonlinearities. When $\hat{a}$ and b are small ($\hat{a},b \ll 1$) the expansions (A.3) and (A.4) convert (A.1) and (A.2) into sets of linear equations. These equations capture the mutual interaction of u and v, but do not account for the bias in the magnitude of u.

An alternate form for the expansions is

$$u = (a^* + \hat{a})\, u_1 + b^2u_2 + \cdots , \tag{A.5}$$

$$v = bv_1 + \hat{a}bv_2 + \cdots , \tag{A.6}$$

where $(\hat{a},b \ll a^* \ll 1)$. This accounts for the bias in u through the additional amplitude a^* multiplying the linear function u_1. For this particular system (A.5) is equivalent to

$$u = a^*u_0 + \hat{a}u_1 + b^2u_2 + \cdots . \tag{A.7}$$

The absence of a u^2 nonlinearity results in u_0 and u_1 having the same governing equation. For the boundary layer, however, there are nonlinear primary terms so that expansions of the forms (A.5) and (A.7) would not be equivalent. (The function u_1 in (A.7) would be parametrically generated, unlike u_1 in (A.5).) The expansion (A.5) is preferred in the analysis of the boundary layer, since it provides for the interaction of the TS wave with the secondary.

Substituting (A.5) and (A.6) into (A.1) and (A.2) and collecting coefficients of the various parameters yields

$$O(a^*): \quad \ddot{u}_1 + u_1 = 0 \ , \tag{A.8}$$

$$O(\hat{a}): \quad \ddot{u}_1 + u_1 = 0 \ , \tag{A.9}$$

$$O(b): \quad \ddot{v}_1 + v_1 + a^* u_1 v_1 = 0 \ , \tag{A.10}$$

$$O(b^2): \quad \ddot{u}_2 + u_2 = v_1^2 \ , \tag{A.11}$$

$$O(\hat{a}b): \quad \ddot{v}_2 + v_2 - a^* u_1 v_2 = u_1 v_1 \ . \tag{A.12}$$

The lowest order u-function, u_1, is given by (A.8). By design, the $O(\hat{a})$ equation is redundant. The lowest order v-function, v_1, is given by (A.10), which contains a parametric forcing term $a^* u_1$. This parametric term results from the initial bias in the u magnitude. The second order equations are of the same form as the first order equations with the addition of lower order forcing terms.

Considering limiting cases of the expansion equations (A.5) and (A.6) yields distinct sets of governing equations. In the limit as $a^* \to 0$, the equations become

$$O(\hat{a}): \quad \ddot{u}_1 - u_1 = 0 \ , \tag{A.13}$$

$$O(b): \quad \ddot{v}_1 - v_1 = 0 \ , \tag{A.14}$$

$$O(b^2): \quad \ddot{u}_2 - u_2 = v_1^2 \ , \tag{A.15}$$

$$O(\hat{a}b): \quad \ddot{v}_2 + v_2 = u_1 v_1 \ . \tag{A.16}$$

These are simply the mutual interaction equations, which are obtained by (A.3) and (A.4). On the other hand, as $\hat{a} \to 0$, the equations become

$$O(a^*): \quad \ddot{u}_1 + u_1 = 0 \ , \tag{A.17}$$

$$O(b): \quad \ddot{v}_1 + v_1 + a^* u_1 v_1 = 0 \ , \tag{A.18}$$

$$O(b^2): \quad \ddot{u}_2 + u_2 = v_1^2 \quad . \tag{A.19}$$

These equations govern a purely parametric interaction. Thus the expansions given by (A.5) and (A.6) provide a generalized parametric interaction, with the mutual resonance and purely parametric interactions as special cases.

The vita has been removed from the scanned document